Lawrence Berkeley Laboratory
UNIVERSITY OF CALIFORNIA

Materials & Molecular Research Division

THE ROLE OF PARTICLE SUBSTRUCTURE
IN THE SINTERING OF MONOSIZED TITANIA

L.H. Edelson
(M.S. Thesis)

December 1986

Prepared for the U.S. Department of Energy under Contract DE-AC03-76SF00098

LBL-22753

DISCLAIMER

LBL-22753

The Role of Particle Substructure in the Sintering of Monosized Titania

Lawrence Howard Edelson

M.S. Thesis

Lawrence Berkeley Laboratory
University of California
Berkeley, California 94720

December 1986

The Role of Particle Substructure in the Sintering of Monosized Titania

By

Lawrence Howard Edelson

Submitted in partial satisfaction of the requirements for the degree of Master of Science in Engineering in the Department of Materials Science at the University of California, Berkeley. December 23, 1986.

Abstract

Results from preliminary coarsening studies on chemically synthesized, monosized, spherical "ideal" titania powders indicated particle coarsening characteristics were strongly influenced by unanticipated particle substructure.[1] Such substructure should also affect sintering, however, particle substructure was not recognized and accounted for in previous sintering studies using this powder. The present study examined the sintering behavior of compacts comprised of monodispersed agglomerates and correlates changes in macroscopic dimensions with changes in particle microstructure and chemistry.

Monosized titania particles (0.35μm) prepared by controlled hydrolysis of titanium tetraethoxide in ethanol were found to be porous agglomerates of approximately 60Å primary particles. The total volume shrinkage during sintering was 84%! Five contributions to the total shrinkage and the temperature ranges for the associated processes were identified: removal of chemisorbed water (approximately 12% linear shrinkage, from ambient to 250°C), crystallization to anatase (approximately 13% linear shrinkage between 250°C to 425°C), intra-agglomerate densification (approximately 13%, 425°C to 600°C), conversion of anatase to rutile (approximately 5% linear between 600°C to 800°C), and interagglomerate densification (7% linear shrinkage above 800°). Thus, approximately half the compact shrinkage is the result of agglomerate substructure changes.

Studies of the agglomerate structural evolution indicate the intra-agglomerate densification crystallite growth rates, rather than crystallization and the polymorphic transformation, are the secondary factors, after compact packing, that influence microstructure development. This indicates control of intra-agglomerate structure is an important and necessary processing consideration even though "particle" size and "particle packing are tightly controlled.

This study has important implications for the processing of other monosized powders. Particle substructure can generate unexpected shrinkage. Failure to adequately control intraparticle structure can deleteriously affect the resulting microstructure finished ceramic.

TABLE OF CONTENTS

Acknowledgements

I would like to thank my research and thesis adviser, Professor A. M. Glaeser for suggesting the original research topic and providing the guidance and motivation to see the project to completion. I am grateful for his advice and friendship. I am honored that I have the opportunity to be among his first advanced degree candidates, and I hope I can continue the trend for my Ph.D.

I would like to thank Professors A. W. Searcy and C. J. Radke, the other members of my thesis committee, for taking the time and effort for reading my thesis. Their comments and suggestions were very helpful and greatly appreciated. I am grateful to Dr. B. J. Dalgleish for reading the manuscript; his assistance with the organization and content were invaluable. I wish to thank Professor R. M. Cannon for his helpful discussions. I am grateful to Professor A. Bleier for his discussion on powder agglomeration.

I would like to acknowledge the hours of effort our laboratory technician Grant Gager expendend trying to maintain our equipment and keep it running despite the best efforts of numerous users to foil him. My research would have been considerably more difficult without his dedication.

Finally, I wish to express my sincerest gratitude to my very special friend, Shelly M. Miyasato. I would not have been able to complete my the thesis without her seemingly endless support, understanding, and confidence.

The author acknowledges the fellowship support of the University of California (Regents, and Richard M. Fulrath Fellowships) for two years, IBM for one year, and the U.S. Department of Energy for their partial support for two-years under contract number DE-AC03-76SF00098.

1.0 Introduction

Future developments in such diverse areas as aerospace, automotive, power production and distribution, materials production, electronics, and biomedical industries will inevitably require the increased use of ceramic materials.[2,3a-g] Ceramic materials possess superior thermal, mechanical, chemical, and electrical properties. However, more extensive use of ceramics is frequently limited by excessive brittleness, high cost, and poor reliability. Inadequate understanding and control during processing can introduce microstructural defects or flaws, compositional heterogeneities, and impurities in the finished product[2] all of which are deleterious to material performance.

Sintering is the predominant fabrication method for polycrystalline ceramics.[4] During sintering, powder particles comprising a compact weld together to form a monolithic body at temperatures below the melting point. The fabrication goal is the production of a material with controlled macroscopic dimensions, and microstructure. Usually, a fine-grained, pore-free material is desired. The green (presintered) compact microstructure largely determines material sintering characteristics.[2,5] Thus, microstructural control in the green compact is important for the success of a sintering process.

In general, densification depends on the coupled processes of pore shrinkage, pore coalescence and grain growth.[6] Scaling laws[7] indicate particle size reduction can enhance shrinkage rates. Grain growth, generally, is undesirable because it does not increase the sintering rate, but can reduce it. Grain growth enhances pore coarsening through grain boundary migration-induced coalescence[8] which reduces the pore removal driving force,[9] and consequently, pore volume shrinkage rates.

Grain growth can lead to pore-grain boundary separation[10-11] which severely limits compact density.[10-12] Narrow size distribution systems develop steady state (normal growth) size distributions after a short induction period.[13-14] Exaggerated grain growth, however, may precede normal growth in wide size distribution systems.[13] Therefore, uniform compacts of fine, equiaxed, narrow sized distribution powders should have increased stability against grain growth,[13] pore coarsening,[14] and pore-grain boundary separation.[2] Uniform compacts do indeed have superior sintering characteristics compared to less carefully controlled compacts made from the same powder.[15]

Powder characteristics (such as particle size, particle size distribution, shape, degree of aggregation and composition) and powder handling determine green compact structure[2,5] and consequently establish a material's potential sintering performance. The starting powder is frequently the limiting factor in ceramic fabrication.[16-21] As a result, control of particle characteristics is an important consideration in ceramics production. Recently, chemical synthesis methods were developed that enable high yield production of monosized, spherical titania powder particles packed in very uniform -- even ordered -- compacts that sinter to full density in 90 minutes at 1050°C (melting point 1800°C).[22-23] This is 300°C below the sintering temperature for conventional titania powders.[24] These results have generated considerable interest in developing characteristic-controlled powder production methods for a variety of other systems.

Packing techniques enabling production of dense-random-packed compacts from mixtures of fine and coarse particles are in development.[25] Properly prepared bimodal or multimodal systems can have much higher initial densities compared to monosized systems and have finer, yet

uniform pore sizes.[25] Potentially superior results are possible with these systems because the higher green densities lead to lower shrinkage while the fine, narrow pore size distribution enables rapid pore elimination.[2,25] Control of the constituent powder characteristics is necessary for optimal performance. Thus, monosized powder synthesis methods also are desirable for the production of rapidly densifying low shrinkage powder compacts.

Arguments favoring monosized powder use to improve material sintering performance are only valid if these powder compacts develop grain and pore size distributions that reflect the particle monodispersity and packing uniformity. The tacit assumption is that monosized powder particles are isotropic, single crystals, lacking internal structure, which are chemically and crystallographically stable during sintering.[2,25] Chemically synthesized powders, though, frequently undergo further chemical (dehydration, decomposition, and/or calcination) reactions and polymorphic transformations during firing.[26-31] Improved characterization techniques are also beginning to reveal considerable internal structure in chemically prepared material.[32-33]

Transformations in apparently "ideal" powders can produce unexpected results in the sintered microstructure. For example, a five-fold grain size increase during the sintering of monosized TiO_2 to full density was attributed to concurrent crystallization and polymorphic transformations.[23] Although no effort was made to optimize conditions, more disasterous results are conceivable. This is illustrated in the sintering of a nominally monosized, spherical alumina in which the gamma-to-alpha polymorphic transformation results in a dramatic increase in grain size as nucleated alpha grains grow through the surrounding

gamma matrix.[26] These growing grains entrain large numbers of formerly intergranular pores, and effectively arrest densification.

Evidence from monosized TiO_2 particles prepared by hydrolysis of titanium tetraethoxide (following the recipe in ref. 23) in the current study, and Bleier and Cannon's investigation[34] of nominally monodispersed m-ZrO_2 prepared by thermal hydrolysis of zirconyl salt solutions indicate these techniques produce powder particles that are actually porous agglomerates of much finer primary units. Van der Woude[35] has reported controlled secondary particle generation in FeOOH, and Matijevic has observed secondary structures in CeO_2.[36] Monosized powders are assumed to develop pore and grain size distributions during sintering reflect this monodispersity, which is the basis for their use. Pore size in a compact of monosized agglomerates, at best, is a bimodal distribution of intra- and interagglomerate pores; primary units comprising the agglomerates may be polydispersed and/or inhomogeneously packed. Thus, considerable driving force for pore coarsening and grain growth may exist in "monosized" powders. As a result, uncontrolled grain growth can potentially limit compact density even when phase transformations are absent or unimportant.

The role of internal agglomerate structure in intra- and interagglomerate densification and grain growth is often ignored. A background section discusses possible agglomerate structural effects on the sintering characteristics of monosized agglomerate compacts, and in this context, includes considerations on grain growth and phase transformations. The remainder of this thesis is devoted to agglomerate substructural effects in the sintering of monosized TiO_2. In this study the powder is first assumed to consist of "ideal" particles, but features in sintered microstructures and shrinkage characteristics are

identified which, in light of the background discussion, are more consistent with powder "particles" that are agglomerates. The agglomerate structure and its evolution are characterized to help explain observed sintering characteristics. A brief discussion of powder synthesis and handling is included because the resulting green microstructures influence sintering properties.

Titania was selected because a synthesis technique exists for the preparation of monosized powder in sufficient quantities for extensive powder characterization and sintering studies, and extensive characterization and sintering studies on conventional TiO_2 have been performed[23,28-30,37-48] Although it is possible to make monosized powders from alternate materials, practical laboratory techniques usually yield small quantities.[49-51] Monosized silica can be prepared in large quantities,[52] but this material remains amorphous and sinters through viscous flow; therefore, many of the internal structure considerations in crystalline materials do not apply.

The primary focus of this research is to explore the possible consequences of particle nonideality on monosized powder densification and microstructure. Titania was selected as a model system for this study; however, the guidelines for synthesis and sintering that emerge are likely to have general applicability to other chemically derived monosized powders. Monosized systems of TiO_2, ZrO_2, CeO_2, and FeOOH are confirmed examples of monosized systems in which the monosized structure is a secondary particle (agglomerate) comprised of much finer primary units. Application of these monosized powder synthesis techniques to other systems is likely to produce, at least in some systems, monosized structures that are secondary particles.

2.0 BACKGROUND

2.1 Agglomerate Structure

The structure of an agglomerate of primary units and the arrangement of particles in a compact are analogous in that they differ only in scale. Sintering in a compact of agglomerates, however, represents an additional complexity in which densification depends on the agglomerate substructure as well as interagglomerate packing in the green compact. It is imperative to consider the effect of grain growth and phase transformations on sintering in the context of the dual microstructure of a compact of agglomerates.

To avoid ambiguity, the following terminology is used: A "particle" is considered to be a non-porous single crystal and is the idealized structural unit in monosized powders. Titania "particle" diameters are generally between 0.1-0.3μm (many monosized powders fall in this size range[49-52]). An agglomerate is an apparent "particle" that is actually an assembly of fine primary units. These primary units are single phase particles in the 10-100Å size range and are considered the fundamental structural units. Porous and/or polycrystalline "particles", for simplicity, are considered to be agglomerates. In an ideal powder, the primary units and "particles" are the same and the powder compact is the structural equivalent of an agglomerate.

A powder's susceptibility to contamination will differ markedly if it is comprised of agglomerates of fine primary units rather than ideal particles. If care is taken to ensure powder purity during synthesis (this is generally necessary for the success of the synthesis anyway), the primary danger is surface contamination during handling. The powder surface area, thus, determines contamination sensitivity. A powder

consisting of open agglomerates of 100Å primary units has a specific surface area that is fifty-fold greater than a powder consisting of 0.5μm particles. Contamination can adversely affect powder suspension stability (resistance to particle flocculation)[23,25,53] and the quality of the resulting compact, alter lattice and grain boundary diffusion coefficients,[45,54] grain boundary mobility,[54-58] phase transformation kinetics,[27-30,42-44] and produce undesirable properties in the finished product (impurities in semiconductors are an excellent case in point).

Conversely, the agglomerate structure is a potential processing advantage in that it facilitates compositional manipulation on a finer scale than in comparably sized dense particles. Since homogenization time scales as the square of diffusion distance, the agglomerate structure can dramatically reduce the homogenization time for doping or the reaction time for the production of spinel phases, for example. Production of the ferroelectric $BaTiO_3$ from TiO_2 suspensions is possible if a suitable barium salt is added. Precipitation at the appropriate conditions can yield a high concentration of barium salt in the intra-agglomerate pores. During subsequent heating in an oxidizing atmosphere, a high volume fraction of titanate forms in much shorter times and lower temperatures than in conventional processes that mix titania and barium carbonate powders.

Intra-agglomerate pore elimination causes additional shrinkage compared to densification of a compact comprised of non-porous particles. Densification of a close packed compact (74% packing efficiency) of particles with 30% porosity will result in more than a 48% volume decrease. Agglomerate porosity exceeds 50% in nominally monosized monoclinic zirconia prepared by thermal hydrolysis of relatively concentrated zirconyl salt solutions.[34] Thus, low densification

shrinkage expectations based on the high apparent packing efficiency of monosized or bimodal powders produced from a mixture of monosized powders (approximately 86% with dense random packing of a mixture of coarse and fine spheres) are deceptive if the "particles" are actually porous agglomerates.

Scaling laws[7] predict intra-agglomerate sintering of primary units occurs much more rapidly than sintering of agglomerate-sized particles. For example, 100Å primary units densify at 50^3 times the rate of 0.5μm particles assuming densification occurs through lattice diffusion, and the diffusional mechanism is size independent.[7,15,59] Hence, the effective intra-agglomerate sintering temperature can be much lower than the interparticle sintering temperature since the fine primary particles accelerate the densification rate at all temperatures (the exact lowering of the temperature depends on the activation energy the rate controlling process causing densification). Significant low temperature shrinkage (>30 vol% for agglomerates of randomly packed spherical primary units) can result from preferential intra-agglomerate sintering.[15,60] In a related process, primary unit sintering between agglomerates can produce interagglomerate necks at temperatures significantly below those expected for agglomerate-sized particles. Interagglomerate neck formation is compared schematically to interparticle neck growth in **Figure 1.** The extent of this process depends on the number of interagglomerate primary particle contacts, which in turn, depends on the agglomerate shape, surface texture, and local packing. Intuitively, rough agglomerate surfaces would be expected to enhance interagglomerate sintering.

Fine primary particles can also enhance interagglomerate densification in a process similar to coalescence of viscous particles.[47,59] The

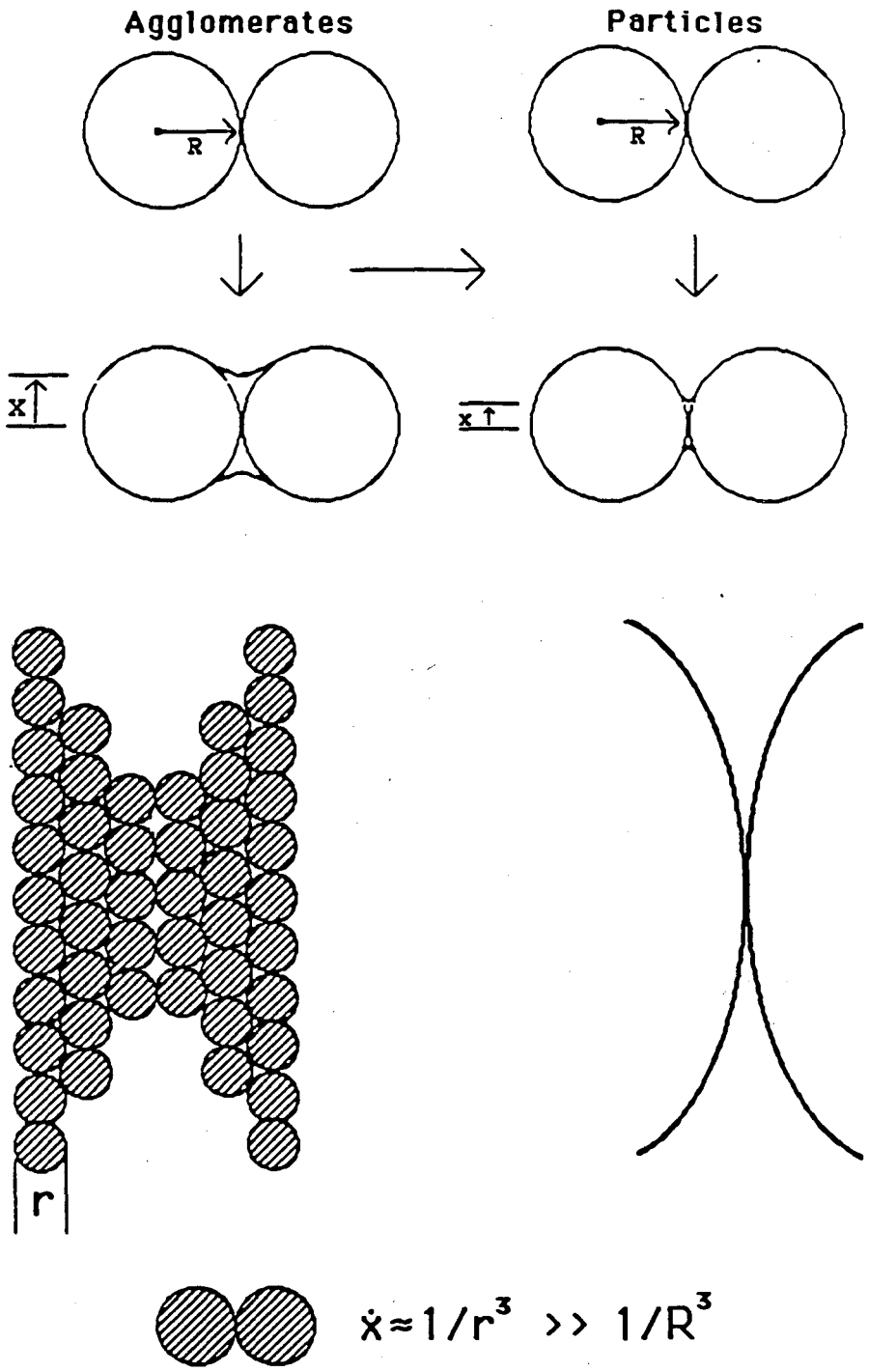

Figure 1. Comparison of interagglomerate to inter-primary particle sintering. The neck between the agglomerate primary particles forms much faster and at a lower temperature than for agglomerate-sized particles. The extent of the low temperature interagglomerate necks depends on the local contact geometry. Rough agglomerate surfaces should "mesh", while smooth agglomerates will have relatively small contact areas.

-- XBL 871-170 --

shrinkage rate $\dot{\varepsilon}$ is given by[47]

$$\dot{\varepsilon}=2\gamma/nR$$

where γ is the solid surface energy, R is the agglomerate radius and n is the effective viscosity for Nabarro-Herring creep, which for a single crystal is[47]

$$n = R^2kT/14Da_o^3$$

where kT is the thermal energy, D is the lattice diffusion coefficient and a_o^3 is the atomic volume. If the particles are now considered to be agglomerates, the viscosity is[59]

$$n = r^2kT/14D_{eff}a_o^3,$$

where

$$D_{eff} = (D_l + \pi\Delta D_b/r)$$

and r is the primary particle size, D_l and D_b are the grain lattice and boundary diffusion coefficients, respectively, and Δ is the grain boundary width. The shrinkage equation becomes

$$\dot{\varepsilon} = \sigma/n = \sigma 14D_{eff}/kTr^2$$

and the stress, σ is

$$\sigma= 2\gamma/R.$$

The shrinkage rate is then proportional to

$$\dot{\varepsilon} \sim 1/Rr^2(D_l + \Delta D_b/r).$$

Thus agglomerate shrinkage through viscous flow is accelerated by $(R/r)^2$ or $(R/r)^3$ depending on the active transport path. For 50Å primary particles in 5000Å agglomerates, these amount to 2500, or 125,000-fold increases in the sintering rate.

Kingery[9] considered the effect of surrounding grains and dihedral angle constraints on pore stability. He found, depending on dihedral angle and number of surrounding grains, that grain boundaries could

prevent pore shrinkage and even cause pore growth. The results of the analysis for space filling grains suggest that in high dihedral angle materials (~150° for Al_2O_3) pores are stable when the ratio of pore size to grain size exceeds only 1.5. The tetrahedral void radius in FCC packing of monosized agglomerates is 15% of the agglomerate radius, and the critical grain size one tenth the agglomerate size. The critical grain size adjacent to the octahedral voids is about one fourth the agglomerate size. 50Å agglomerates in 5000Å particles are substantially below the critical size for pore stabilization. Thus, substantial grain growth may be necessary before interagglomerate pore shrinkage begins.

2.2 Grain Growth in Polycrystalline Particles

Grain growth is an Ostwald ripening process in which large grains eliminate adjacent smaller grains to reduce the total grain boundary energy. In the initial stages of sintering, grain growth through the interparticle or interprimary unit neck is impeded because boundary movement through the neck requires its extension. As a result, grain growth does not take place before significant neck growth and, usually, densification has occurred.[23,61] This limitation applies to both intra-agglomerate grain growth and interparticle growth.

Intra-agglomerate densification in closely packed agglomerates occurs preferentially over interagglomerate densification.[60] As intra-agglomerate porosity is reduced, crystallite growth will begin. The rate and extent of this intra-agglomerate grain growth depends on the grain size distribution and packing within the agglomerate.[61] At a critical porosity, exaggerated grain growth may occur. Exaggerated growth is more likely in fine crystallite coarsening because there is a greater possibility that some grains that develop during normal growth will be

of sufficient size undergo exaggerated growth when compact porosity falls below a critical porosity.[19,61]

As long as grain growth is confined within an agglomerate, the consequences for sintering probably are not serious. Even intra-agglomerate voids, isolated from internal primary unit boundaries during growth, should not limit compact density. Diffusion distances to the relatively large interagglomerate pores are short (<0.1μm), compared to pores inside grains exceeding 1μm; furthermore, the proximity of the comparably large interagglomerate pores to the fine intra-agglomerate pores creates a high driving force for intra-agglomerate pore removal.

Exaggerated primary unit growth that occurs before appreciable interagglomerate sintering can produce grain size distributions that at the outset of interagglomerate sintering are near the steady state distribution. This is desirable, because then the expected low grain growth rate for monosized powders are likely to be realized. The stochastic nature of grain growth, though, can lead to grain size differences between adjacent agglomerates (**Figure 2**) that are sufficient to stimulate exaggerated grain growth. Growth can isolate interagglomerate pores as rapidly growing grains in dense regions grow around pores, as shown in **Figure 3**. Normal grain boundary-pore separation can also occur. If densification occurs rapidly compared to the grain growth, exaggerated growth in the dense material is a potential problem. At any rate, significantly more grain growth may occur in monosized agglomerate powders than is expected in an "ideal" powder.

The grain boundary in the neck between two dissimilar size, single-crystal particles is in a state of local equilibrium: the large grain should consume the smaller grain, but further movement increases the grain boundary area and thus the total energy of the pair (**Figure 4a**).

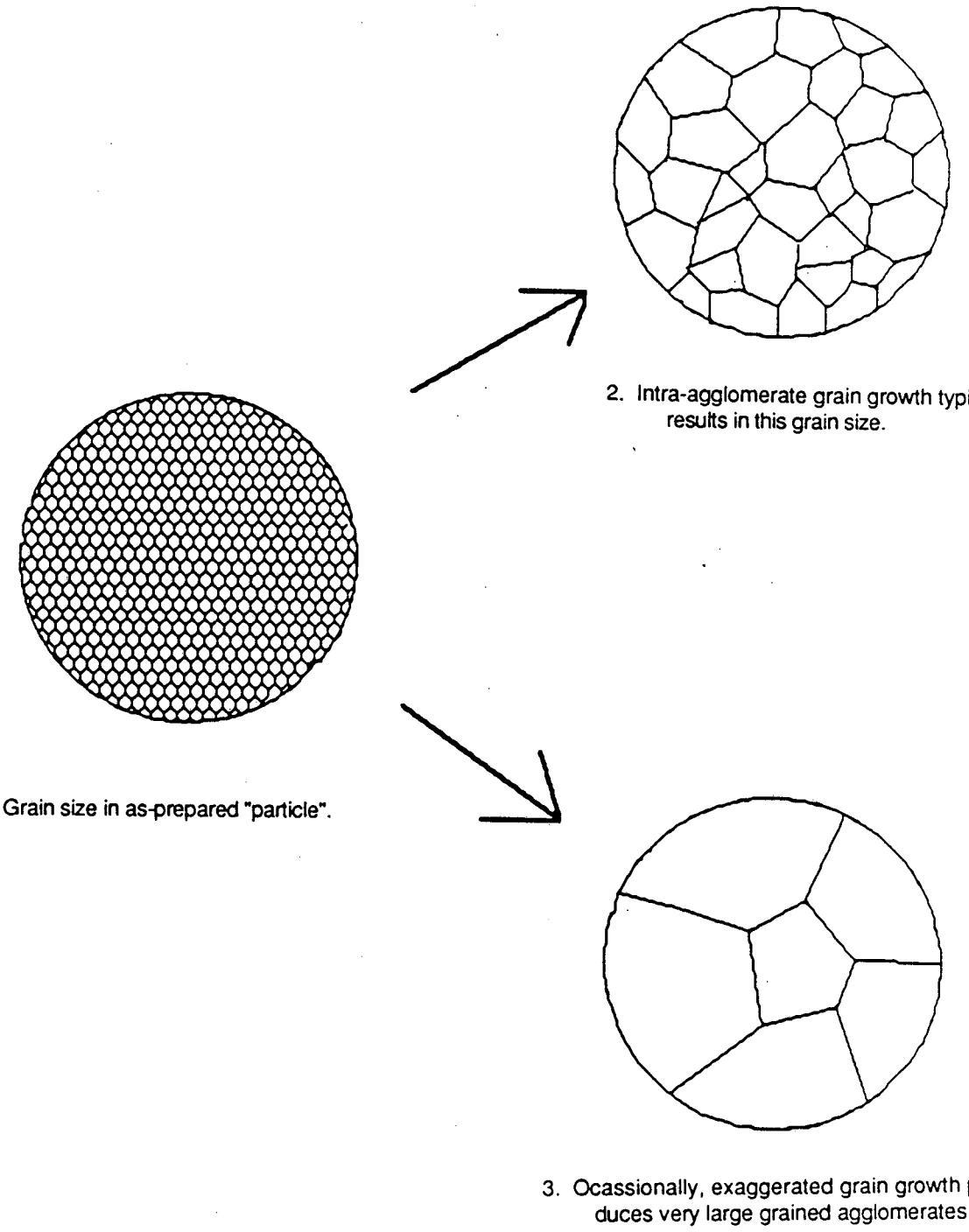

Figure 2. Intra-agglomerate grain growth can result in large differences in grain size in adjacent agglomerates. The starting size distribution is small. In (2), normal grain growth has produced a relatively fine grain size. In (3), exaggerated grain growth of a few grains has produced very coarse grains. In each case the size distribtion is narrow. The large difference in average grain size between adjacent particles can stimulate rapid grain growth in the latter stages of interagglomerate sintering.

-- XBL 871-171 --

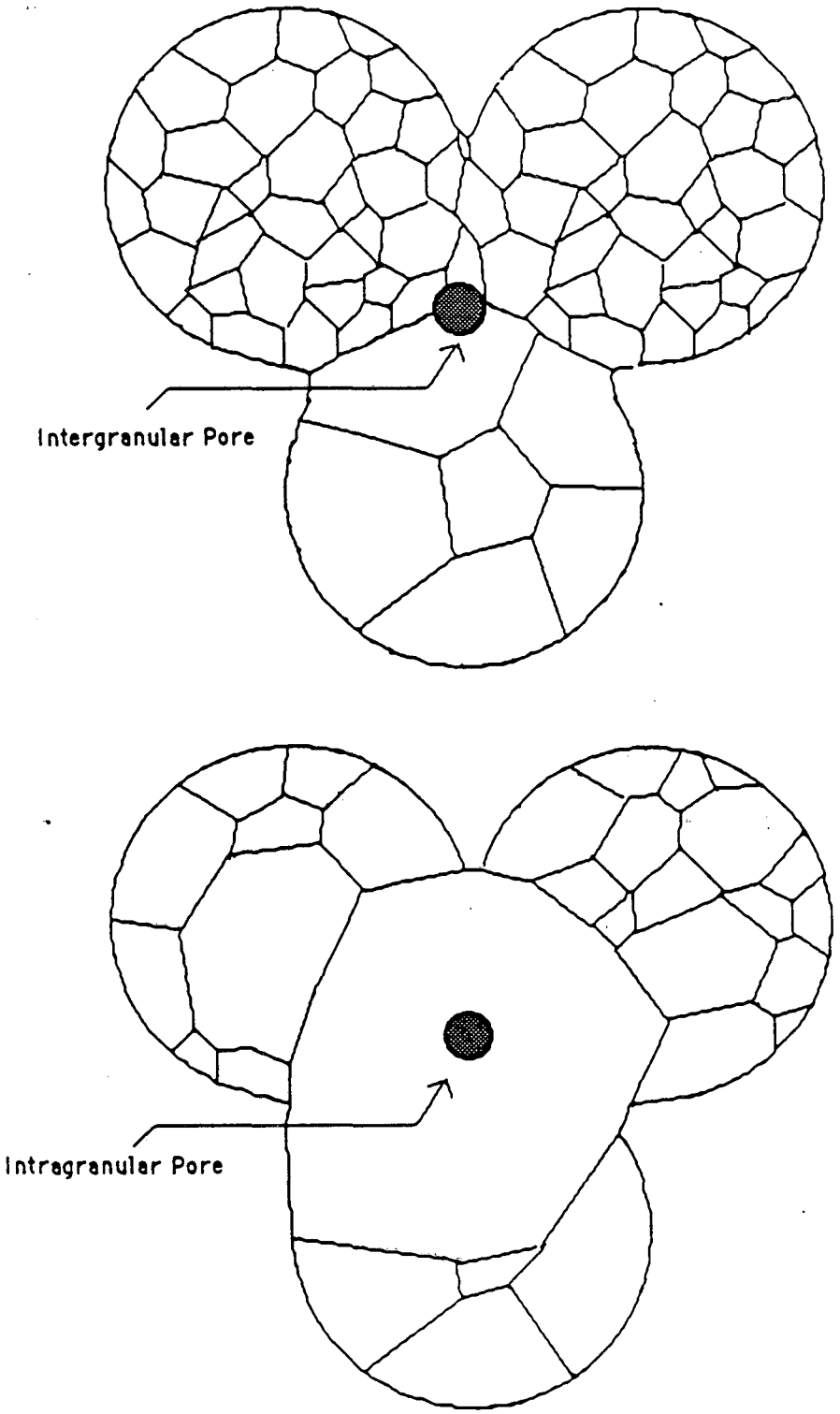

Figure 3. Intra-agglomerate grain growth has resulted in a large difference in the grain size between adjacent grains. During interagglomerate sintering, a large grain in the bottom agglomerate consumes adjacent smaller grains, and in the process isolates a interagglomerate pore.

-- XBL 871-172 --

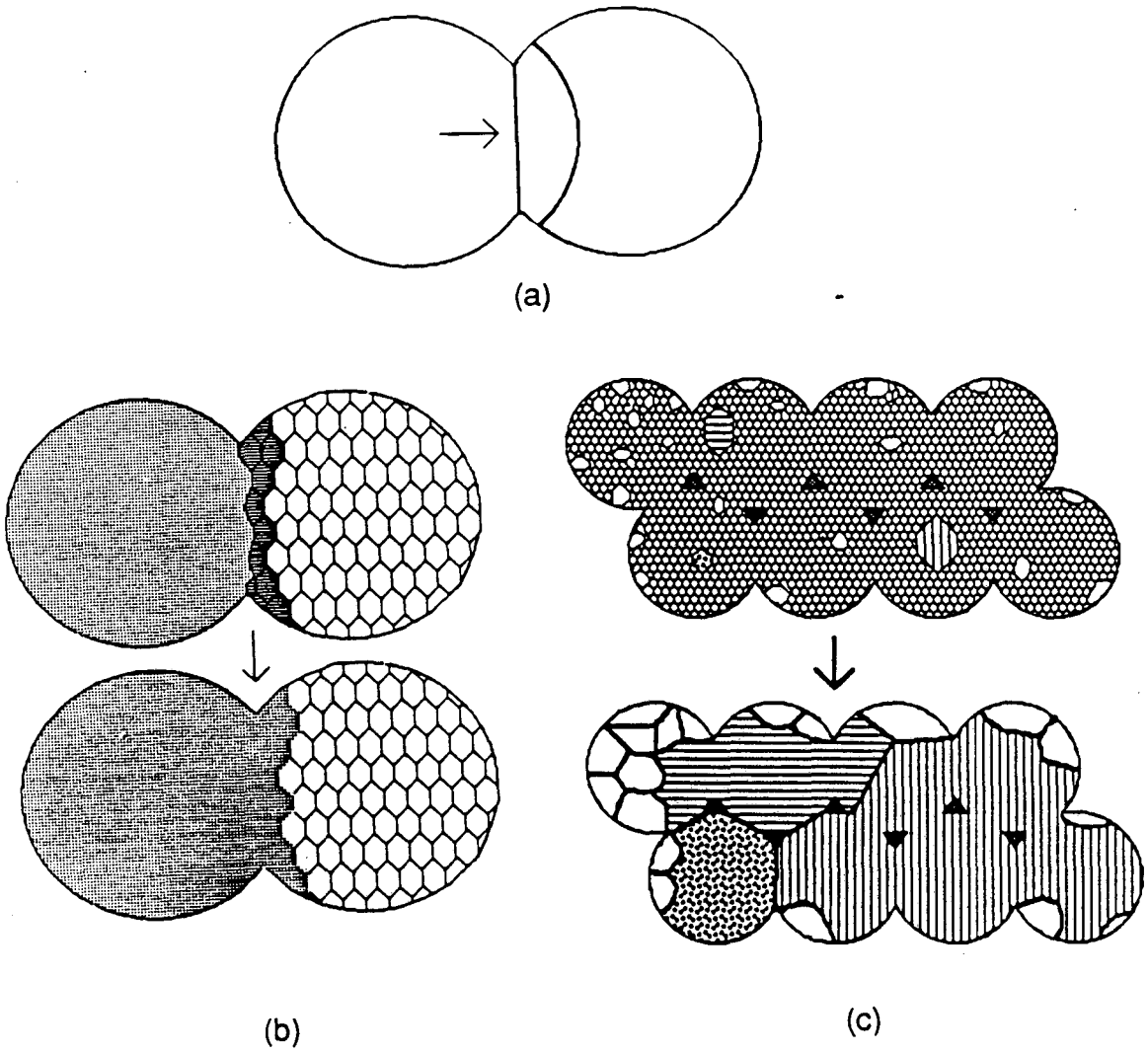

Figure 4. Growth of intra-agglomerate grains through polycrystalline necks.

(a) Growth of a grain boundary between two particles causes an increase in boundary area, and the dihedral angle constraint at the free surface creates a boundary curvature that opposes further grain growth.

(b) Growth of a large grain can proceed across a polycrystalline neck by incrementally consuming smaller grains.

(c) Exaggerated intra-agglomerate crystallite growth results in large grains developing in the early sintering stages. The resulting grain structure may contain some very large grains that undergo exaggerated grain growth in the latter stages of interagglomerate sintering.

Grain boundaries are effectively pinned to their adjacent interparticle pores. As sintering progresses, pores shrink until pore movement and possibly grain boundary separation can occur at the existing grain growth driving force. Interparticle or interprimary unit grain growth in uniform, narrow size distribution systems does not occur before the local density exceeds approximately 85% of theoretical.[23] In wide size distribution systems, grain growth occurs at lower relative densities, but this reflects, in part, greater density variation which permits growth in localized dense regions while other areas are still too porous to support grain growth.

Grain growth between polycrystalline particles can occur at low relative densities if the neck diameter exceeds grain size. **Figure 4b, 4c** illustrate how large grains can "incrementally" cross polycrystalline necks without grain boundary extension. Substantial growth may take place before a growing grain encounters another grain exceeding the neck size and is pinned. Wide grain size distributions can develop with some grains substantially larger than the original particle size. Subsequent exaggerated grain growth can result as the interagglomerate porosity is reduced and the grain boundary pinning is diminished. Low intra-agglomerate grain growth rates, paradoxically, can increase the extent of low density interagglomerate grain growth because relatively large interagglomerate necks can form before the onset of exaggerated grain growth. Conditions that enhance intra-agglomerate densification and grain growth, but delay interagglomerate sintering would reduce low density grain growth. Alternatively, grain boundary mobility reduction with dopants can, if done correctly, maintain a fine grain size.

Dopants and impurities cause significant changes in the grain boundary mobility (eg. MgO in alumina[56], LiF[57]). In certain cases,

additives to the powder may be necessary to control grain growth during sintering. In polycrystalline particles, additives admixed after the synthesis step may be ineffective if they do not penetrate to the internal boundaries, since control of intra-agglomerate growth is their intended purpose. In this situation, dopants must be incorporated directly in the powder synthesis. Furthermore, sufficient dopant concentration is necessary to ensure the growth of all grains is retarded. Insufficient dopant concentration can enable a few grains to grow extremely large.[19,58]

2.3 Transformations

Phase transformations change solid density and compact porosity. Transformations can convert particles into agglomerates.[27] Transformations may influence the densification rate through alterations in the diffusion coefficients, grain boundary mobility, and the pore and grain size distributions. In compacts of "ideal" monosized powders or bi- or polymodal mixtures of monosized powders, phase transformations can dramatically alter the uniform pore and/or grain size distribution[27] which was the basis for using these powders.

Polymorphic transformations are the most frequently encountered phase transformation during processing of single component ceramics. These transformations alter the crystal structure without modifying composition. Polymorphic transformations can be classified as either displacive or reconstructive. Displacive transitions (such as the martensitic transformation of cubic to tetragonal (ferroelectric) $BaTiO_3$, or the monoclinic-to-tetragonal inversion in zirconia) change the secondary coordination distances without breaking primary chemical bonds, and are accomplished by coordinated displacements of atoms from their

starting positions. Since these reactions are diffusionless, they occur rapidly, at a definite temperature. To minimize strain energy, new lenticular phases form along crystallographically invariant habit planes. These orientational constraints generally confine newly formed grains within their parent grain. Often several crystallographically equivalent variants will form in a parent grain. Large volume changes can cause cracking and are the most serious consequence of displacive transformations. Displacive transformations modify the grain size distribution, and therefore may alter subsequent grain growth rates, possibly causing exaggerated grain growth.

Reconstructive transformations (e.g. the cubic (gamma) to hexagonal (alpha) transition in alumina) involve substantial changes in secondary coordination, and require bond breakage and reformation in a new structure. Reconstructive transformations require thermal activation to form critical nuclei in the parent phase. High temperature phases, therefore, can exist metastably at low temperatures, and even polymorphs that lack an equilibrium temperature range may exist (e.g. gamma alumina, or martensite in steel). Nucleation and growth rates for the new phase largely determine the effects of processing temperature and heating rate on the grain structure after a reconstructive transformation. Some reconstructive transformations have kinetically unfavorable orientational relationships with the parent phase that can constrain a growing grain within the properly oriented parent grain. Growth into adjacent grains is orientationally impeded, and other nucleation events are likely to occur before earlier nucleated grains grow through adjacent untransformed regions. In other cases, nucleation is the limiting kinetic factor, and grain growth is not confined within the parent grain.

The homogeneous nucleation rate for a reconstructive phase transformation, I, is given by[9]

$$I = I_o \exp\{-\Delta G_m/kT\} \exp\{-16\pi\gamma^3 T_o^2/3kT\Delta H_v^2(T_o-T)^2\},$$

where $I_o\exp\{-\Delta G_m/kt\}$ is the collision frequency of atoms at the interface, ΔG_m is the activation energy for transport across the nucleus matrix interface, γ is the interfacial energy, T_o and T are the respective equilibrium and actual transformation temperatures, and ΔH_v is the enthalpy change per unit volume for the transformation. The factor $\Delta H_v(T-T_o)/T_o$ is the approximate free energy change (this approximation is good when the heat capacities of the new and parent phase are close) and is the effective transformation driving force.

At low temperatures, the nucleation rate is nearly zero. As the temperature is raised, nucleation rate can increase dramatically. Near the transformation temperature, the driving force is low and nucleation rate is low. At low temperatures, growth rate can increase substantially as the temperature is raised; at high temperatures, growth rate is temperature independent. As the temperature of a highly undercooled phase is raised, the nucleation rate increases rapidly, and substantial nucleation will occur before growth. This transformation produces a uniform, fine-grained microstructure. Transformations with comparable nucleation and growth rates are expected during heating of moderately undercooled phases at lower temperatures, and will develop a wide grain size distribution. Finally low driving force reactions will have high relative growth rates compared to the nucleation rate and will develop coarse-grained microstructures. This final category often has the most deleterious affect during sintering; for example, the gamma to alpha transition in alumina falls in this category. High heating rates can lower the effective driving force in high driving force reactions, and

consequently produce coarse-grained material. Conversely, high heating rates, in certain low driving force transformations*, can enhance nucleation at constant growth rate, and consequently, reduce grain size.

Transformations in agglomerates occurring before interagglomerate neck growth simply modify the grain size distribution within the agglomerates. This does not substantially alter the sintering problem which still involves simultaneous intra- and interagglomerate sintering and grain growth, although it can change grain growth stability. Low driving force transformations without orientational constraints can convert a polycrystalline agglomerate into a porous single crystal (a similar process is shown schematically in **Figure 5a**) isolating fine porosity within agglomerates. Isolated intra-agglomerate pores, though, are expected to shrink rapidly in contrast to their interagglomerate counterparts.

In a low driving force reconstructive transformation with favorable (and conversely, kinetically unfavorable) growth orientations with respect to the parent phase, a nucleated grain is likely to consume the parent grain without encountering another growing crystallite; however, orientational constraints will prevent the growth from continuing into adjacent grains (**Figure 5b**). Slow nucleation will occur in until the transformation is complete. Displacive transformations in a low-symmetry parent phase can also convert single grains in the parent phase to single grains in the product phase since the number of crystallographically equivalent variants is low. These two types of transformations produce grain size distributions in the product phase

*These transformations have a low, effectively temperature independent, driving forces. These transformations are characteristic of metastable phases that have no effective equilibrium temperature range (T_o is infinite), but have a very small transformation enthalpy change.

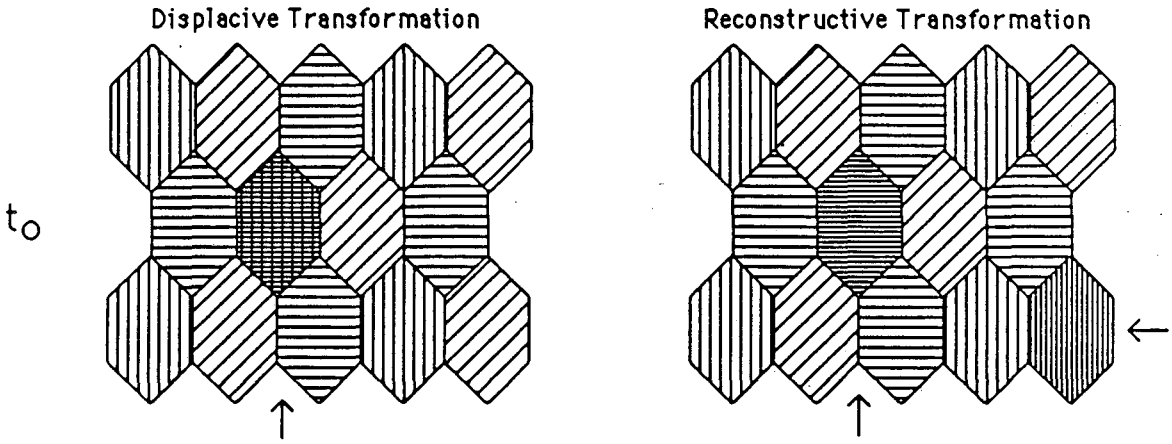

Displacive transformation produces new phase grains that are orientationally constrained to their parent grains

Reconstructive transformations can produce a new phase that is NOT orientationally constrained within its parent grains.

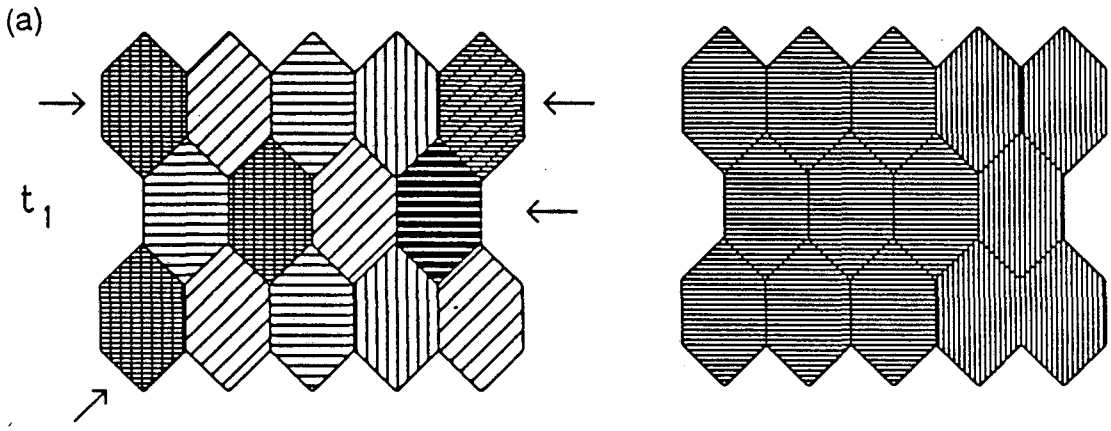

Subsequent transformations are also confined within parent grains

In the reconstructive transformation, the newly formed phase can grow rapidly. Grains of the growing phase can consume many adjacent untransformed grains before encountering another transformed grain.

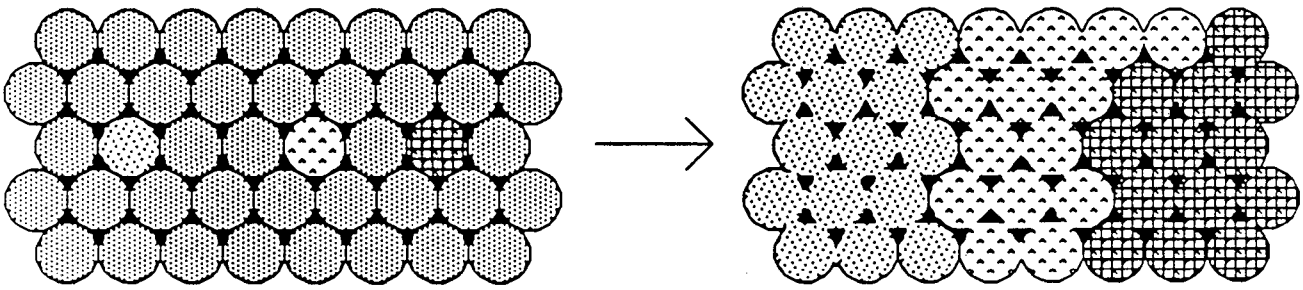

(b) Reconstructive phase transformations can dramatically change the pore/grain boundary structure. Here, a slow driving force reconstructive reaction produces a few transformed grains that grow rapidly through the surrounding matrix. This can isolate many intergranular pores within "vermicular" single grains. Such a structure is impossible to densify because intragranular pores are removed through lattice diffusion; the corresponding removal time is excessive compared to removal through the much faster grain boundary transport path.

Figure 5. Comparison of the grain structures before and after low driving force reconstructive and displacive phase transformations.

that are very similar to the grain size distribution in the parent phase since there is a one-to-one correspondence between parent and product grains.

The most serious possibility is that of low driving force reconstructive transformation without orientational constraints, schematically illustrated in **Figure 5c.** In this transformation, the new phase, once nucleated, can grow through many adjacent grains and particles before encountering another transformed grain. This occurs in the gamma-to-alpha transition during the sintering of the monosized alumina.[26] The result is an extremely large-grained vermicular structure which does not densify.[26] Seeding the phase change[31] or doping the powder may circumvent this problem. Low temperature sintering of agglomerates provides a path for rapidly growing grains of the new phase grains to cross through adjacent agglomerates at much lower temperatures than expected for agglomerate-sized particles. A bimodal pore size structure of vermicular grains, interagglomerate, and intra-agglomerate grains can result.

3.0 Experimental Method

3.1 Powder Synthesis

Monosized spherical TiO_2 powders were prepared by controlled hydrolysis of titanium tetraethoxide (Aldrich Chemical, Milwaukee, WI) in ethanol (as developed in refs. 22,23). The synthesis was performed in a controlled atmosphere glove box (#50004, Labconco, Kansas City, MO) with dry N_2 since ambient moisture can cause premature ethoxide hydrolysis. To ensure a dry environment, tank N_2 was dried in drierite columns (-100°F dew point column specification), open containers of drierite were placed in the glove box, and all glassware was dried overnight at 150°C before use.

Anhydrous ethanol was filtered through 0.2μm cellulose acetate membrane filters and divided into two equal portions. Based on the total ethanol volume, water and ethoxide were mixed into separate portions of filteredethanol to concentrations of 0.45 M and 0.15 M, respectively. These concentrations were selected because they represent the optimum of monodispersity and yield.[23] In contrast to the original procedure, 0.005g/cc (based on total ethanol volume) of the surfactant hydroxypropylcellulose (HPC, Aldrich Chemical) was dissolved in the ethoxide-containing ethanol portion to inhibit agglomeration.[62] Dissolution of the HPC at ambient temperature requires from 5-10 minutes with rapid agitation. This ethanol portion was refiltered through the membrane -- additional filtering of the water-containing portion was not required since both the water and ethanol were filtered before mixing. The two ethanol portions were rapidly mixed at ambient temperature with a magnetic stirrer for only three seconds -- longer times resulted in a higher percentage of agglomerates and poorly formed particles. The

onset of turbidity occurred 8-12 seconds after mixing. The contents were intermittently mixed at slow speed for an additional 10 minutes before removal from the glove box.

3.2 Powder Classification

After synthesis, a two-step centrifugal classification procedure was used to narrow the powder particle size distribution. In the first step, the ethanolic suspension produced in the powder synthesis reaction was briefly accelerated for three minutes at 3600 rpm (2800 g) to remove coarse material. This centrifuge cake, which was enriched in coarse particles, was discarded. After acceleration, approximately the top fifth (7 mm) of the suspension was clear, which indicates that 20% of the powder in the suspension had settled. This is the settling rate of the average particle size, and its value allows the separation to be estimated. Settling of submicron particles at mm/min rates occurs in the Stokes regime;[63] the settling rate for spheres is proportional to the square of their diameter. (Actually, drag is proportional to the hydrodynamic radius times the settling velocity, while the mass scales as the cube of the radius of gyration $r_g = V^{0.33}$; balancing forces results in $V_s = r_g^3 / r_h$.) Roughly, all particles with a diameter greater than 2.2 times the average diameter should end up in the cake because they settle at five times the rate of the average. Doublets, which have twice the mass of singlets, have nearly a singlet hydrodynamic radius -- since they minimize drag when they settle -- should settle at twice the rate of singlets and their concentration is reduced by 40%, but the amount relative to monosized particles is only reduced 20%. After the first centrifugation step, the remaining suspension was rehomogenized and subjected to another 15 min cycle to remove fine material. The

supernatant, which was enriched in fine material, was discarded. No further classification was performed.

The centrifuge cake obtained from the classification procedure was redispersed in basic (pH=10) NH_4OH solution (measured before powder dispersion) with an ultrasonic probe (#W-375, Heat Systems-Ultrasonics, Farmingdale, NY). Compaction with 15 minute centrifugation and redispersion at pH=10 was repeated five times to remove the remaining ethanol. The volume fraction of solid was adjusted in the final redispersion step. The suspensions served as the starting material for a variety of compact preparation techniques.

3.3 Compact Fabrication

3.3.1 Centrifugation

Centrifuge compacts were prepared from electrostatically stabilized aqueous suspensions with roughly 40 vol% solid loading (based on the volume of the centrifuge cakes). This concentration was estimated from the volume of the centrifuge cake before the final dispersion step. The pellets were compacted at 800 rpm for 24 hrs and then accelerated to 3600 rpm for 15 min in flat-bottomed polypropylene centrifuge tubes. After compaction, the cakes were dried in the centrifuge tubes at ambient conditions until they separated from the tube. The drying time varied from three days to a week. Tube-compact adhesion caused extensive cracking in pellets. After removal from the centrifuge tube, the compacts were stored in a dessicator with drierite dessicant.

3.3.2 Slip Casting

Two-piece plaster-of-paris molds were used to facilitate pellet removal. A two-piece mold was poured around a cylindrical form. The mold

halves were allowed to set for 24 hours. They were then soaked in distilled water to remove any unreacted material. The quality of the seam between the two mold halves proved to be a particularly difficult problem in this study. Excessive quantities of slip were frequently lost between the halves of poorly prepared molds. The mold preparation technique was never completely mastered.

Standard base-stabilized suspensions with 30-40% solids loading were used as slips for slip casting. The slips were poured into a two-part plaster-of-paris mold. Additional slip was added to maintain the fluid level at the top of the mold. Initially, extra slip additions were required frequently, but the period decreased to several hours after a few additions. When the mold cavity was filled with solid, the mold and entrained pellet were allowed to stand overnight. The compact was then removed from the mold and dried for 24 hours in a small cardboard box that was previously dampened to reduce the drying rate and prevent cracking. Following this, pellet were dried at ambient conditions for another day and was then stored in a dessicator.

3.3.3 Gravitational Sedimentation

The strongest compacts were obtained using this method. Samples were settled from a base-stabilized (pH=10) suspension with approximately 50% solids loading. The pH may decrease during settling due to NH_3 loss and CO_2 pickup, but this was not measured. No additional ammonia was added during settling. Settling in long tubes was abandoned in favor of settling in petri dishes to reduce the time needed to make compacts. The supernatant that formed at the top of the suspension was removed with a pipette every two or three days. When the thickness was too thin (<1mm) to remove without disturbing the opaque portion of the

suspension, the remaining liquid was allowed to evaporate, and the compact was dried at ambient conditions. These compacts required two to three weeks to prepare. Some cracking occurred, but it may be possible to eliminate this cracking by controlling the drying rate at the end of the settling period, and proper container material selection. The fragments were relatively large -- often around 1 cm^2 and slightly more than 0.1 cm thickness.

3.4 Sintering

All samples used in sintering studies, except those used in dilatometry, were slowly heated in air to 450°C and annealed for at least one hour before being subjected to high temperatures. The purpose of this low temperature treatment was to reduce the extent of cracking by removing volatile and combustible organics. Slow heating (~75°C/hr) through the 300°C to 450°C range corresponding to anatase crystallization (see section 4.2.3) was required to prevent excessive crumbling, especially in the less densely packed centrifuge and slip cast compacts. After this low temperature treatment, gravitationally settled compacts could be introduced directly into a hot furnace for isothermal studies; however compacts formed using the other two techniques could only be used in constant heating rate experiments.

Isothermal treatments at 800 and 1000°C were chosen to study the contribution of differently sized structural features within the monosized powder particles -- which should have different "sintering temperatures" -- to the densification of monosized powder compacts. These temperatures correspond to the sintering temperatures observed for fine TiO_2 (100-700Å) particles[23,47] and monosized spherical TiO_2 in the 0.2-0.45μm size

range, respectively. These sizes respectively correspond to the approximate substructure and particle size in the current study.

In the isothermal treatments, gravitational compacts were introduced directly into a furnace at temperature. Approximately 1200°C/hr heating rates (maximum furnace rate) from room temperature to 800°C or 1000°C were used to study sintering in centrifuge and slip cast compacts, which could not withstand the isothermal treatments without excessive crumbling. Although the heating periods are not included in descriptions of the overall sintering time of slip cast and centrifuge pellets, the 40 to 50 minute heatings represent a significant portion of the overall treatment time and are therefore considered implicit in the description. For example, a centrifuge pellet that has been treated for one hour at 1000°C has actually been heated at 1200°C/hr for 50 minutes to 1000°C, annealed for one hour and then removed from the hot furnace.

The extent of densification after treatments at various times and temperatures was assessed from SEM images of the compact surfaces. All compaction techniques produce very smooth surfaces that required no polishing after sintering. As-sintered grain boundary thermal etches produced good contrast in SEM images. Generally, the particle or grain size was below the resolution limit for optical microscopy. Time limitations prevented compact sectioning for microscopic study of the bulk structure of the sintered compacts. Surface morphology changes were considered representative because good agreement was obtained between surface observations and bulk measurements of shrinkage and porosity.

3.5 Characterization

3.5.1 Dilatometry

A horizontal loading dilatometer (Harrop, Columbus, OH) with aluminum oxide rams and boat was used for shrinkage studies under a 10g load at a 4°C/min (measured at the sample) heating rate. A 4°C/min heating rate was selected for comparison with Barringer's TGA-DTA data which was also collected with a 4°C/min ramp. Initially, slip cast compacts were used in these experiments, however overcoming apparatus difficulties required many samples. Therefore, slip cast compacts were abandoned in favor of the more easily prepared centrifuge compacts. As expected, cracks formed in centrifuge compacts, but the ram pressure prevented transverse cracks from forming; at the end of the dilatometry run, little material was lost from between the rams. Specimen-ram friction created transverse tensile stresses as the compact shrank and caused extensive cracking parallel to the pellet axis. However, these cracks should not affect the results since continuous material remained between the rams.

3.5.2 Mercury Porosimetry

Interparticle porosity in gravitationally settled powder compacts were measured on a scanning mercury porosimeter (Quantachrome, Syosset, NY). The mercury solid contact angle was taken as 140° and the surface tension of mercury of 480 ergs/cm^2 was used;[64] both were assumed to be pressure and curvature invariant. The specific porosity is the ratio of the intrusion volume to the compacts mass. The minimum pore size intruded was determined from the Washburn equation[65]

$$r = -(2\gamma\cos\theta)/P$$

where r is the pore radius, γ is the mercury surface tension, θ is the

contact angle, and P is the intrusion pressure. Although pore radii as small as 18Å are accessible at the 60 kpsia maximum apparatus pressure, mercury compression makes the results for small samples unreliable above 7500psia. With an accessible minimum pore radius of 240Å at 7500psia, all pores between 0.3-0.45μm particles were assumed to be intruded.

Surface areas were calculated by graphical integration of the penetration curves and compared with the BET data. The surface area, S, was estimated from[64]

$$S = F\ \{1/(\gamma\cos\theta)\cdot\int PdV\}$$

This equation assumes cylindrical pores open at each end, which is far from the actual pore geometry in the monosized powder compact. Thus, the factor, F, corrects for the actual compact geometry. The model used to calculate F is described in Appendix I.

3.5.3 SEM Imaging and Analysis

High resolution images were obtained on the high resolution stage of an ISI DS-130 SEM with a tungsten hairpin filament. The optimal accelerating voltage was about 25KV. Since the ceramic powder is non-conductive, SEM samples were coated for 2.5 minutes in a gold coater at a sputtering voltage of 20KV in a 40 millitorr vacuum.

The surface structure observed in the SEM should accurately reflect the true structure of rough surfaces. As surfaces smooth, however, the deposited gold layer becomes thicker and can conceal the finer structure of these surfaces. Low temperature (800°C) sintered compacts were coated for only 1.5 minutes to reduce the smoothing of the fine structure. Charging and local heating reduced the lifetime of illuminated areas and made high resolution imaging more difficult in the more thinly coated samples. High resolution image quality involves a degree of

luck; daily and even positional variation in image quality make structural comparison of different samples based on SEM images alone difficult and of dubious accuracy.

Particle size distributions were estimated directly from SEM images of compact surfaces. The estimate involved measurement of only a few particles (~100) selected at random. Computer aided image analysis was difficult and did not improve the qualitative estimates appreciably. Some size distribution biasing may result from settling rate disparities between differently sized and shaped particles. Porosity was estimated from SEM micrographs of compact surfaces using a line intercept method: the fraction a line, drawn across low magnification micrographs of compact surfaces, intersecting pores is to a first approximation, the pore volume fraction.[66] To ensure representative sampling, micrographs were used that contained at least 50 distinct pores.[66]

3.5.4 Chemical Analysis

Semiquantitative metal oxide impurity content was measured with plasma emission spectroscopy (American Spectographic, San Francisco, CA). Powders from the slip cast and centrifuge compacts used in the study of the polymorph transformation kinetics were used in the semiquantitative chemical analysis. Temperature scanned mass spectrometry (Mass Spectrometry Laboratory, Dept. of Chemistry, U.C.B) was used to identify the material expelled from powder during low temperature heating. The maximum temperature was 370°C. The signal of a particular species (water at MW 18, for example) is proportional to the pressure of the species in the heating chamber. Large signals indicate that a copious amount of a particular material is being evolved. Since the residence time in the mass spectrometer system is small compared to the

measurement time, a persistent high signal indicates the powder is evolving material at a relatively high rate, while a low signal indicates a low rate.

3.5.5 Surface Area Measurement

Powder surface areas were determined from N_2 gas adsorption data using the single point BET technique.[67] An adsorption gas of 30% N_2 in He was used for the single point measurement following the procedure of the adsorption system manufacturer (Quantachrome).[68] Samples were outgassed for 24 hours under flowing N_2 at ambient temperature (~25°C) before measurement. This treatment removes most physically adsorbed water, however chemically adsorbed water remains.[69]

The thermal evolution of surface area was followed on a single powder sample so changes in absolute area could be determined. The room temperature surface area of this powder was measured using the standard technique. The powder was subsequently annealed at 250°C for one hour while still in the adsorption tube. The standard outgassing and measurement procedure were then followed. Surface area measurements were repeated after 350°C and 450°C anneals. The tube material (i.e. glass) limited the maximum temperature in these measurements.

3.5.6 X-ray Diffraction

X-ray powder diffraction was performed on a Siemens diffractometer with a copper anode was used for polymorph identification, qualitative polymorph volume fraction measurements, and x-ray line broadening measurements of crystal growth. Standard collimators were usually used; narrow collimators were used to reduce instrumental broadening in x-ray line broadening measurement. After annealing at the desired temperatures for specified times, powder samples were ground with a silica mortar and

pestle. A line of the powder was spread on a quartz holder with a thin layer of petroleum jelly as an adherent.

X-ray line broadening of the primary anatase and rutile peaks was used to determine qualitative anatase and rutile crystal sizes from the Sherrer formula.[70] Crystallite growth was studied using both isothermal and constant heating rate heat treatments. Instrumental broadening was not assessed, but instrumental broadening results in a systematic underestimation of the grain size that is more serious at larger grain sizes. Crystallization and polymorph transformation kinetics were also investigated with isothermal and constant heating rate treatments. Semiquantitative rutile volume fractions were estimated as the ratio of the integrated intensity of the primary rutile peak and the sum of the integrated intensities of the primary anatase and rutile peaks

$$V_r = P_r/(P_r + P_a)$$

where the r and a subscripts denote the rutile and anatase polymorphs, respectively, V_r is the rutile volume fraction, and P is the integrated intensity of the primary peaks.

4.0 Results and Discussion

4.1 Synthesis and Compaction of Monosized Titania

4.1.1 Formation of Monosized "Particles"

Particle agglomeration is usually associated with highly heterogeneous, porous structures. Formation of monosized agglomerates is not expected, and monosized growth techniques seek to avoid agglomeration. Ideal monosized particle formation requires that nucleation from a supercritical solution occurs rapidly, without nuclei coalescence during subsequent growth.[71] In contrast, a possible formation mechanism for monosized agglomerates has rapid nucleation and growth that produces a suspension of ultrafine particles. These fine particles subsequently coalesce into monosized agglomerate structures. Either a kinetic limitation prevents coalescence on large agglomerates and results in essentially monosized agglomerates at the limiting size, or in a physical analog to the chemical process, nucleation and growth of monosized agglomerates proceeds from a "critical suspension" of fine primary particles. Rearrangement of primary units into more densely packed configurations during agglomeration would increase agglomerate stability. These two monosized agglomerate growth mechanisms of monosized agglomerates are discussed in greater detail in Appendix II.

The effect of reactant concentrations and synthesis conditions on particle size, size distribution and yield is discussed elsewhere.[23] Particle size measurements on compact surfaces yield average particle sizes between 0.33 and 0.37μm, and are in excellent agreement with the reported sizes for the same synthesis conditions[23,62]. Little batch-to-batch variation is evident in the average particle size or size distributions. Prereaction was a persistent problem before adequate care was

taken to ensure a dry glove box atmosphere. "Prereacted" powders are nominally monosized, however, they contain a higher fraction of fine and large, irregularly shaped particles. Only non-prereacted powders were used in sintering and morphology evolution studies.

4.1.2 Incorporation of Impurities During Handling

Semiquantitative chemical analysis data are presented below:

Table I. Semi-quantitative Spectrographic Analysis for Monosized Titania, reported as oxides

	Centrifuge Compact	Slip-Cast Compact
Ti	Principal Const.	Principal Const.
Al	0.03%	0.04%
Si	0.02	0.05
Ca	0.003	0.35
Mg	<.002	.01
Sr	<.003	<.003
Cu	<.002	<.002

Since these data were obtained from powder compacts after several processing steps, the data reflect impurities incorporated in handling and compaction. An interesting feature is the large amount of calcium acquired from the slip cast mold. At the slip conditions, the powder has a negative surface charge[23] which will enrich the calcium concentration adjacent to the solid surface. Specific adsorption (adsorption on the solid surface due to short-range physical forces) of alkaline earths on rutile[53] and of Ba^{2+} on amorphous, monosized TiO_2[22] at basic pH, indicates calcium also specifically adsorbs at basic conditions. Acidic slip conditions can reduce the susceptibility of monosized titania to alkaline earth contamination.

High surface area monosized TiO_2 powders are potentially useful ion exchange media or wet catalysts, but the same properties that make TiO_2 useful in these services makes careful handling essential to ensure

success in sintering. Specific adsorption can adversely affect suspension quality and consequently the green compact quality and subsequent sintering behavior. Furthermore, calcium and other contaminants[41-45] affect the anatase grain growth, and the anatase-rutile polymorphic transformation (this is discussed later). Surface adsorption data suggest suspension stabilization at acidic conditions may reduce contamination susceptibility.

Silicon and aluminum are most likely leached from glassware. Substitution of plastic for glass container material should reduce these impurities. Other sources of contamination include refractory insulation in the annealing furnace and ambient dust.

4.1.3 Compact Fabrication From Aqueous Suspensions

Conditions that may cause heterogeneous compacts, cracking, or introduce impurities are important because they can degrade the sintering characteristics of a powder. A crack or large heterogeneity in the powder compact is likely to be a feature of the sintered microstructure regardless of the sintering performance of the powder. The particle morphology is an important factor in the compaction method because it influences particle interactions which affect particle suspension rheology, stability, and ultimately the compact density. Careful attention to compaction can enhance powder compact densification kinetics, while carelessness can ruin a good powder. These three types of powder compacts had significant <u>but</u> <u>reproducible</u> differences in their sintering behavior. A brief discussion of the characteristics of the three compaction techniques use in this study is appropriate before sintering and "particle" structure are discussed.

4.1.3.1 Centrifugation

This method enables the rapid preparation of pellets for subsequent sintering studies. A centrifuge compact surface is shown in **Figure 6.** Packing is moderately dense, but exhibits considerable variation in packing efficiency. These pellets are the least densely packed of the three compact preparation methods discussed. The rough particle surface and the rapid settling rate cause significant interparticle friction and prevents formation of densely packed, ordered arrays even if the suspension is correctly stabilized to prevent flocculation. Coating particles surfaces with low viscosity resins to reduce roughness and reduce interparticle friction may improve centrifuge compact quality. The lower density and packing consistency make centrifuge compacts more prone to cracking. This cracking can be minimized by reducing compact-container adhesion with additives and/or alternate container materials, as well as by cautious handling.

4.1.3.2 Slip Casting

Slip casting produces denser compacts and makes possible the production of more complex shapes. A slip cast compact surface is shown in **Figure 7.** The packing is somewhat better than in centrifuge compacts: packing flaws are smaller, packing uniformity is greater, and even some regions are present that have close packing of particles. The compact can be classified as disordered with some short-range six-fold coordination.

The plaster mold is a source of calcium. The suspension is stabilized against particle flocculation at pH=10 with NH_4OH. Calcium ions can detrimentally affect the slip properties. At this pH, the particles have negatively charged surfaces. Calcium, which is a divalent cation,

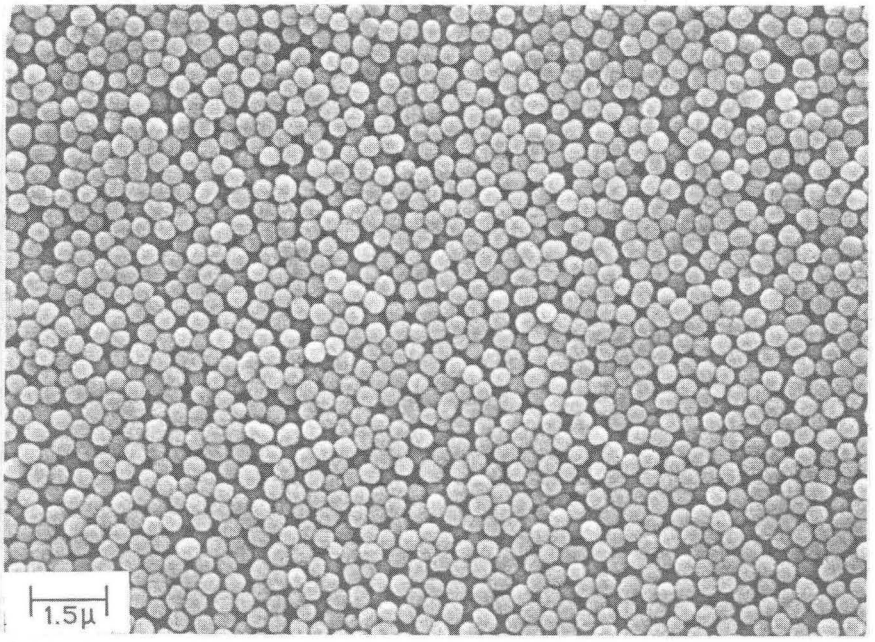

Figure 6. SEM micrograph from the top surface of a centrifugally compacted pellet. Particle packing efficiency is <55%. The average particle diameter is ≈0.35μm.

XBB 864-3352A

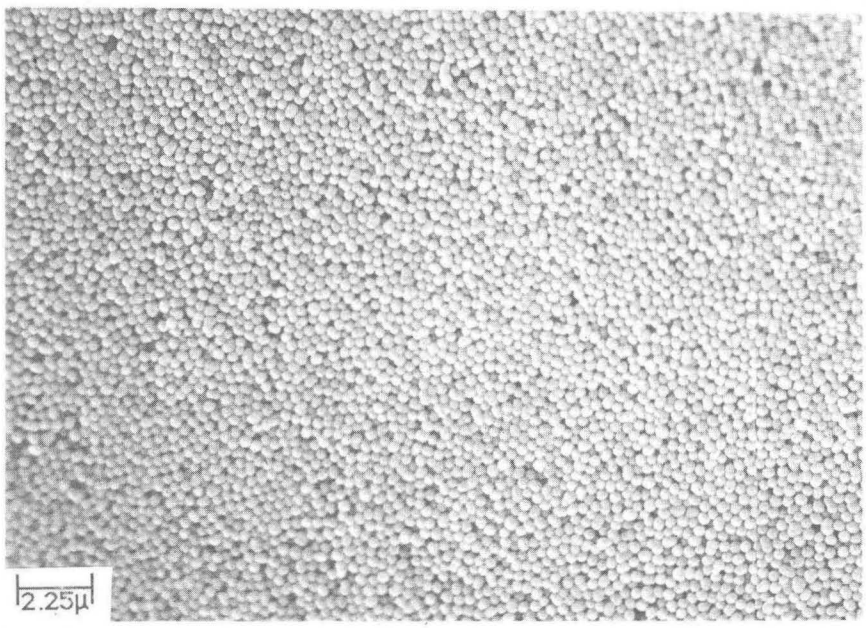

Figure 7. SEM micrograph from the top surface of a slip-cast compact. Some close-packed areas are evident, but packing is largely disordered. Average particle size is ≈0.35μm.

XBB 8612-9982

segregates to particle surfaces and screens the negative surface charge. This screening lowers the particle-particle repulsion (see Appendix II), allowing particles to flocculate (stick) in open, irregular structures that do not pack well. Specific adsorption of a counter ion (e.g Ca^{2+} on titania at basic conditions), enhances ionic flocculation strength; specific adsorption of Ba^{2+}, for example, destabilizes monosized TiO_2 suspensions at are normally stabilizing conditions,[23] and can cause surface charge reversal (negative to positive) at high enough concentrations.[23]

Calcium must diffuse against the water leaving the compact and entering the mold, and the extent of calcium intrusion will depend on the water removal rate. In a slip-cast cylinder, for example, there will be a radially increasing calcium concentration from the compact axis to the mold surface. Variation in calcium concentration with depth changes powder flocculation rate, which causes the packing density and uniformity to vary. Since packing density directly affects sintering rate, calcium may indirectly cause nonuniform shrinkage, prevent complete densification, promote cracking, and produce nonuniform properties in the densified material.

4.1.3.3 Gravitational Sedimentation

This method produces the most densely packed compacts of the three methods explored. Small ordered domains (with both six- and four-fold coordination) are evident in the SEM micrograph from a gravitational compact surface in **Figure 8.** Interdomain regions are also well packed, with voids rarely exceeding particle dimensions. A small fraction of doublet and large, poorly shaped particles apparently prevent the development of long-range order in the compact. The irregular particles

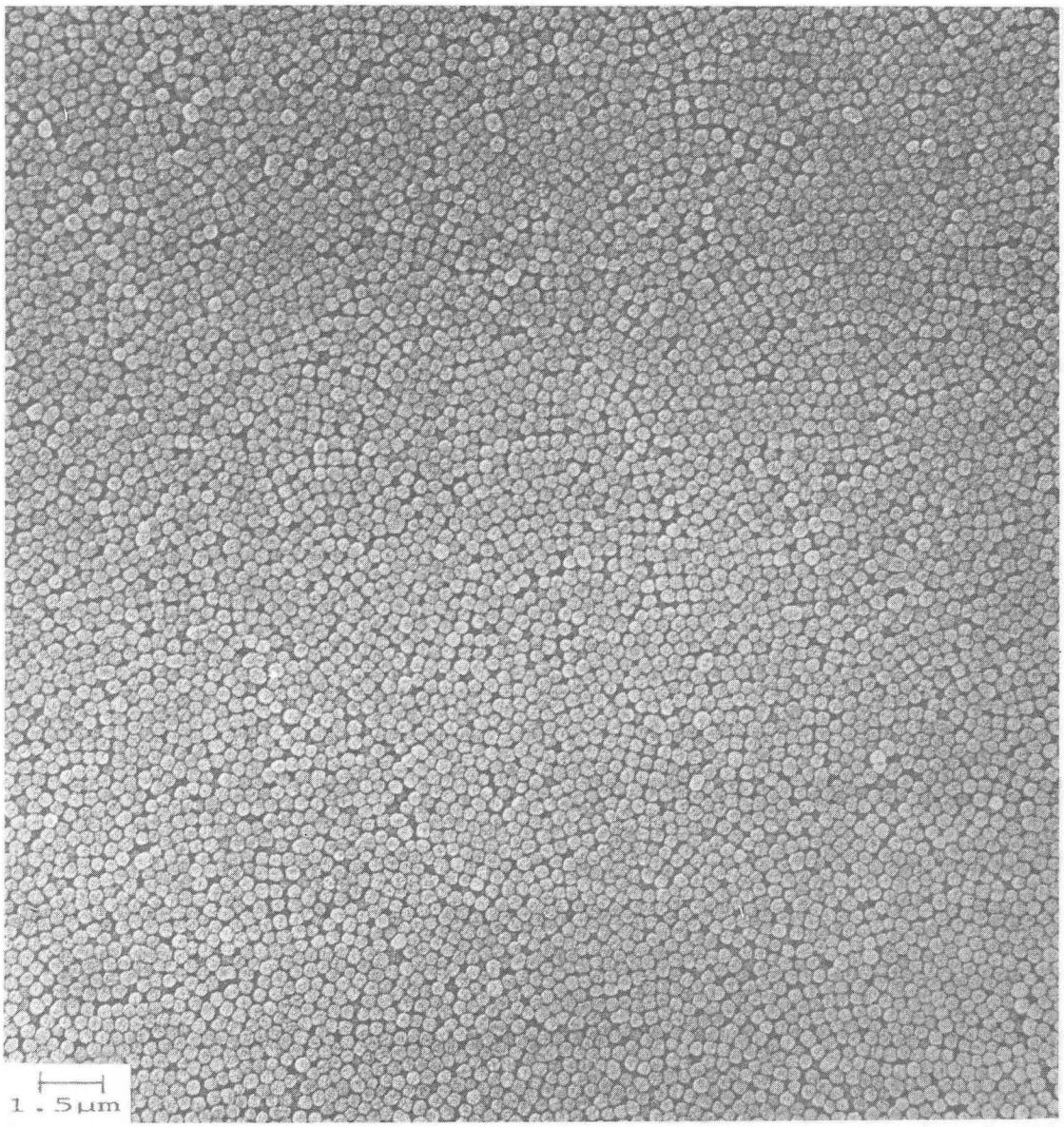

Figure 8. SEM micrograph from the top surface of a compact gravitationally settled from an electrostatically stabilized (pH 10 ammonium hydroxide) aqueous suspension. Six-fold and four-fold two-dimensional ordered domains are evident. The packing efficiency exceeds 65%. (Compare with 74% for FCC).

XBB 8612-9983

cannot be easily accommodated in an ordered structure; doublets are somewhat easier because they can occupy a pair of adjacent sites without introducing much distortion into the packing arrangement. Offending particles can disrupt packing several particle diameters distant. If a compact of nearly monosized particles contains, perhaps, as little as approximately 2% irregular particles in a uniform dispersion throughout the compact, long-range ordering may not occur. To prevent ordering these irregular particles would have to disrupt packing at distances on the order of their mean separation (this is less than five particle diameters for a 2% concentration of irregular particles).

The shapes that can be produced using this compaction method are limited; vertical sections are possible, but difficult. The settling time is excessive: weeks are required to settle thin layers. Upon drying, the compacts crack due to excessive friction with the container. Alternate container materials with less friction and slower drying rates can alleviate this problem. The fragments that remain after drying show much greater resistance to further crumbling during heat treatment than compacts produced by the other methods. Gravitational compacts, probably are more durable because of their greater packing density.

4.2 Sintering of "Monosized" Powder

4.2.1 SEM Observations

Preliminary observation of the sintering behavior of monosized TiO_2 compacts at 1000°C (**Figures 9a,b, 10a,b**) does not indicate any manifestation of internal agglomerate structure in the sintered microstructure. Individual particles in unfired gravitational and centrifuge compacts (**Figures 6 and 8**, respectively) produce single grains during sintering (**Figures 10a and 11a,b**). After one hour at 1000°C, the

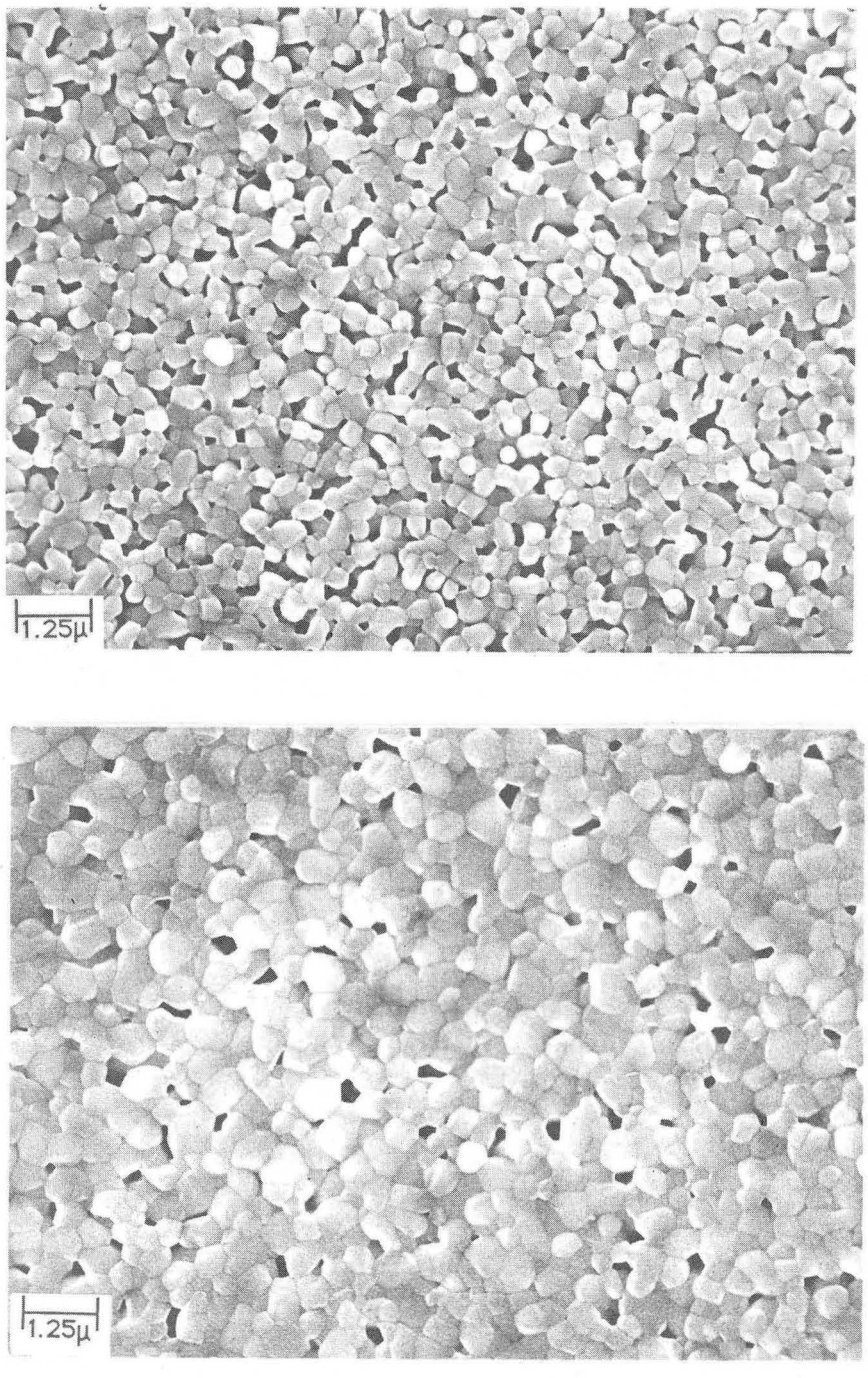

Figure 9. Top surface of a centrifuge compact after sintering in air at 1000°C. (a) After 1 hr, compact is approximately 91% dense with a grain size of about 0.5μm. (b) After 2 hr, density is around 96% of theoretical and the grain size is 0.7μm. Large pores in (b) are probably the result of large packing flaws in the green compact; Ostwald ripening initially causes large pores to grow until the final sintering stages.

XBB 8612-9984

(a)

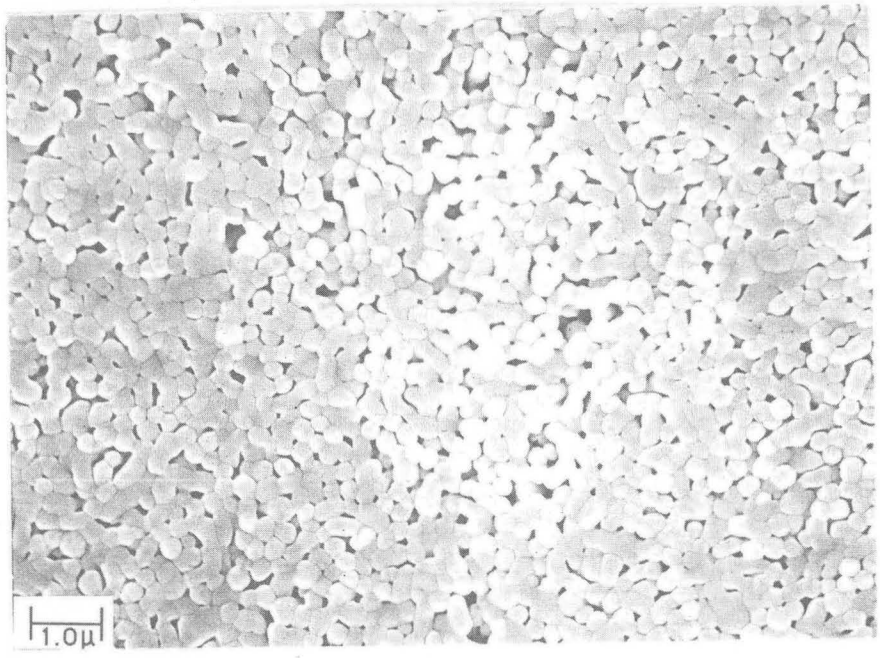

(b)

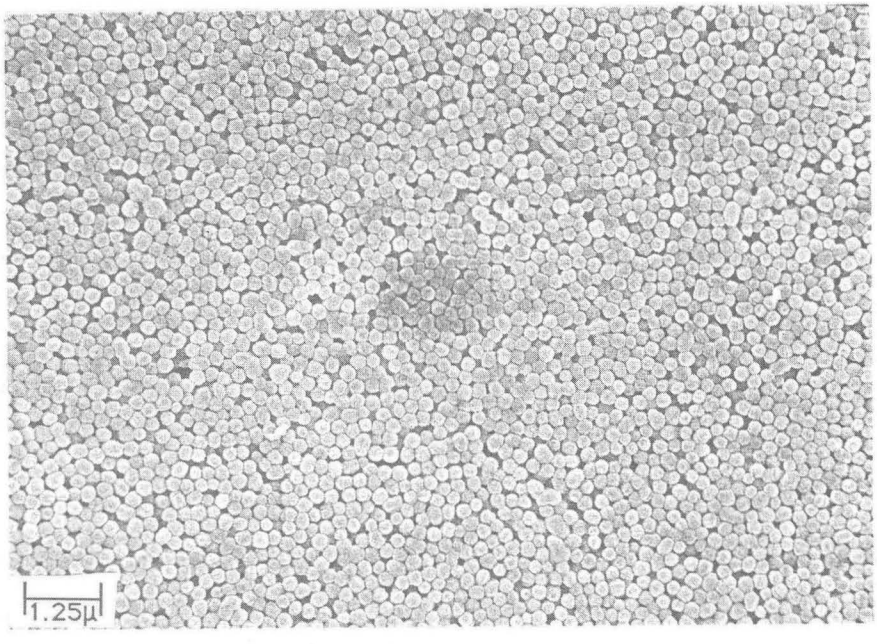

Figure 10. Gravitational compact surfaces after sintering in air at 1000°C for 1 hr. Compact (a) 95% dense (the central region is about twice the porosity of the outer portions). Grain size is about 0.5μm. (N.B. magnification is 25% greater than Fig. 9.) (b) Compact is near 94% density, but ordered domains are >98% of theoretical. (This is more clearly evident at higher magnifications.) The grain size is **less** than the 0.35μm original particle size.

XBB 8612-9985

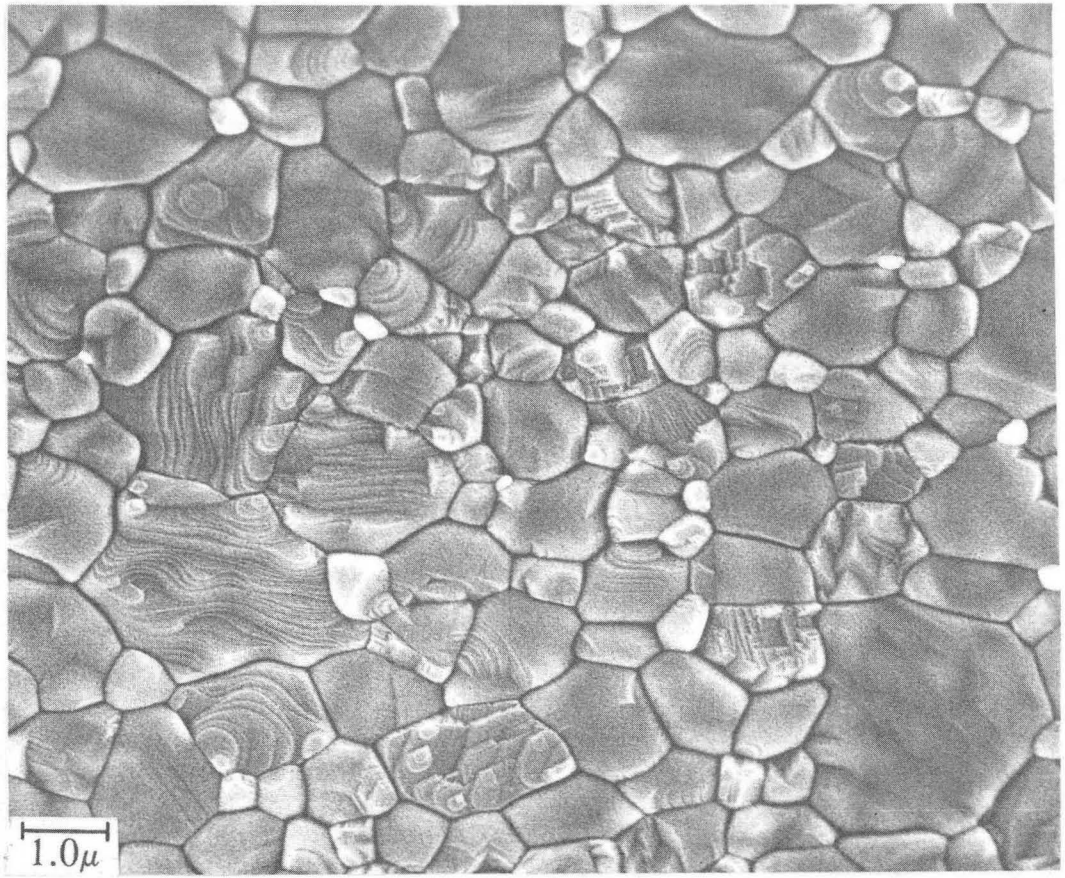

Figure 11. Theoretically dense centrifugal compact produced after approximately 4 hrs at 1000°C. The grain size is about 1.9μm or ≥5 times the original particle size.

XBB 8612-9986

densities of the more uniformly packed gravitational compacts (**Figure 10a,b**) exceeds the density of the slip cast compact after one and almost two hours of sintering (**Figures 9a,b**). In addition, the grain size in both **10a and b** is considerably smaller than in **9b**. The uniformity and density of the unfired compact microstructure, as expected, has a significant influence on densification kinetics and structural evolution. Compacts displaying greater packing uniformity have superior densification properties to the less homogeneous compacts.

The unfired gravitational compact (I) (**Figure 8**)-- with few voids larger than particle dimensions and extensive short-range order -- is considerably more uniform than the centrifuge cast compact (II) (**Figure 7**), which has a largely disordered structure with considerable variation in packing uniformity. **Figures 9a and b** suggest large packing flaws persist in the sintered microstructure. Approximately 4 hours are required to sinter centrifuge compacts to full density, and the grain size in **Figure 11** is approximately six times the original particle size. The relative densities and corresponding grain sizes for the centrifuge compact conform to the grain growth trajectory (after ref. 23) in **Figure 12** for disordered monosized titania compacts.

The gravitational compacts in **Figures 10a,b** have sintered so that a uniform distribution of fine pores remain in a fine grained matrix. The gravitational compact in **Figure 10a** has a grain size that falls on the trajectory of ordered TiO_2 compacts[23] in **Figure 12.** Significant grain growth is not expected to occur before relative density exceeds approximately 90%. However, higher magnification in **Figure 13a** readily shows a significant number of grains that have grown through several adjacent particles before, apparently, being arrested at interparticle necks. This is the microstructure that is expected to result from incremental

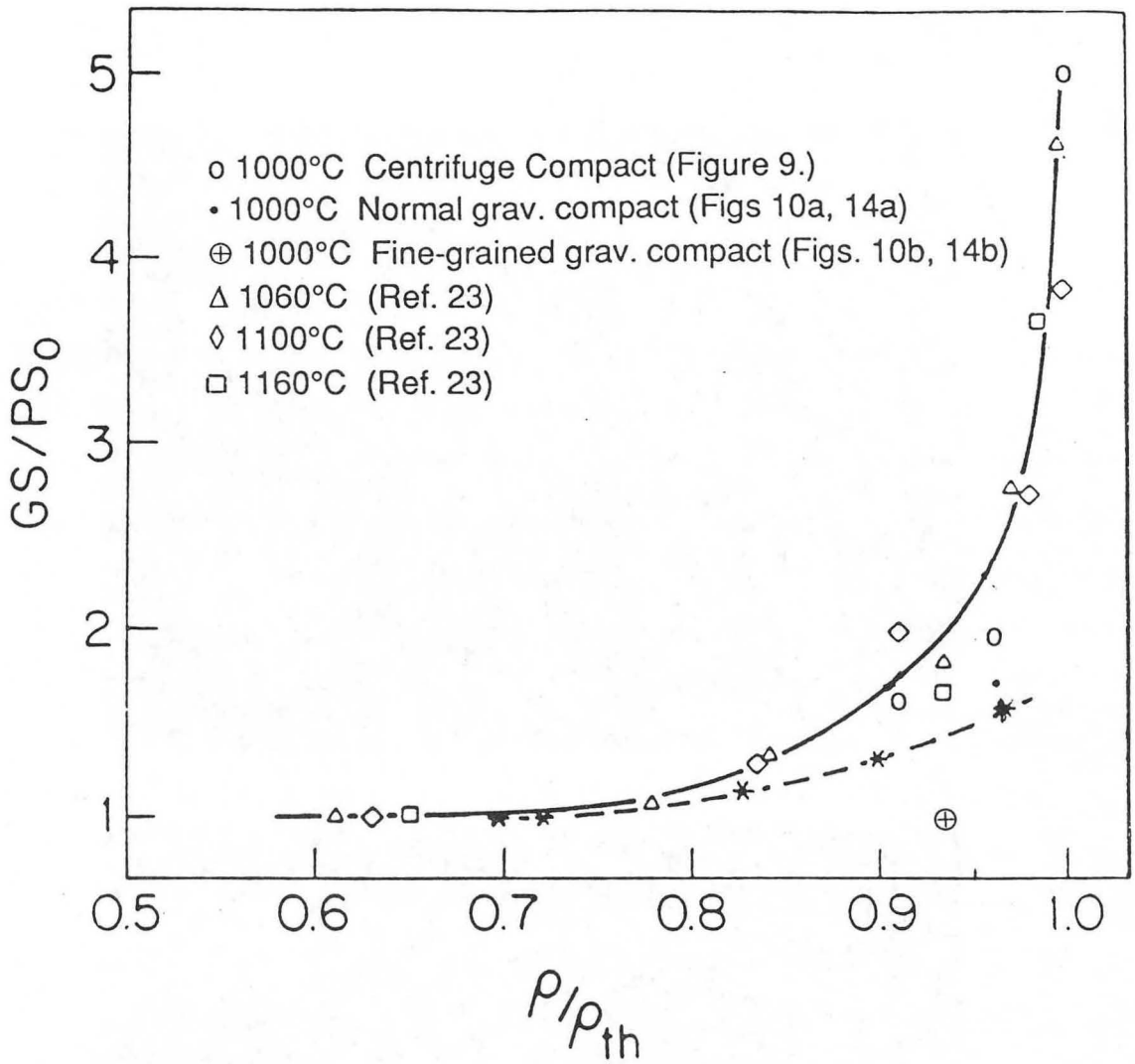

Figure 12. The approximate grain size as a function of relative compact density. Barringer's data for ordered compacts (-*-) corresponds to nearly ordered gravitational compacts in the current study. Dense, uniform packing in Barringer's study (——) corresponds to centrifuge and slip cast compacts. GS refers to the average grain size, and PS_0 is the initial particle size (≈0.35μm). Grain size trajectories after ref. 23.

-- XBL 871-175 --

(a)

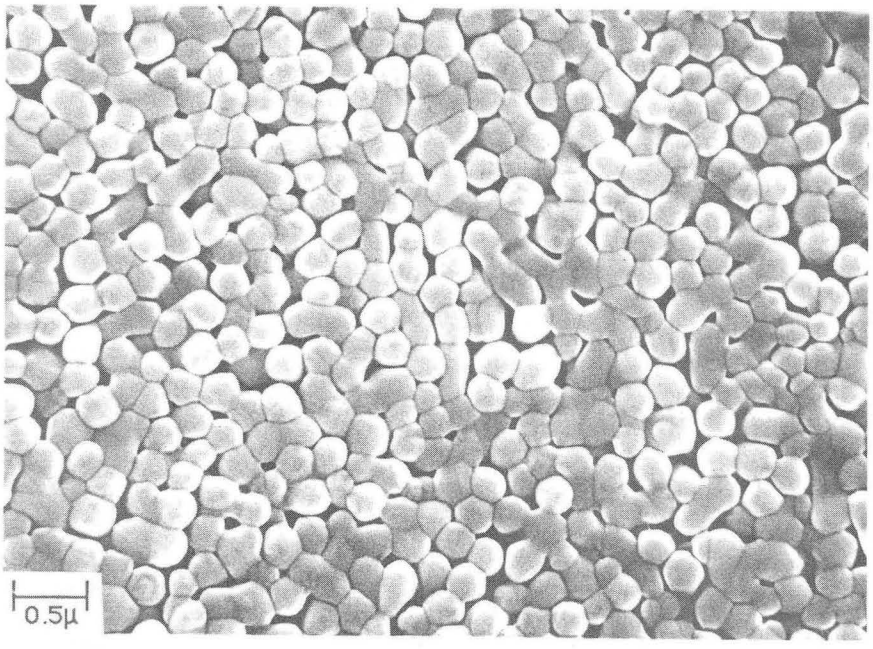

(b)

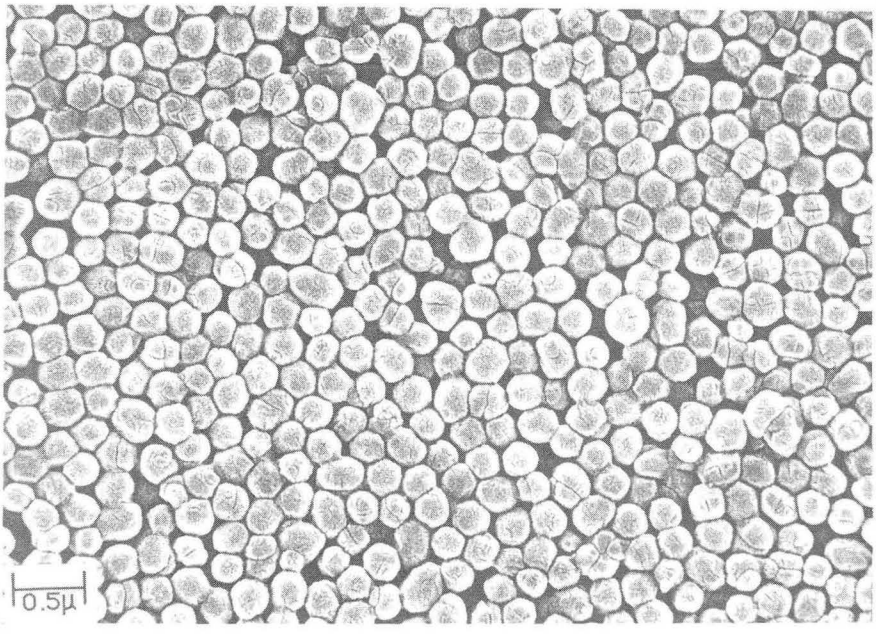

Figure 13. Higher magnification images of the sintered gravitational compact showing the grain structure differences more clearly. (a) Some grains have grown through several adjacent particles, while in (b), grain boundaries are pinned at interparticle necks.

XBB 8612-9987

grain growth (see sec. 2.2) between polycrystalline particles in early sintering stages.

In contrast, the grain size in **Figure 10b** falls below(!) the trajectory of even ordered compacts. No grains are evident in the higher magnification image (**Figure 13b**) that have crossed into adjacent grains. In fact, some ordered regions have sintered to full density and have formed ideal hexagonal grains. This grain structure is desirable because it should be very resistant to grain growth even in dense materials, and it is a useful model system as well.

The difference in the grain structure development in two apparently identical gravitational compacts is possibly due to a differences in the relative intraparticle grain growth and interparticle neck growth rates between the two samples. The initial grain growth rate in the sample that lacks "transparticle" grains may be sufficiently rapid to maintain a grain size that is always larger than the interparticle necks. In this case, grains can never cross an interparticle neck in an incremental growth process, and all coarsening is confined to the parent grain. The explanation for the existence of both grain structures assumes the powder particles, initially, are polycrystalline. However, more detailed description of the particle infrastructure and structural evolution are necessary before more definite conclusions are possible. Reproducing these microstructures was somewhat difficult; the relative rates of intra-agglomerate sintering and grain growth and interagglomerate neck growth are possibly sensitive to trace impurities and/or subtle morphological differences between batches.

Closer inspection of the gravitational compact in **Figures 14a** and **b** show grain boundaries **within** individual powder particles. This proves there is not a one-to-one correspondence between the grain size and

(a)

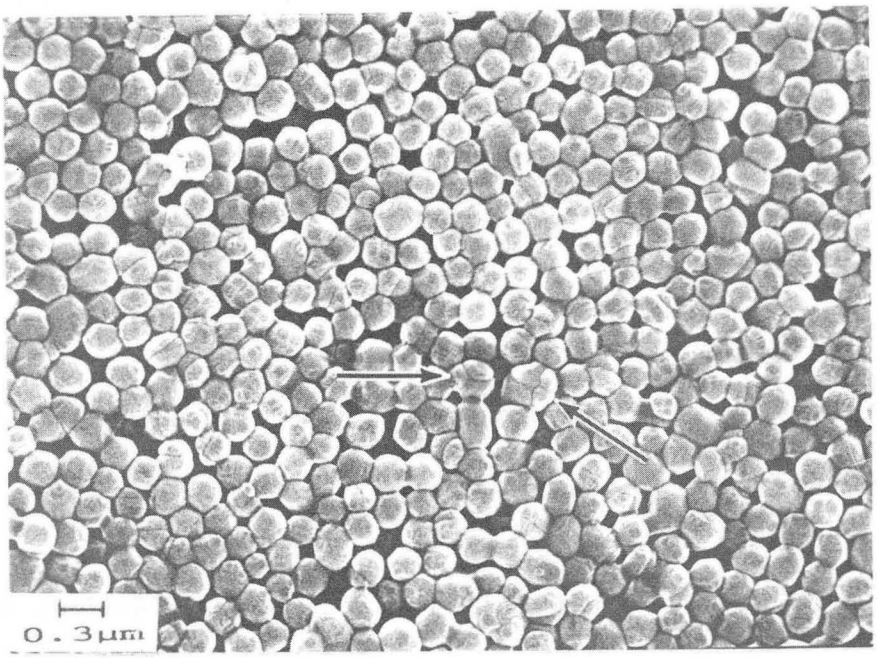

(b)

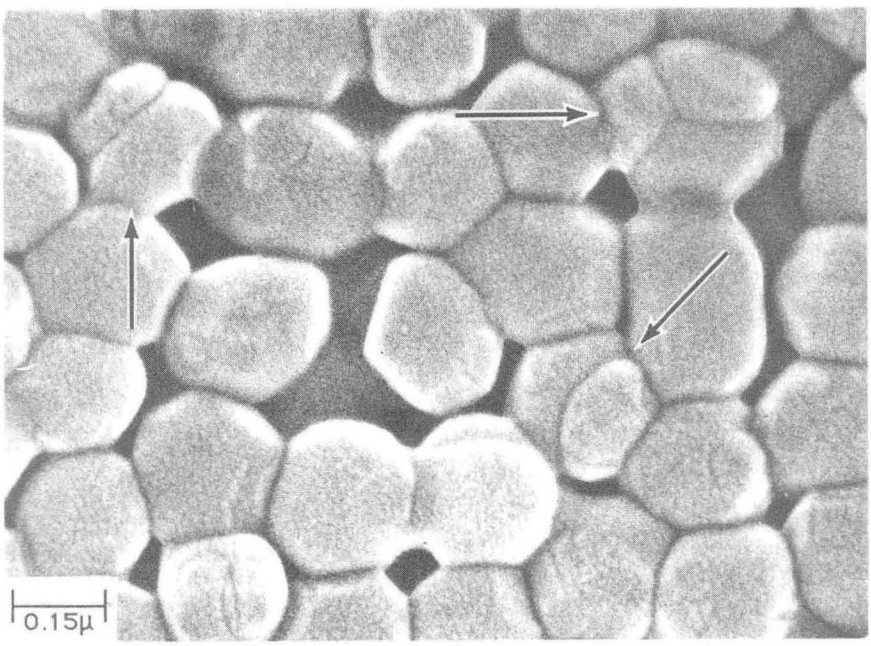

Figure 14. High magnification images of "ideal" grain structure clearly show grain boundaries within former "particles." Arrows in (a) point at a three- and a four-grained particle in the center-right portion of the micrograph. (b) Two- and three-grain particles are easily seen. Treatment: 1000°C for 1 hr.

XBB 8612-9988

apparent particle size. It also indicates that the initial grain size is smaller than the initial particle size. Phase transformations, though, may change an initial grain structure in which the grain size corresponds to the particle size into one in which the grains are smaller than the particle size.

There is a significant increase in mechanical strength after as little as 10 min treatment at 800°C. For this increase to occur, a substantial number of interparticle necks must have formed. **Figure 15a** shows interparticle bridging, after 1 hr at 800°C, to the extent that little of the original "particle" identity remains. **Figure 15b** compares structural development at 1000°C. Interestingly, the apparent grain sizes in **Figure 15a** are much smaller than the original 0.35μm apparent particle size, but are similar to the feature size in high resolution micrographs of prefired particle surfaces shown in **Figures 16a,b.** Apparently, structural units near 100Å scale are participating in a low temperature sintering process. Other ultrafine (particle size 0 n) TiO_2 powders[23,28-29,47] show extensive sintering at 800°C. The low temperature sintered microstructure indicates that structural units much smaller than the apparent particles are participating in sintering, and indicates assumptions of ideal particle structure (non-porous, single crystal) are not accurate.

4.2.2 Dilatometry

The total shrinkage of a monosized compact provides additional evidence that "particle" infrastructure is a significant consideration in monosized TiO_2 sintering. The dilatometry plot in **Figure 17** shows 50% linear shrinkage (>87% volume shrinkage!) in sintering a centrifuge compact to theoretical density. Using the 3.1g/cc as-prepared particle

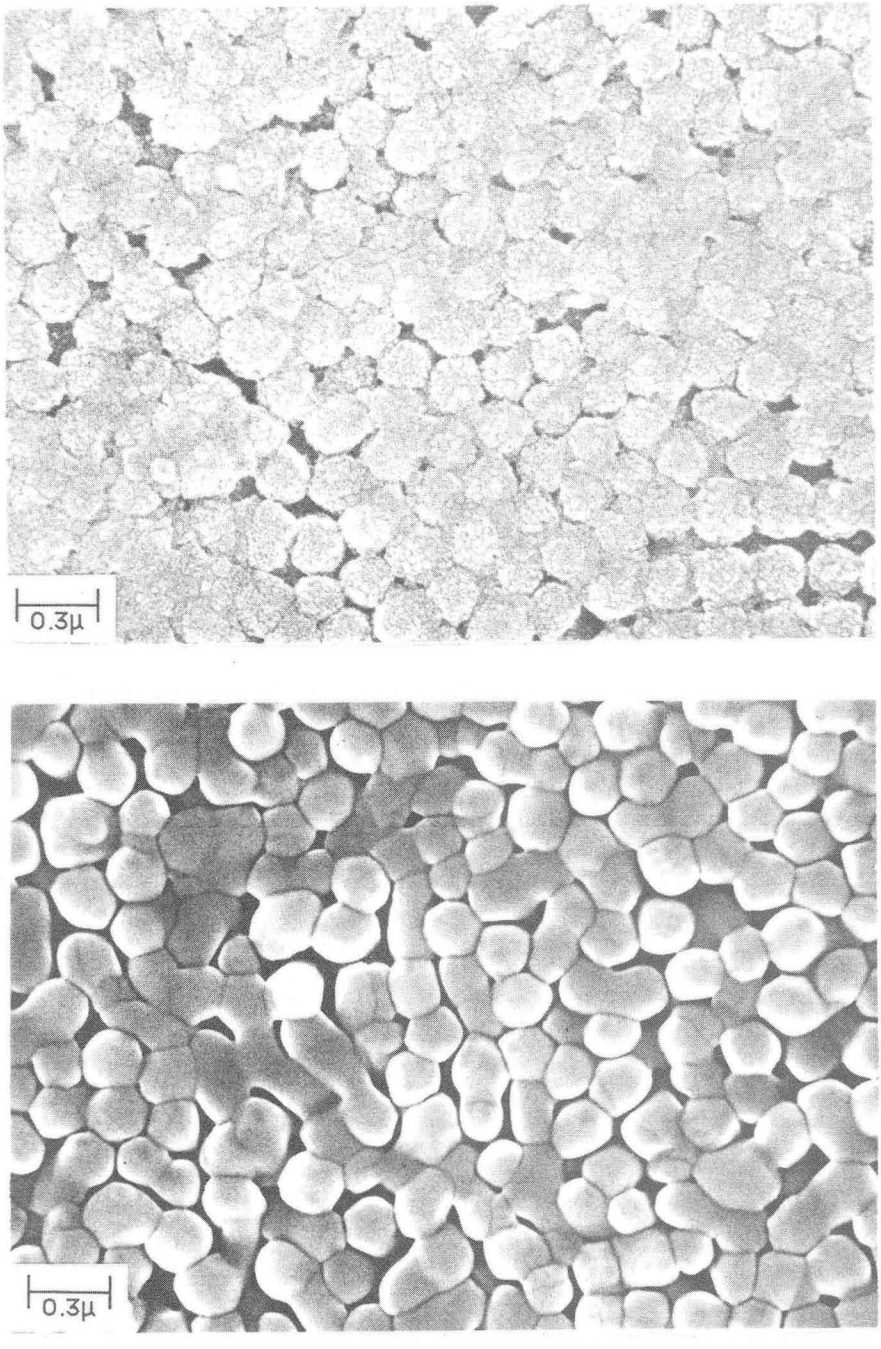

Figure 15. Comparison of the sintering behaviour of a gravitational compact after 1 hr at (a) 800°C, and (b) 1000°C. Sintering in (a) is on the scale of much finer structural units than what is expected for 0.3μm, single-crystal particles. (b) For comparison, "normal" sintering at the higher temperature is shown.

(a)

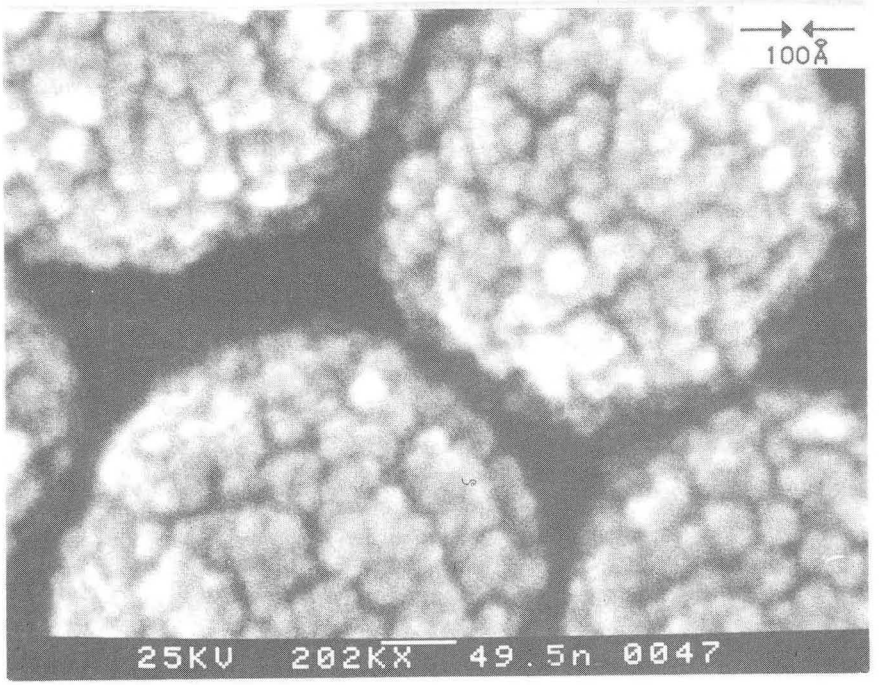

(b)

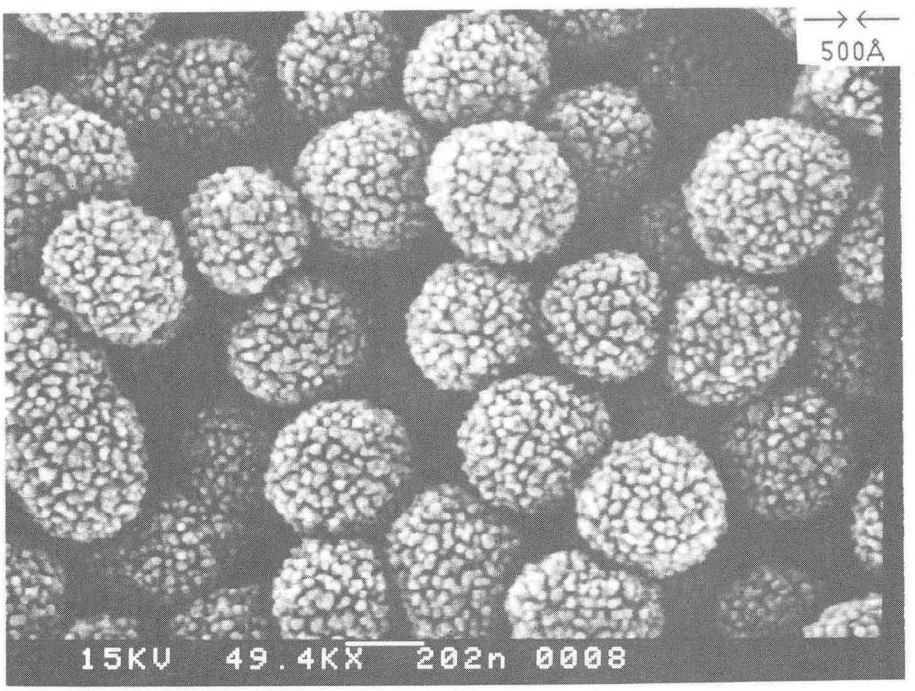

Fig 16. High resolution SEM micrographs of monosized titania particles suggest the "particles" are composed of much finer particulates. Features smaller than 100Å are visible in (a). (b) is from a different powder batch; both particle size and particle morphology are nearly identical.

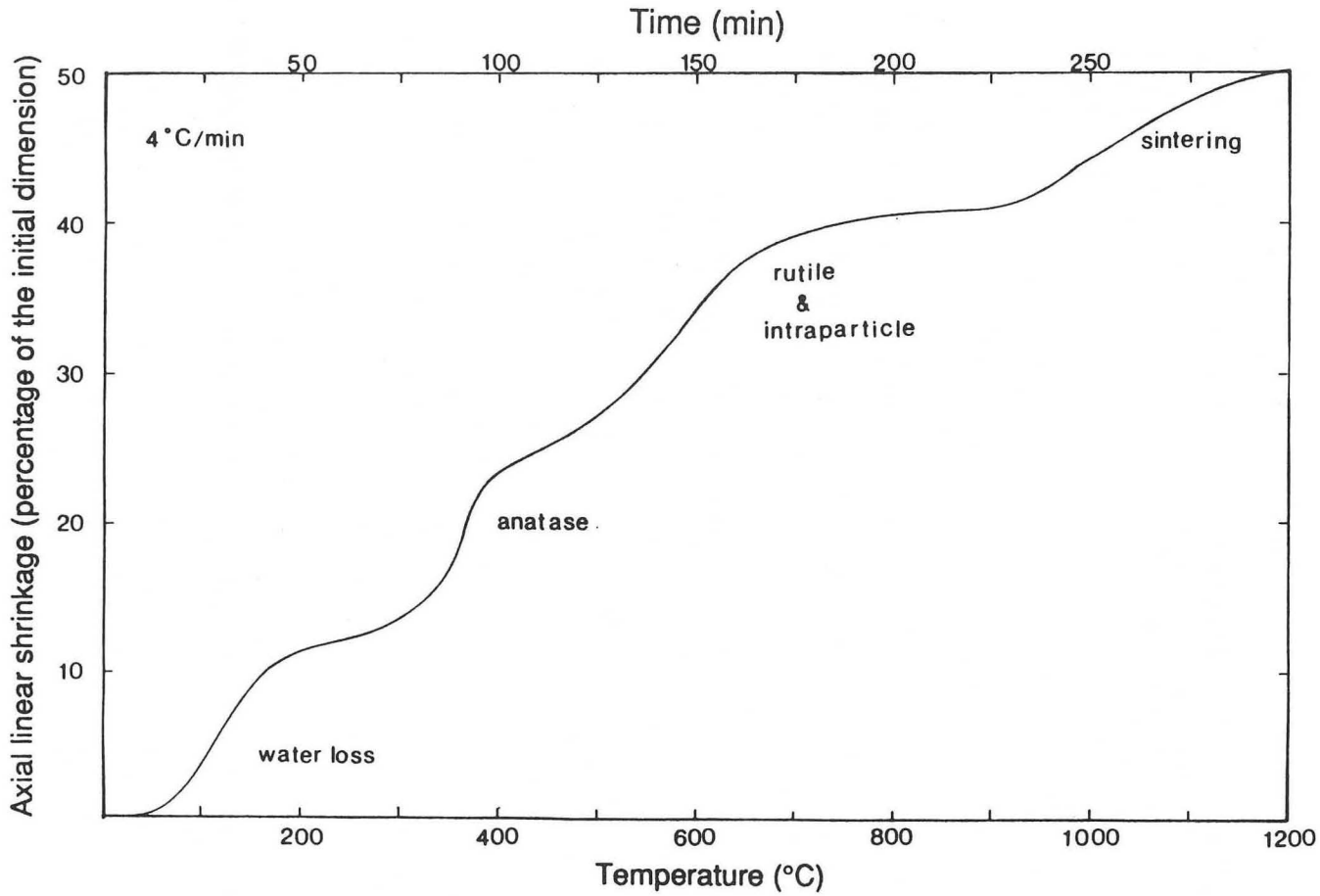

Figure 17. Constant heating rate shrinkage of a centrifuge compact. Features are labelled with the likely mechanism producing the observed shrinkage.

-- XBL 871-176 --

density of amorphous TiO_2 reported by Barringer, and assuming an overly conservative 40% packing efficiency for gravitationally settled compacts results in only 70% volume shrinkage in sintering to theoretically dense rutile (4.2g/cc). Thus, there is additional shrinkage that is due to other processes than interparticle sintering and phase transformations.

Four distinct regions of accelerated shrinkage indicate several different thermally activated processes occur during heating:

1. From ambient to 250°C, approximately 12% linear (32% volume) shrinkage occurs. The maximum shrinkage rate falls between 100-150°C and corresponds very well with the TGA-DTA measurements of Barringer that show a broad endothermic peak with significant mass loss characteristic of evaporation of water of hydration. The mass spectrometry water signal in **Figure 18** provides direct verification that water loss is the primary cause of shrinkage between ambient (~30°C) to 250°C. The maximum signal in **Figure 18** occurs at 130°C and is near the temperature of maximum shrinkage rate (the disparity reflects differences in heating rate and temperature measurement apparatus). The signal drops significantly at temperatures above that corresponding to the maximum signal. The persistence of a small, but decreasing, mass spectrometry water signal suggests some water loss continues to at least 370°C, the maximum device temperature. The contribution of other species to the total mass spectrometry signal is insignificant.

Water removal mass loss is approximately 34%, however because small quantities of material were used, the mass loss was difficult to measure accurately. (This estimate is most likely low since weighing was not performed *in situ* and some reabsorption of ambient atmospheric water occurred during measurement.) True mass loss probably exceeds 36% at 250°C. Unfortunately, mass loss measurements were performed on powders

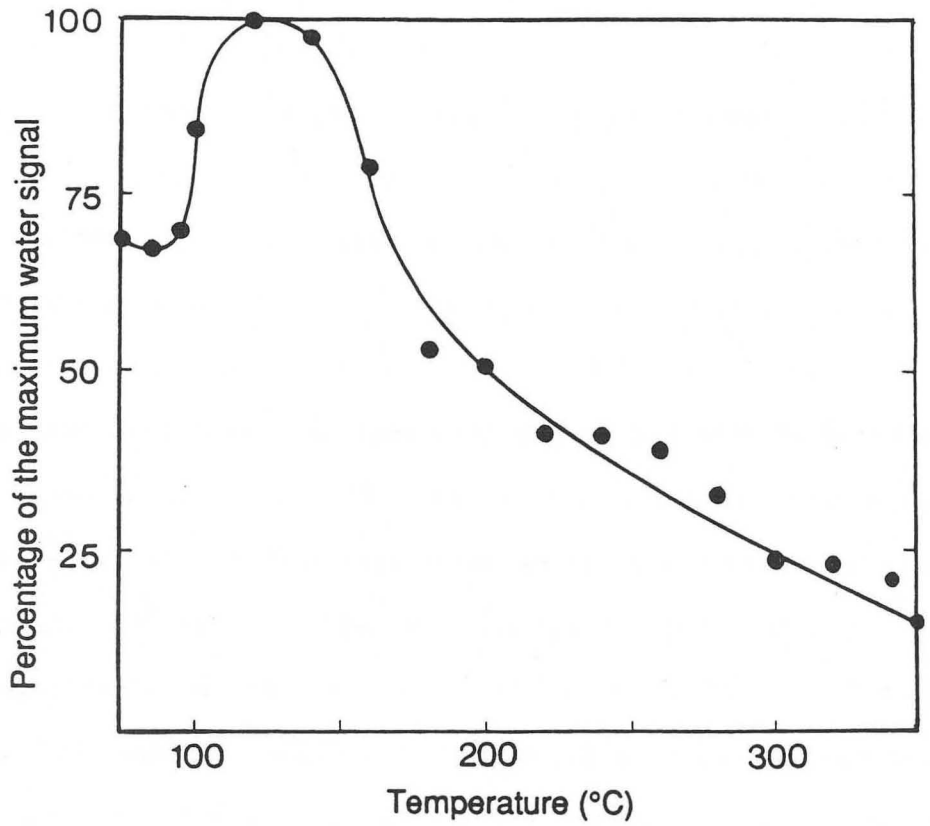

Figure 18. Temperature scannned mass spectrometry water signal.

-- XBL 871-177 --

that spent extensive periods at ambient humidity so significant amounts of physisorbed water are present; mass loss in dessicator-stored material is most certainly lower.

The water layer thickness on 0.35μm diameter (this is the average as-prepared "particle" size) particle surfaces must be 210Å (12% of the particle radii) to account for 12% linear shrinkage associated with water loss. However, a layer of this thickness should have the characteristics of bulk water, and is not expected to persist even at ambient humidity. TGA-DTA, mass spec, and shrinkage data, which were collected on dessicator-dried powder, though, indicate the water layer is stable in dry environments and is only eliminated with heating. Hydration (chemisorption) can stabilize water monolayers in dry environments.[69] Water monolayer thickness on TiO_2 is about 3Å, and a multilayer thickness up to 10Å develops before vapor saturation is attained.[72] Thus, water is most likely present as a thin layer on fine primary units comprising monosized agglomerates or in very fine penetrating capillaries, rather than as a surface coating on relatively large particles. In the latter structure, water loss must cause collapse of capillaries in order to cause shrinkage, while in the former structure water monolayer removal cause shrinkage of the primary units and consequently causes agglomerate shrinkage. A primary unit with a 3Å chemisorbed water layer corresponding to 12% of the total particle radius is about 50Å diameter. Since some ambient moisture is reabsorbed before dilatometry measurements, the water layer and consequently the estimated primary particle diameter are perhaps 50% larger at typical ambient humidity (~30% relative).

2. The region in **Figure 17** between 250°C and 425°C contributes an additional 12% linear shrinkage between 250°C to 425°C for a total linear shrinkage of 24% and a volume shrinkage of 56%. The relative volume shrinkage is 35%; it is determined from

$$\Delta V_{rel}=1 - \{(1 - \Delta L_2)/(1 - \Delta L_1)\}^3$$

where ΔL_1 and ΔL_2 the linear shrinkages at the beginning and end of the region, respectively. The maximum shrinkage rate occurs from 325°C to 390°C and corresponds very well with the temperature range for crystallization of the amorphous, as-prepared phase to anatase, as determined from powder x-ray diffraction spectra. The end-point for the crystallization process occurs at approximately 425°C and is assumed to occur when the integrated intensity of the primary peak stops increasing.

The 390-400°C sharp exothermic peak in Barringers work that was attributed to organic combustion can also be due to crystallization. Mass spectrometer limitation prevented verification of this; however, there is a significant increase in the total organic signal between 350°C to 370°C that may indicate the onset of organic volatilization or combustion; the magnitude of this signal is small and indicates only small quantities of organic material are evolving. Organic pyrolysis rather than combustion may occur since the mass spectrometry data are collected **in vacuo**. Organic combustion, though, is not likely to generate the relatively large shrinkage observed in the 390-400°C temperature range; in Barringer's material, total carbon content amounted to less than 0.18 wt.%.

Most powder compact cracking during heating takes place in the crystallization temperature range. Interestingly, it is possible to crystallize these powders with hydrothermal aging for 22 hours in boiling water. By properly stabilizing the suspension during hydrothermal

aging to prevent agglomeration, it may be possible to produce dense compacts of crystallized powders that do not suffer the severe cracking problems of amorphous material. The absence of shrinkage between 320°C and 420°C with all other shrinkage regions present would provide independent confirmation that shrinkage in that temperature range is induced by crystallization induced.

The density of the as-prepared amorphous material can be back-calculated from the anatase polymorph density using the mass loss and shrinkage data; the mass loss and shrinkage are taken to the anatase crystallization completion temperature, approximately 420°C. At 420°C, the material is 44% of its room temperature volume and 64% of its room temperature mass. Applying these factors to the anatase polymorph density of 3.8g/cc yields an estimated density of 2.6g/cc for the hydrated, amorphous as-prepared material. This is the approximate density of the solid and adsorbed water and does not reflect the contribution of intra-agglomerate porosity to the apparent agglomerate density. The 2.6g/cc density is somewhat lower than the 3.1g/cc measured in Barringer's stereopyncometry work. Revision of the water mass loss to a more credible 12% lowers the density measurement of solid and adsorbed water to 2.0g/cc. At 250°C, the calculated solid density is 3.1g/cc, and is in very good agreement with the other reported data[23].

3. An additional 16% linear shrinkage occurs over the broad temperature range of 425°C to 800°C in **Figure 17.** The total volume decrease to 800°C is 78% with a relative volume contraction of 50% in the 425-800°C temperature range. X-ray diffraction data (discussed later) shows the polymorphic transformation from anatase to rutile begins, and is largely completed in this temperature range. Based on the densities of

anatase and rutile (3.84g/cc and 4.26g/cc, respectively), only 10% relative volume shrinkage is expected if shrinkage in this temperature range is due entirely to the anatase to rutile transformation. If the difference is attributed to densification within microporous agglomerates, an agglomerate density of approximately 60% theoretically (40% intra-agglomerate porosity) is inferred. This probably overestimates the particle porosity because some additional mass loss and anatase crystallization probably occur in the lower end of the temperature range, while some interagglomerate sintering can contribute to shrinkage in the high end of region 3.

Figures 19a-d and **20a-d** compare the agglomerate size and substructural evolution in the as-prepared powder after sequential, one-hour anneals at 250°C, 450°C, and 800°C, respectively. The change in average agglomerate size in these SEM micrographs agrees well with shrinkage to the corresponding temperature. The considerable coarsening of the agglomerate substructure evident in 800°C annealed material certainly indicates intra-agglomerate densification and grain growth has taken place between 450° and 800°C. Agglomerate structure is discussed in a later section.

4. Finally, the 10% linear shrinkage from 800°C to 1200°C in **Figure 17** is due to interparticle sintering. **Figures 19a-d** and **20a-d** show that shrinkage up to 800°C is confined to intra-agglomerate processes. This final shrinkage region, therefore, is most likely due to interagglomerate sintering. The relative volume shrinkage is 42% indicates packing efficiency is 58% in centrifugal compacts, which compares well with the observed packing in **Figure 7.** Surprisingly, only one-fifth of the shrinkage measured in dilatometry is due to "normal" sintering processes.

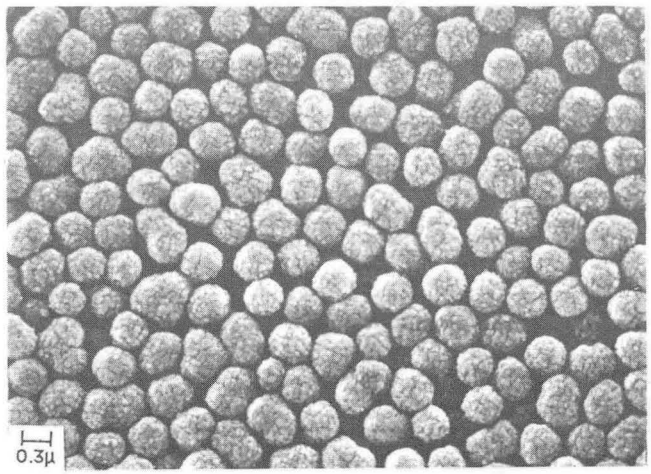

(a) Room temperature

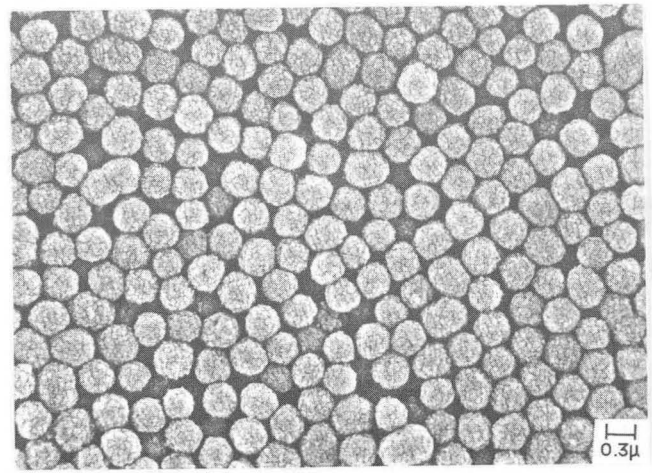

(b) 250°C (water loss)

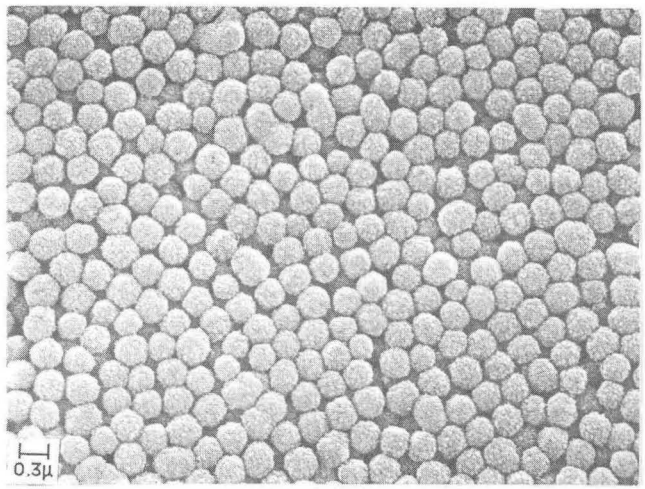

(c) 450°C (anatase crystallization)

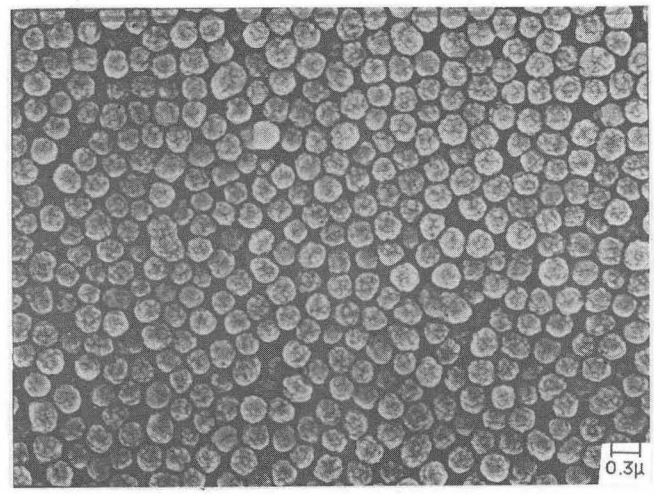

(d) 800°C (rutile formation and intraparticle densification)

Figure 19. Particle shrinkage after incremental isothermal annealing at (a) room termperature, (b) 250°C , 1 hr, (c) 450°C, 1 hr, (d) 800°C, 1 hr. The likely processes contributing to shrinkage are listed next to the corresponding temperature.

XBB 8612-9980

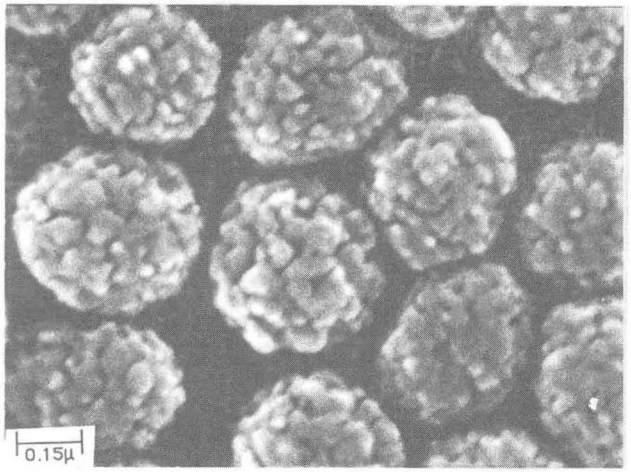

(a) Room temperature

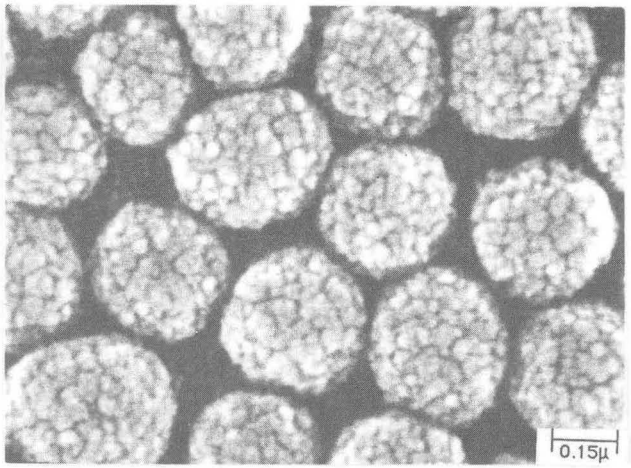

(b) 250°C (water loss)

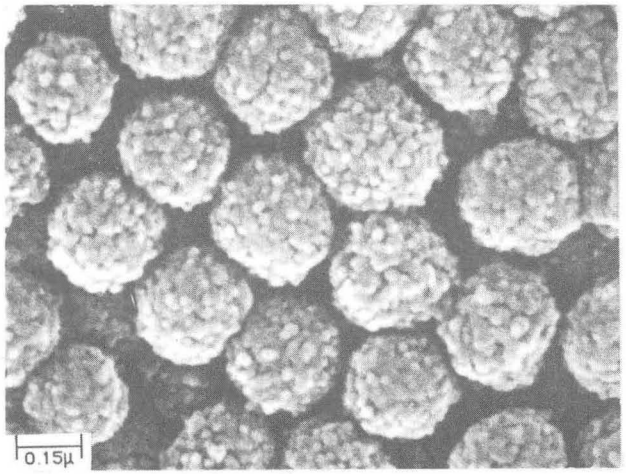

(c) 450°C (anatase crystallization)

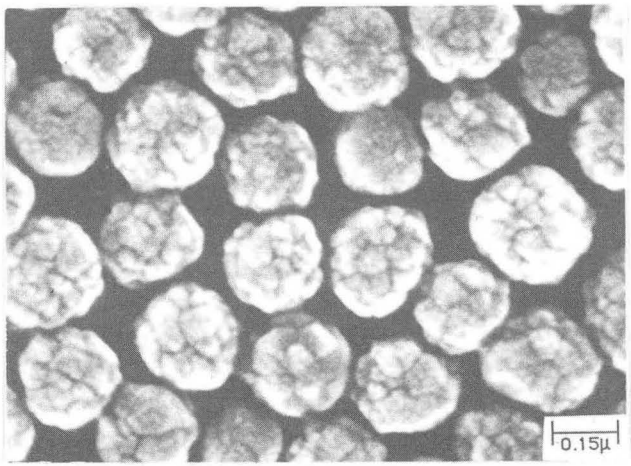

(d) 800°C (rutile formation and intraparticle densification)

Figure 20. High resolution images of the particle surfaces after incremental isothermal anneals showing the change in particle structure at (a) room temperature, (b) 250°C, 1hr, (c) 450°C, 1 hr, and (d) 800°C, 1hr. The likely processes contributing to particle shrinkage are listed next to the corresponding temperature.

XBB 8612-9981

4.2.3 X-ray diffraction

X-ray diffraction spectra of the as-prepared material in **Figure 21a** shows it be amorphous to the crystalline phase detection limit (approximately 1%). The broad anatase peaks in **Figure 21b** of a powder annealed at 400°C for one hour indicate the anatase crystallite size is significantly smaller than the particle size. The 100Å crystallite size, calculated from the Scherrer formula, is similar to the surface feature size observed in high resolution SEM micrographs (**Figures 16a,b**) of powder particles. At this size, there are nearly 50,000(!) anatase crystallites per 3500Å agglomerate. The initial grain size distribution, therefore, does not correspond to the "particle" size distribution. Clearly, grain growth in polycrystalline agglomerates is an important consideration in the sintering of monosized TiO_2. Indeed, with more than a thirty-fold increase in grain size ($4x10^4$ volume increase) during sintering to full density, monosized TiO_2 exhibits more grain growth than many conventional powders.

Figure 21c shows the diffraction spectrum of a powder during transition from anatase to rutile after half an hour at 700°C. The narrow anatase peaks indicate considerable growth has occurred since crystallization. Although the anatase-to-rutile transition temperature shows a batch-to-batch variation between 600 and 800°C, anatase grain growth appears to be a general prerequisite for the transformation. Rutile formation does not significantly change the grain size, but low sensitivity of the broadening technique at detecting grain size variations above 1000Å, makes this conclusion uncertain.

X-ray line broadening measurements place the rutile grain size at about one-third the particle size at the transformation. This agrees reasonably well with **Figures 14a and b** which show grain sizes as small

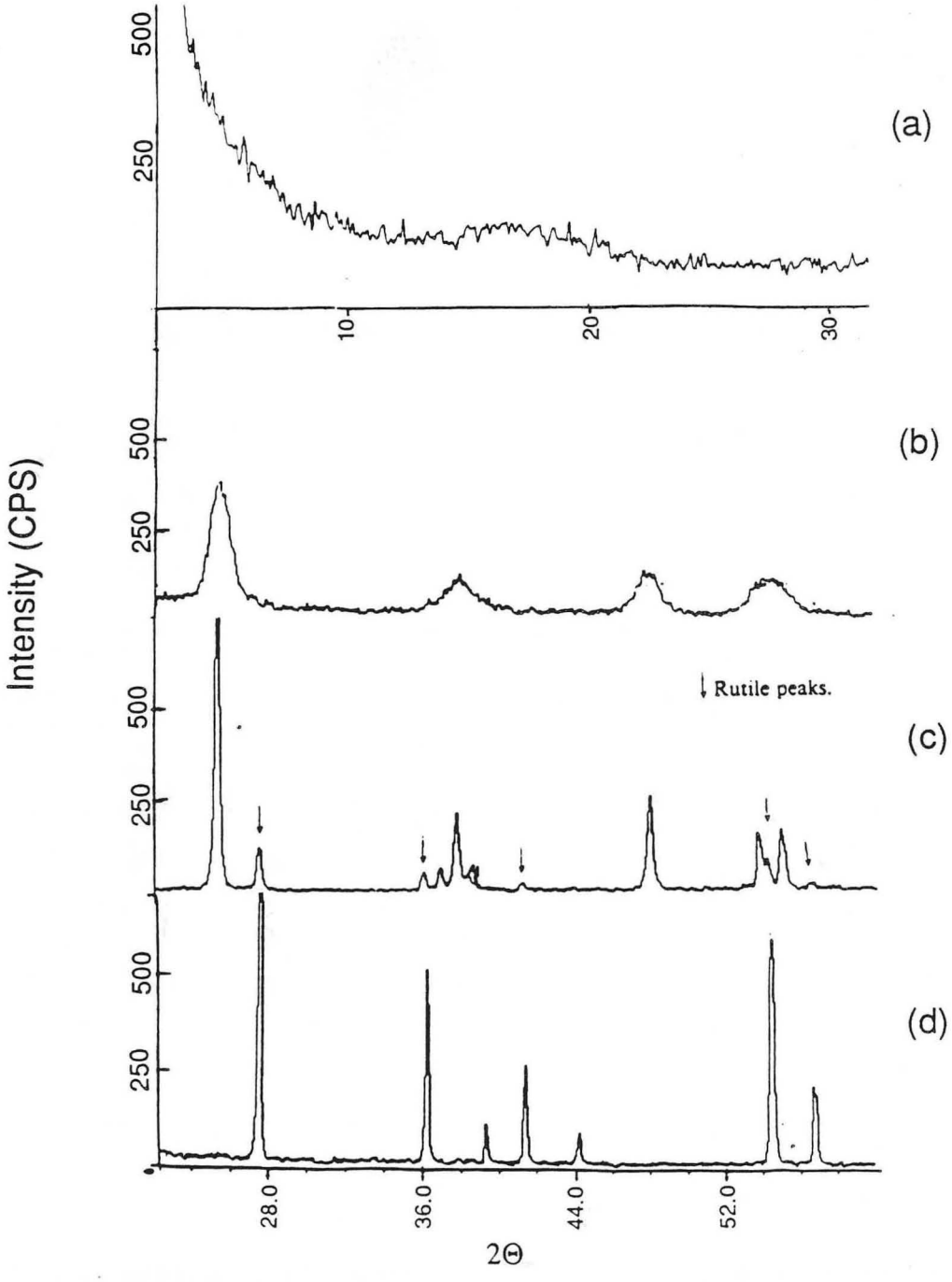

Figure 21. X-ray diffraction spectra from monosized TiO_2 powder.
(a) Amorphous as prepared. (b) After one hour at 400°C, powder has transformed into fine anatase crystallites (note the broad peak width). (c) Peak narrowing after 0.5 hours at 700°C is evidence for considerable coarsening before transformation to rutile. (d) After one hour at 1000°C, the material is 100% rutile.

as one-third the agglomerate size (the minimum grain size, presumably, is smaller than one-third as only a fraction of a agglomerate surface is visible in the SEM micrograph. If the grain diameter is one-third the agglomerate diameter, there are potentially 27 grains per agglomerate) after one hour at 1000°C in a compact that is 100% rutile (**Figure 21d**). Since the rutile transformation, in most cases, is largely complete below 900°C, the rutile grain size at transformation should be smaller than the average grain sizes in **Figure 21a,b**. X-ray line broadening cannot confirm the presence of relatively large grains that may form during incremental growth because instrumental broadening dominates above approximately 1000Å.

4.2.4 Summary

Low temperature sintering on the scale of particle substructure, and shrinkage and water loss characteristics all indicate monosized "particles" are agglomerates of much finer structural units. Shrinkage measurements indicate agglomerate porosity is approximately 40%, and SEM (**Figures 8a,b**) images suggest the primary unit size is between 50-100Å. Since small deviations in the rather subjective assignment of the anatase crystallization and rutile conversion completion temperatures can result in moderately large changes in the porosity estimate, the accuracy of this estimate is low. In order to support this estimate, porosity was assessed using two additional independent techniques. Furthermore, additional characterization techniques were used to confirm that the agglomerate-like morphology seen in SEM images is a bulk characteristic.

4.3 "Particle" Structure

4.3.1 Intra-Agglomerate Porosity

The specific interagglomerate pore volume (volume per unit mass) of a powder compact, $\bar{V}$, measured using mercury intrusion, can be used to estimate the intra-agglomerate pore volume fraction, v, if the solid density, ρ, and interagglomerate packing efficiency, PE, are known. The average agglomerate density, P, is expressible in terms of v and ρ as

$$P = (1-v) \cdot \rho$$

Where the factor (1-v) is the relative volume of the solid in the agglomerate. Similarly, the relative volume of interagglomerate pores is (1-PE). This is the ratio of the interagglomerate pore volume, V, to the total volume of the compact, V_t. V_t can be set equal to one, and the total mass of the compact is simply P(PE) since agglomerates are equivalent to particles of density P. Applying the definition of $\bar{V}$,

$$\bar{V} = (1-PE)/(P \cdot PE)$$

$$= (1-PE)/\{(1-v) \cdot \rho \cdot PE\},$$

and rearranging, we find that

$$v = [PE \cdot \{(\bar{V} \cdot \rho) + 1\} - 1]/(PE \cdot \bar{V} \cdot \rho).$$

Interparticle gravitational compact porosity, $\bar{V}$, was measured at 0.26g/cc. 65-68% agglomerate packing efficiency was estimated from SEM images of the top surface of gravitational compacts (**Figure 8**). The intra-agglomerate porosity is between 20-30% or 33-42% if the solid density is taken as 2.6 or 3.1g/cc, respectively.

Barringer determined the micropore volume in fresh, water-rinsed powder at 0.19cm^3/gm using the α_s method[73] of analyzing adsorption data. Using the same notation as that of the previous paragraph

$$\bar{v} = v/\{(1-v) \cdot \rho\},$$

where $\bar{v}$ is the micropore volume. Rearrangement gives the following,

$$v = (\bar{v} \cdot \rho)/\{1 + \bar{v}\rho\}$$

A porosity of 33% or 37% is calculated at 2.6 or 3.1g/cc density, respectively. This method does not measure the contribution of isolated porosity; however, it does provide the best estimate of agglomerate porosity because it is relatively insensitive to variation of the assumed solid density and the micropore volume measurement is reasonably accurate. Considering the limitations of the three assessment techniques, 35% is probably a very good estimate of the intra-agglomerate porosity.

4.3.2 Primary Unit Size

The surface structure visible in high resolution SEM micrographs of the powder "particles" in **Figures 16a,b** provide an indication of the internal particle structure. These images certainly suggest the monosized particles are agglomerates of very fine particles. The smallest feature size is approximately 50Å which is close to the ultimate 38Å point-to-point apparatus resolution specification, but most readily visible features are in the neighborhood of 100Å. The agglomerate surface is very heterogeneous with considerable variation in the packing of these apparent particles. This surface texture may reflect local variation in the coalescence of fine primary units at the agglomerate surface.

Single point BET measurements from dried and outgassed powders, prepared with the standard technique that includes several water rinses immediately after hydrolysis, consistently yielded surface areas between 310-350 m^2/g and agree with the results of Barringer for water-rinsed

powder. This is more than 120 times greater than the $2.5 m^2/g$ expected for a powder consisting of dense, 0.45μm, 2.7g/cc spherical particles. Adsorption isotherms[23] from water-rinsed powder show that the onset of capillary condensation begins above 30% N_2, thus capillary condensation may be a problem with 30% N_2, 70% He adsorption gas mixture used in this study. Graphical integration of the mercury penetration curve (below 15,000 psia) yields a surface area of 14 m^2/gm which is still a little greater than expected for 0.45μm particles. Part of this additional surface area is a consequence of the geometrical simplification used to model the pore structure; a more refined model (see Appendix I) places the surface area at 4.3 m^2/g. This is significantly lower than the BET surface area, and reflects the difference in penetration characteristics of mercury and nitrogen -- in the former technique, the particles behave as solid spheres, while in the latter they are porous agglomerates.

The corresponding sphere size for $310 m^2/g$ surface area and 2.7g/cc particles is about 70Å diameter which is in good agreement with the apparent primary particle size in the SEM. The chemisorbed water layer is most likely present during room temperature surface area measurements; as discussed earlier, Yates[69] found chemisorbed water layers persist even after extended outgassing (>30 hrs) under flowing N_2. Therefore, the actual solid diameter is around 64Å. This diameter is somewhat larger than the primary unit diameter estimated from dilatometry data assuming shrinkage to 250°C was due to water monolayer loss, and indicates physisorbed water loss in addition to chemisorbed water loss contribute to the shrinkage. Underestimation of the water layer thickness results in a low estimate. The 20Å average pore size calculated from nitrogen desorption isotherms of water-rinsed powder

compares reasonably well with the 11Å minimum pore diameter between 70Å particles.

Barringer attributed particle porosity and high surface areas of water-rinsed powders to fine surface precipitates that form when unreacted ethoxide contacts water. The thickness of this precipitate layer is between 100 and 200Å Such a morphology could produce the surfaces seen in high resolution SEM images. However, such a morphology is inconsistent with porosity and surface area measurements:

1. At 200Å, the surface precipitate layer volume does not exceed 35% of the volume of the 0.35μm "particles" used in pore volume measurements. Earlier calculations indicate this surface layer must account for the entire 35% particle porosity. This is clearly impossible in a layer that is only 35% of the particle volume.

2. The entire powder must be composed of particles that do not exceed 70Å diameter in order to account for the very high powder surface area measurements. In order to generate the measured surface areas, the precipitate size in a surface layer 35% of the particle volume cannot exceed 25Å. This is inconsistent with SEM (Figures 17a,b), TEM measurements[23] that place the crystallite size between 50-100Å, and capillary condensation pore diameters.

3. Dense 0.35μm particles are not consistent with the observed water loss shrinkage and adsorbed water stability. A maximum water layer thickness of 15Å at saturated humidity would produce less than 1% linear shrinkage when removed from dense 0.35μm particles.

4.3.3 Adsorbed Water Layer

The surface area evolution associated with water desorption provides another indication that the "particles" are agglomerates of fine structural units. A surface area decrease in direct proportion to the square of the decrease in agglomerate diameter is expected if shrinkage is due to evaporation of a thin water layer coating the primary units comprising the agglomerate. On the other hand, evaporation of water from pores in rigid particles will cause an increase in surface area. The absolute surface area of a powder sample after a one hour anneal at

250°C drops to 79% of its room temperature value. Dilatometry measurements and SEM images indicate the agglomerate size decreases to 88% of the room temperature value. The square root of the surface area decrease is 0.89, and indicates water loss from the surface of fine primary units does indeed cause agglomerate and consequently compact shrinkage to 250°C.

A water layer thickness of 4.2Å on 70Å primary units can account for agglomerate shrinkage. Hydration of the solid surface probably stabilizes this water layer so that it persists in a dry atmosphere. The 70Å estimate includes the thickness chemisorbed water layer thickness; primary particle diameter without a chemisorbed water layer is 64Å and assuming this is the diameter produced after removal of the physi- and chemisorbed water layers (D/D_0=0.88) results in a 4.4Å water layer thickness estimate. The water layer coating on the primary structural units in the monosized agglomerate corresponds to roughly 3-4 water molecules, assuming bulk water molecule geometry. IR spectroscopy could confirm the presence of, and provide structural information on, the hydrated surface layer. Changes in pH which alter the surface charge, and adsorption of ions can possibly change the stability of the water coating, and can have potential processing applications such as an enhanced drying rate.

4.3.4 TEM Analysis

Pickles and Lilley's[32,33] TEM work on ultramicrotomed anatase-crystallized powders shows essentially random packing of nearly spherical particles within monosized agglomerates. The maximum particle size is around 100Å. The porosity, between 30 and 40%, is in good agreement with most of the previous observations. Images of the amorphous

material show intra-agglomerate porosity, but do not indicate a particulate structure. SEM and surface area measurements, though, suggest the amorphous material is also particulate. The lack of images of unique primary units within the monosized "particles" is probably a consequence of the uniform absorption of amorphous material which makes contrast variation between adjacent primary units low. In crystallized material, different crystallographic orientations of adjacent units produces good diffraction contrast.

4.4 Structural Evolution During Processing

4.4.1 Surface Area Evolution

The surface area of monosized TiO_2 is a function of the size distribution of the primary particles comprising the agglomerates. The surface area evolution gives an indication of intra-agglomerate structural changes. It was stated in section 4.3.3 that the surface area decrease accompanying the loss of the water film on primary particle is simply proportional to the square of the ratio of the average primary particle size shrinkage. This is a property of any homogeneous contraction or expansion of a particle size distribution. This assertion is simply proved. Mathematically, the average surface area of a powder composed of spherical particles is determined as follows:

$$\bar{S} = 4\pi \cdot z \cdot (R_{rms})^2$$

$$\bar{S} = q \cdot 4\pi \cdot z \cdot (\bar{R})^2$$

where q is defined as

$$q = R_{rms}/\bar{R}$$

and R_{rms}, $\bar{R}$, are defined using the normalized particle size distribution function, F(R), such that

$$R_{rms} = \{(\Sigma F(R)R^2)/(\Sigma F(R)\ (=1))\}^{0.5}$$

is simply the square root of the second moment of the size distribution and

$$\bar{R} = \Sigma F(R)R/(\Sigma F(R) \ (=1))$$

is the first moment of the distribution. Applying these definitions to the definition of q yields

$$q = (\Sigma F(R)R^2)^{0.5}/(\Sigma F(R)R)$$

Particle shape and roughness are accounted for with a constant correction factor, z. Water loss simply changes the primary particle size by a constant structural factor L, such that $R'=L \cdot R$, where R' is the particle radius after water loss; a homogeneous size change does not change particle shape (including roughness) and, therefore, does not change the shape correction factor. The resulting change in $\bar{R}$, and q are

$$R'_{rms} = (\Sigma F(R)(L \cdot R)^2)^{0.5} = L \cdot R_{rms}$$

$$\bar{R}' = \Sigma F(R)(L \cdot R) = L \bar{R}$$

and

$$q' = q$$

The new surface area is simply

$$\bar{S}' = L^2 \cdot \bar{S}$$

which is the L^2 dependence originally described.

If the surface area is calculated on the basis of the agglomerate size distribution instead of the primary particle size distribution, z becomes a roughness factor for the agglomerates and is a function of the primary particle size distribution. The surface area for any homogeneous change of the primary particle size distribution will scale as L^2 for the agglomerate since it is identical to L^2 for primary particles; z does not change. The surface area (normalized with the room temperature surface area) will decrease more rapidly than the expected L^2 dependence for homogeneous shrinkage when intra-agglomerate sintering occurs. For example, a 65% dense agglomerate with a surface area

100-fold greater than a smooth sphere decreases its surface area by a factor of 1/237 (= $0.65^2/100$) during 35% shrinkage (L=65%) to full density, while 35% agglomerate shrinkage (L=65%) decreases surface area by only L^2=43% when shrinkage is the result of primary particle contraction.

Figure 22 shows the variation of normalized absolute surface area with the normalized average agglomerate size squared, L^2 (both are normalized by the room temperature values). The factor L is obtained from dilatometry measurements: L=1-ΔA, where ΔA is the axial shrinkage. The corresponding temperatures are listed next to each data point. The solid diagonal line is the path the surface area would follow if decreases were the result of homogeneous primary particle shrinkage. The surface area data points fall along the solid line below 350°C. Negative deviation from the line above 350°C indicates intra-agglomerate sintering is occurring. Neck growth between primary particles by surface diffusion is most likely the predominant sintering process above 350°C.

Below 350°C, water loss from the surfaces of the primary particles causes a uniform decrease in all the primary particle dimension that is reflected in the surface area evolution. The slight positive deviation from the line indicates that some additional surface sites have become accessible. After the water is removed, the TiO_2 surfaces are in contact. Mass transport at this point probably forms interparticle necks within the agglomerates that cause the smoothing seen in the surface area data. This smoothing corresponds to the anatase crystallization; possibly, heterogeneous anatase nucleation takes place at two-particle contacts, but the correspondence may be coincidental. Microscopic (SEM)

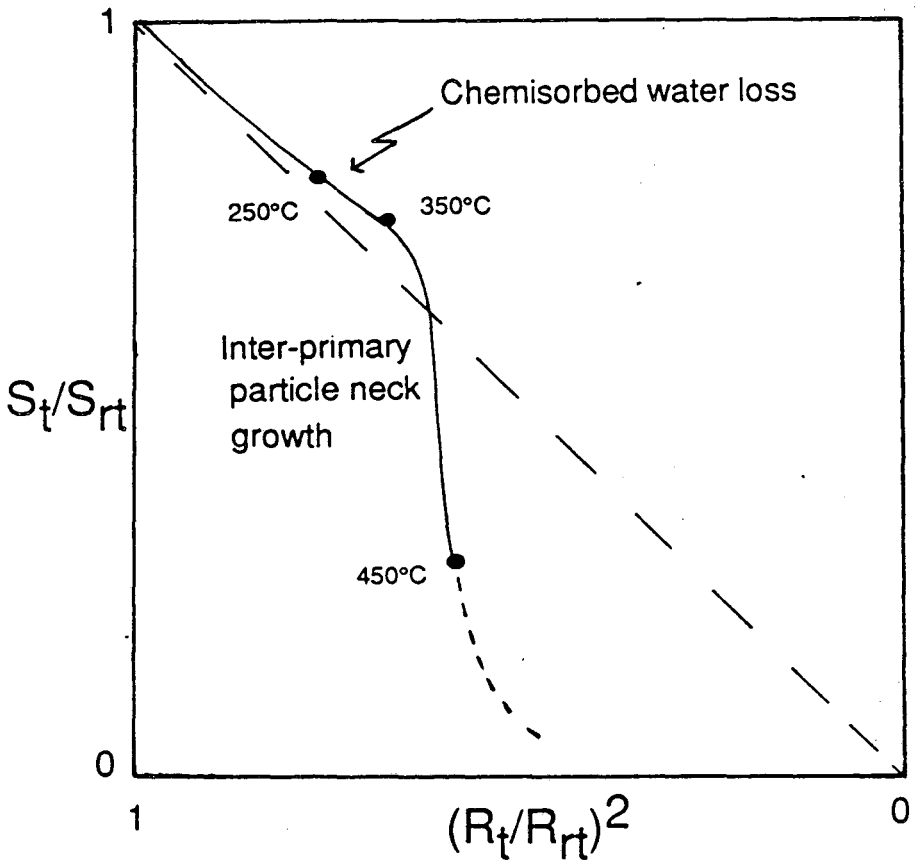

Figure 22. Surface area evolution during incremental isothermal anneals of a powder sample. S_t/S_{rt} is the normalized surface area after annealing at temperature t, and S_{rt} refers to the room temperature surface area. R_t/R_{rt} is the agglomerate radius after annealing at temperature t, and rt is the room temperature agglomerate size. This ratio is the equivalent to $1-\Delta L_t$, where ΔL_t is the relative compact shrinkage to temperature t, and is obtained from dilatometry measurements.

-- XBL 871-179 --

evidence of smoothing is not expected because the feature sizes corresponding to 100-350m^2/g surface areas (~100-70Å) are near the microscopic resolution limit.

4.4.2 Crystallization

Anatase crystallization in a dry atmosphere possibly initiates at contacts between primary particles that form after water removal. During hydrothermal aging, water-aided mass transport may accelerate the transformation at primary particle surfaces. Perhaps crystallization directly to the rutile polymorph is possible in hydrothermal conditions if the correct ions are present in the solution. Use of hydrothermal rutile crystallized powder suspensions would significantly reduce compact shrinkage. Investigation of the anatase crystallization with micrographic and spectrographic techniques might reveal intermediate structures that can be altered with dopants to yield different TiO_2 polymorphs upon crystallization.

4.4.3 Anatase Grain Growth

The results of x-ray line broadening studies of isothermal anatase grain growth are shown in **Figure 23**. The study was done on fragments of a centrifugally compacted powder. Material from this compact also underwent semiquantitative chemical analysis. The heating time is negligible because these are small samples of ground powder. Negligible grain growth occurs at 400°C, while grain growth at 600°C is initially very rapid. The anatase grain growth rate slows at a grain size of ~1000Å (0.1μm), which appears to be the maximum anatase grain size before rutile formation begins. Some of the drop in growth rate is due to the low sensitivity of the x-ray line broadening technique for grain sizes above 0.1μm as well as instrumental broadening, but micrographic

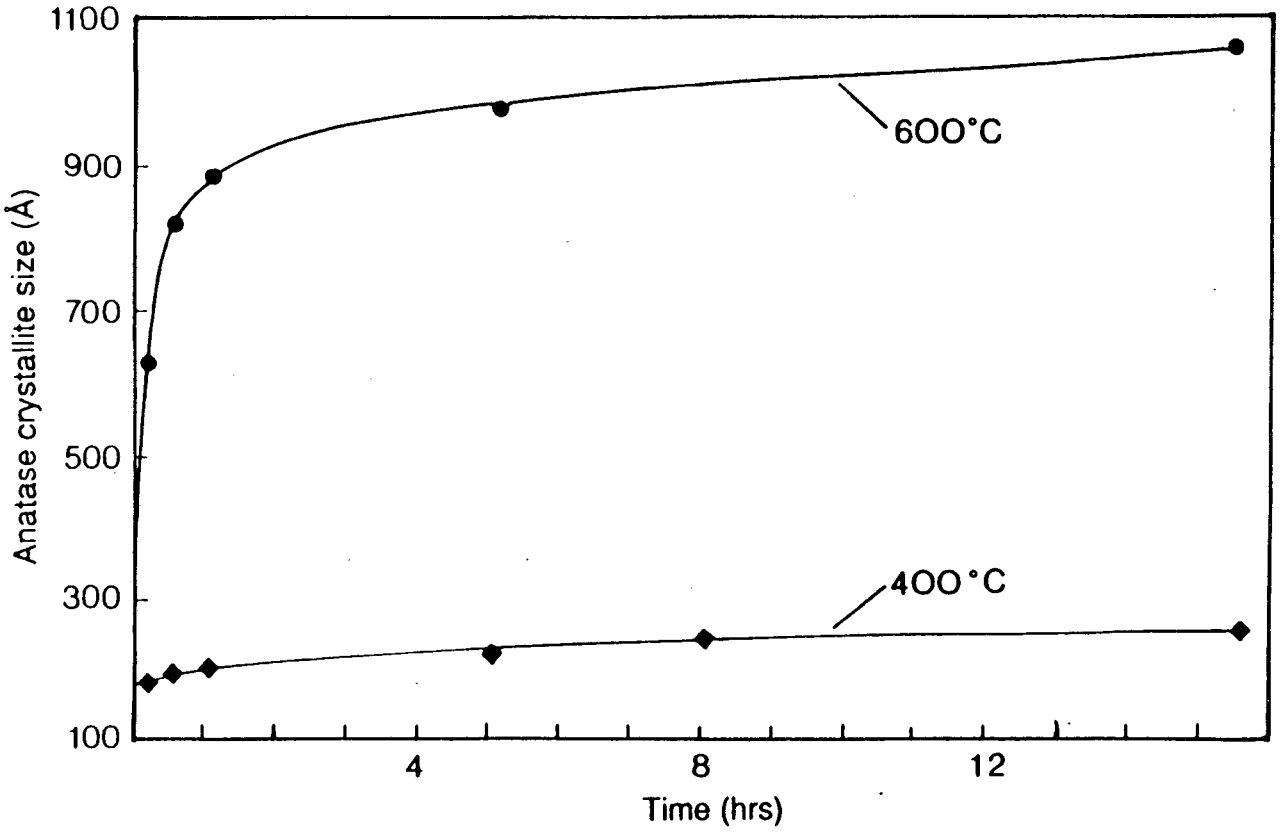

Figure 23. Isothermal anatase crystallite growth

-- XBL 871-180 --

evidence indicates that this is an accurate limiting value. The grain growth work was performed on ground powder samples, so grain bridging between agglomerates is not expected to occur with great frequency.

Constant heating rate (4°C/min) anatase crystallite growth was followed in a sample of slip cast powder. Slip cast powder was used because the centrifuge stock was depleted. The results of the grain size versus temperature measurements in **Figure 24** suggest the grain growth rate in the s/c powder is somewhat slower than the centrifuge powder. The grain growth rate at 600°C is much lower than growth rate for centrifugally compacted powder at a similar grain size. Since the powder morphologies of s/c and centrifuged powder are identical prior to settling, calcium is the obvious cause of the difference between these two samples. Calcium, evidently, is an effective grain growth inhibitor in TiO_2. The calcium was leached from the plaster-of-Paris mold during slip casting. The calcium ions probably penetrate the monosized agglomerates and adsorb on the primary particle surfaces.

Impurity segregation, second phases and pores at grain boundaries all reduce grain boundary mobility. Assuming the only grain boundary drag sources in the pure (centrifuge) powder sample are pores. The grain boundary velocity for a boundary with containing mobile pores is[10]

$$v_b = F_b \, M_p M_b / (N M_b + M_p)$$

where v_b is the boundary velocity, F_b is the force across the boundary, M_b is the boundary mobility, M_p is the pore mobility, and N is the number of pores per boundary. Generally, large pores limit boundary velocity. As densification progresses, pore shrink and grain growth accelerates. If the assumption is made that pore size is proportional to grain size[74] then grain growth follows a cubic[75]

$$G^3 - G_o^3 = K_2 t$$

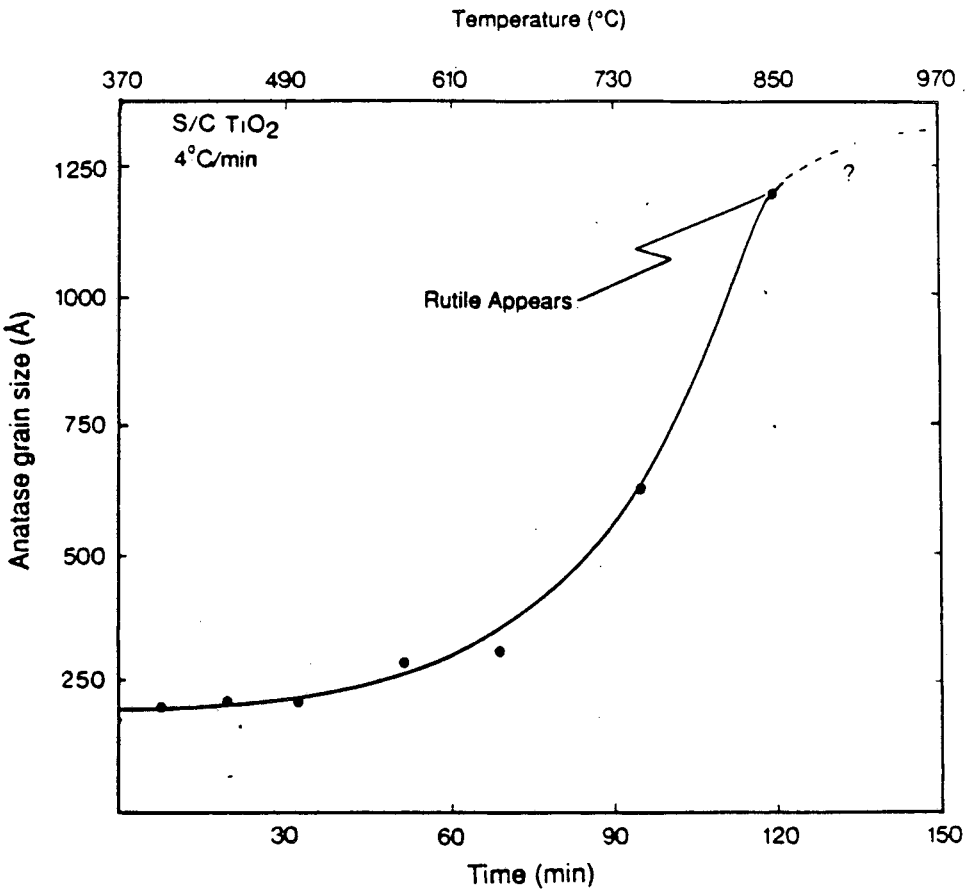

Figure 24. Constant heating rate anatase crystallite coarsening.

-- XBL 871-181 --

growth law when diffusion through vapor or solid phases enables pore migration, or quartic

$$G^4 - G_o^4 = K_3 t$$

growth when pore movement involves surface diffusion.

Figure 25 is a plot of the isothermal (600°C) grain size GS^4 versus t, and shows that at grain sizes below 900Å time dependence for GS^4 if roughly proportional to t. The correlation of the data to a straight line is poor, but the quartic rate law produces the closest fit. If $G^4 >> G_o^4$, then G_o can be neglected and the data can be plotted as G vs $t^{0.5}$. This grain size dependence indicates surface diffusion in pores is the limiting factor in the initial grain growth. Extensive negative deviation at larger grain sizes is due to systematic grain size underestimation from x-ray line broadening data. At larger grain sizes, dihedral constraints at the grain boundary-surface junction (grooving), and a lower grain growth driving force reduce growth rates below the quartic dependence. (The grains cannot grow larger than the agglomerate size in the ground powder samples used in the grain growth studies). Calcium may reduce anatase grain growth by inhibiting anatase surface diffusion and thereby decreasing pore mobility.

Since grain growth cannot proceed at low relative densities, the slower grain growth rates in calcium-contaminated powders may be the consequence of a lower intra-agglomerate densification rate that is calcium induced. Preliminary dilatometry measurements attempted on slip cast pellets indicate that after crystallization, further shrinkage does not occur until the temperature reaches 900°C. The magnitude of this high temperature shrinkage (>800°C) is is roughly large enough to account for intraparticle shrinkage, rutile formation and interparticle

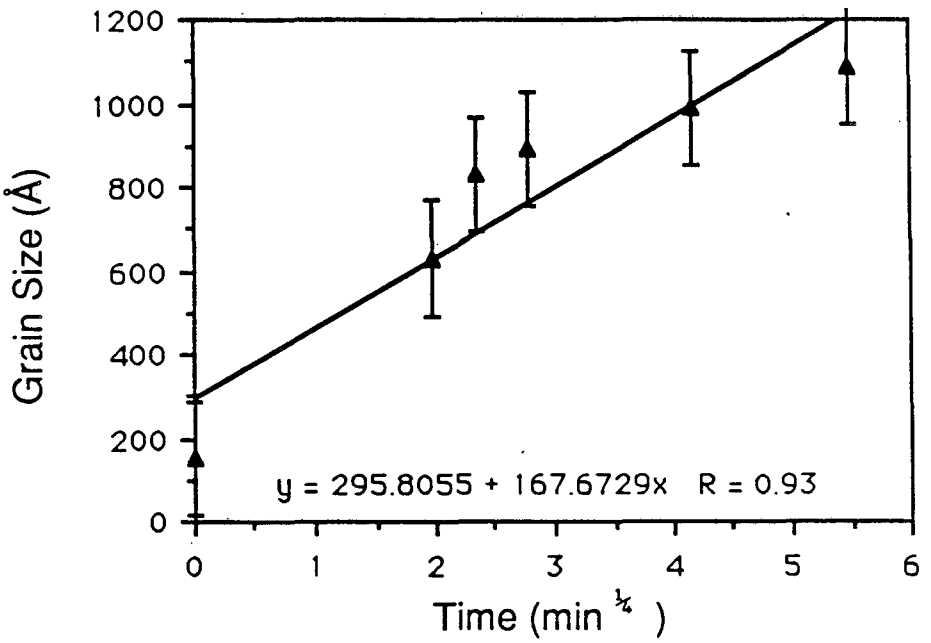

Figure 25. Kinetic analysis of isothermal anatase coarsening at 600°C. The data roughly conform to the fourth order coarsening kinetics expected for pore-limited grain growth if pore movement is accomplished through diffusion of material along the pore surfaces. The poor fit, though, suggests several additional factors are active. However, fouth order kinetics provides the closest fit to the data.

-- XBL 871-182 --

sintering. This indicates calcium displaces the intra-agglomerate densification to higher temperatures, and that it is this slower densification that forestalls grain growth until higher temperatures are attained. Additional dilatometry and careful X-ray thermal/kinetic experiments are needed to confirm the actual grain growth kinetics law and verify the grain growth and densification mechanisms. Since the manner in which x-ray line broadening averages the grain size distribution is uncertain, more direct TEM measurements of grain size distributions in quenched powder particles is desirable. Microtomy techniques combined with TEM microanalysis can yield structural and chemical information from the intra-agglomerate the bulk and grain boundaries. Until these experiments are undertaken, the kinetic growth law developed herein should be considered **highly conjectural.**

4.4.4 Anatase to Rutile Transformation

The transformation data are semiquantitative in that no standards were used to calibrate the x-ray diffraction data. Standards must be prepared from samples of monosized TiO_2 because the particle density of other powder sources will not match and data biasing will result. There is some difficulty in producing large-grained anatase in monosized TiO_2, but short heat treatments at moderate temperatures (eg. 600°C) should be adequate. No attempt was made to fit the data to existing models since the results are semiquantitative.

Figure 26 shows the results of the anatase to rutile transformation study. More than 15 hours is required for complete conversion to rutile at 600°C, but 1 to 3 hours are required at 800°C. At 900°C, the rate is too fast to follow accurately in quench experiments and requires in situ measurements. However, the most interesting result of this study

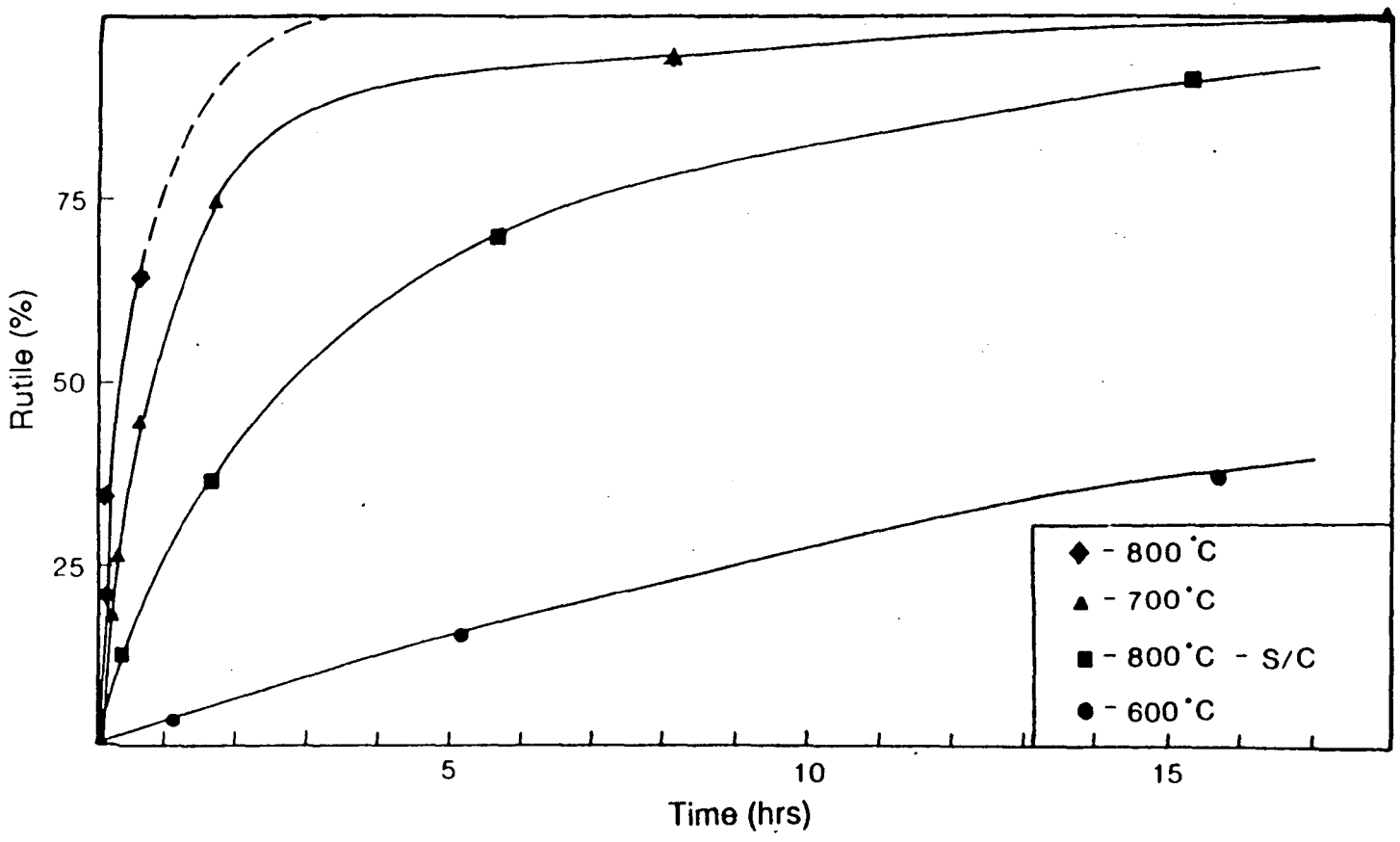

Figure 26. Isothermal anatase to rutile inversion kinetics.

-- XBL 871-183 --

is not the characteristics of the centrifuge powder, but the much slower transformation kinetics of the slip cast powder. The transformation rate of the s/c powder at 800°C is equivalent to centrifuged powder at approximately 650°C — 150°C lower. Again, the agent suspected to cause this difference is calcium.

McKenzie performed extensive studies of the anatase to rutile transformation including the effect of various dopants.[43,44]. He observed that dopants (including divalent ions) tend to increase, not hinder, the transformation. McKenzie attributed this increased rate to the greater defect concentration (anion vacancies and interstitial cations) associated with the introduction of divalent metal ions into tetravalent sites which increases lattice diffusion and catalyzes the transformation. Although no explicit data was collected for calcium, based on the impurity influence mechanism that is discussed calcium impurities would be expected to accelerate the anatase to rutile transformation. This prediction contradicts the observations in the current work on monosized TiO_2. Earlier work on chemically derived powders pure[28-30] indicate impurities reduce the transformation rate. The transformation temperatures in these earlier studies are in good agreement with the transformation temperatures for monosized TiO_2.

All observations in this study indicate that rutile does not form before the anatase grain size, measured with X-ray line broadening, exceeds approximately 900Å. Calcium slows the anatase grain growth, and apparently displaces the rutile transformation to higher temperatures. The anatase to rutile transformation in monosized TiO_2 -- even with calcium -- proceeds at lower temperatures than the minimum temperature in McKenzie's work. McKenzie also observed enhanced particle sintering in material doped to accelerate the rutile transformation. These enhanced

sintering rates were attributed to enhanced oxide lattice diffusion that facilitates both rutile formation and interparticle sintering. Miller[45] cites cation interstitial and oxygen vacancy diffusion mechanisms as the active mass transport paths in the sintering of rutile. Most recent and accepted studies on sintering of TiO_2 have concluded oxygen lattice diffusivity controls densification.[45,47,48] Based on these interpretations a possible mechanism for calcium retardation of the anatase to rutile transformation assumes the presence of interstitial calcium defects. Interstitial calcium will reduce the oxygen vacancy concentration and consequently decrease oxygen lattice diffusivity.

The anatase to rutile transition does not substantially alter the grain size. The rutile grains essentially continue growing along the anatase grain growth trajectory. Exaggerated growth of a few transformed grains is not a problem in the sintering of monosized TiO_2. The five-fold grain size increase in sintering monosized TiO_2 to theoretical density is a consequence of anatase and rutile grain growth, rather than simultaneous crystallization and phase transformations, as originally suggested by Barringer. Therefore, intra-agglomerate grain growth is the secondary factor, after green compact microstructure, that affects monosized titania densification and grain structure development.

4.4.5 Intra- and Interagglomerate Sintering

Changes observed in region 3 of the dilatometry curve (425-800°C) were attributed to both the anatase to rutile transformation and intra-agglomerate sintering. However, the curve provides no indication of the actual kinetics of each of these process. The thermal/kinetic data for anatase grain growth and the polymorphic transformation allow the description of region 3 to be refined. It is possible to deduce that rutile

transformation shrinkage is not significant below 600°C in a 4°C/min run since the anatase grain growth has not proceeded to the point that the rutile transformation occurs. Hence, below 600°C intra-agglomerate sintering is the major cause of agglomerate and, consequently compact, shrinkage. These results agree with earlier observations of the sintering behavior of ultrafine anatase particles.[28].

Dilatometry evidence indicates intra-agglomerate densification begins at temperatures at least as low as 425°C. If it is assumed grain growth does not begin below about 90% relative agglomerate density, then significant grain growth in the constant heating rate dilatometry experiment probably begins above 570°C. The selection of 90% as the critical relative density for grain growth is based on grain growth trajectories for compacts with high (>60%) initial packing efficiency; grain size 90% relative density is less than twice the initial grain size, but at 95% relative density, the grain size is greater than three times the initial size.

Micrographic evidence for low temperature interagglomerate sintering was originally cited as evidence for the existence of fine primary units in what are apparently ideal "particles". Some interagglomerate neck growth at primary unit contacts would be expected as low as 425°, however there is no micrographic evidence for this process, and there is no appreciable increase in compact strength. Micrographic evidence for interagglomerate neck formation after one hour at 600°C is inconclusive, but strength does increases slightly after on one hour at 600° and indicates interagglomerate neck growth has occurred.

Grain structures in sintered compacts, described earlier (section 4.2.1), indicate grain growth between particles at low relative

densities may occur through an incremental growth process. Initially, particles must be polycrystalline for incremental growth to occur. Evidence gathered from various characterization techniques strongly indicates "particles" are polygranular agglomerates of fine primary units. There is no evidence that phase transformations cause any significant changes in the grain structure or the relative compact density. Some intra-agglomerate densification is required for grain growth to begin. If intra-agglomerate densification and interagglomerate neck formation occur at the same temperature, grains that begin to grow above a critical relative density would be expected to cross between agglomerates. Intra-agglomerate densification, must occur more rapidly than interagglomerate neck growth if grain growth is to be confined within agglomerates until late in the final sintering stages when the compact attains high relative density.

The relative agglomerate densification, intra-agglomerate grain growth, and interagglomerate neck growth rates determine whether incremental grain growth will occur at low relative densities. Agglomerate morphologies that permit rapid grain growth at low relative densities and/or inhibit low temperature neck formation are desirable because compacts produced from these powders will develop uniform grain sizes with lower grain growth. The example of calcium illustrates the point that small impurity concentrations might substantially change microstructure development.

It is important to re-emphasize the point that the grain sintered grain structure in monosized titania is a product of intra-agglomerate grain growth rather than growth of initially monosized grains. In the former case significant grain growth occurs during densification, while in the latter, grain growth is small. In reality, monosized titania

does not reduce grain growth (as the ratio of final to initial grain size) compared to conventional powders, but instead controls the limiting size during exaggerated intra-agglomerate grain growth so that at the outset of interparticle sintering, a uniform grain size is on the order of the apparent particle size is produced. At the outset of interagglomerate sintering, this new grain size distribution is relatively stable, and a second exaggerated growth process involving these larger grains does not take place. Low grain growth during interagglomerate sintering results in grain structures that are superior to conventional powders. This controlled grain growth is fortunate, but not necessarily the rule in monosized systems.

The extent of the low temperature interagglomerate sintering in **Figure 15a** suggests grain boundary stabilization of pores may not be occurring. This sintering behavior indicates a viscous coalescence process is operative. This behavior, though is not generalized over the entire sample. Areas that undergo no low temperature sintering often are adjacent to a regions that exhibit extensive low temperature densification. Impurities are a possible cause, but sensitive spatially resolved chemical analysis techniques (scanning auger, x-ray microprobe and STEM/TEM characterization -- ESCA, EELS, and x-ray microanalysis) are required to detect small spatial variations in impurity concentration.

Powder synthesis and compaction techniques that eliminate the agglomerate "intermediate", and instead pack primary units in uniform compacts can reduce the sintering shrinkage by more than 50% in the absence of complicating factors such as phase changes and dehydration. Grain boundary stabilization of the relatively large (compared to the

initial crystallite size) interagglomerate pores is no longer a possibility. In the case of monosized TiO_2, a potential densification temperature as low as 600°C is possible if methods are developed to break-up the monosized agglomerates and form compacts from the primary particles. In the absence of phase transformations, this would cut densification shrinkage in half. However, without the intermediate barriers to further grain growth at agglomerate sizes, substantially more grain growth may occur in these systems.

Summary

Monosized, spherical 0.35μm titania particles were prepared by controlled hydrolysis of 0.15 M titanium tetraethoxide with 0.45 M water in ethanol. Particle structure characterization with direct (SEM and TEM) and indirect (e.g. dilatometry, gas adsorption, and mercury porosimetry) techniques indicate the powder particles are actually dense-random-packed agglomerates of 60Å primary units. This structure contains approximately 35% porosity. This substructure has important manifestations in the sintering properties of monosized titania powder compacts:

1. The total linear shrinkage in dilatometry experiments is double the amount that is expected if the monosized particles are assumed to be dense primary particles. (a) Loss of chemisorbed water from primary particle surfaces in dessicator-dried powder compacts occurs between ambient and 250°C, and results in approximately 12% linear shrinkage. Total shrinkage for dense, 0.35μm particles would be less than 1%. (b) Approximately 13% shrinkage between 250°c and 425°C is the result of anatase crystallization. (c) Approximately 13% shrinkage between 425°C and 600°C is the result of intra-agglomerate densification. Again, this shrinkage source would be absent in "ideal" powders. (d) Between 600°C and 800°c, there is approximately 5% linear shrinkage that is the result of the anatase to rutile polymorphic transformation. (e) Finally, above 800°C normal interagglomerate sintering takes place.

2. Low temperature (<800°C) microstructures indicate primary particle-aided viscous coalescence of monosized agglomerates, may occur, although this process is not generalized. Stress gradients and impurities may cause some areas to exhibit low temperature sintering.

3. Differences in the relative rates of intra- and interagglomerate densification and intra-agglomerate grain growth can account for the different sintered grain structures that developed in the gravitational compacts (**Figure 10a and 10b**). Preferential intra-agglomerate densification and subsequent rapid intra-agglomerate grain growth may produce the grain structure in **10b**. The structure in **10a** may result from initial intra- and interagglomerate densification rates that are similar. This permits rapidly growing grains to cross between adjacent agglomerates resulting in grains that may encompass several adjacent agglomerates. The origin of these different growth and densification rates is unknown, but impurities may be important. Calcium, for example, has inhibits anatase grain growth, the anatase to rutile transformation, and possibly intra-agglomerate densification.

4. Thermal/kinetic crystallographic studies indicate phase transformations (crystallization, and the anatase to rutile polymorphic transformation) do not alter the grain size significantly. Thus, grain structure evolution within the monosized agglomerates is the primary factor (aside from green compact packing and "particle" size distribution) that influences grain structure development. Intra-agglomerate grain growth begins at approximately 90% relative agglomerate density. The grain growth very roughly obeys fourth order growth kinetics characteristic of pore drag-limited growth.

5. The agglomerate structure permits large contamination levels because these powders have intrinsically high accessible surface areas. The expected calcium content in "ideal" monosized powders is expected to be 100 times lower (less than 0.0035%) than the 0.35% calcium content in agglomerate powders.

6. Finally, difference in the sintering characteristics of the gravitational and centrifuge compacts, as expected, reflect differences in the compact density and uniformity: the "ordered" gravitational compacts sinter to higher density, in shorter time, with less grain growth than uniform, but disordered, centrifuge compacts. the centrifuge and gravitational compacts fall along the uniform and ordered compact density–grain size trajectories in **Figure 12**, respectively.

Conclusions

1. The agglomerate structure in monosized titania particles has important manifestations in the sintering characteristics and sintered microstructure of monosized titania.

2. Grain growth is an important consideration in the sintering of monosized titania. The actual grain size increase in gravitational compacts is approximately fifty-fold rather than less than five-fold as previously reported[23]. Grain growth control may be required in the sintering of other monosized systems; the uniform grain size that develops in titania may not be a general property of all monosized systems.

3. Inter-primary unit sintering below 600°C indicates that densification of uniform compacts of fine primary particles may be possible at 600°C (~900°K, or T/T_m=0.43). This indicates that 100Å alumina particle compacts, for example, can densify below 1000°C if packing is carefully controlled.

4. Other monosized systems -- specifically those prepared by alkoxide hydrolysis -- might, in fact, consist of monosized agglomerates. These systems should show relatively large water loss shrinkages between at low temperatures. While intra-agglomerate densification would cause shrinkage at moderate temperatures. In addition, intra-agglomerate grain growth and phase transformations may have deleterious consequences.

5. The formation mechanism of monosized agglomerates warrents further study. Controlled agglomeration of 100Å or smaller particles may provide a practical and powerful method for preparing polymodal powders and/or controlled primary particles packing in green structures.

Appendix I: Surface Estimation From Scanning Mercury Porosimetry on Monosized Powder Compacts

A more accurate estimate of the surface area is possible if the compact is assumed to have settled in a FCC structure. The smallest passage in this structure is the three-fold coordinated pore between through close packed (111) planes. When the primitive (rhombahedral) cell is considered in isolation with a close-packed plane taken as the upper surface, there are two channels that run from the upper surface to the lower surface (Figure line drawing) that intersect the tetrahedral and octahedral voids within the cell. In this analysis, these two pores can be considered a complete set for the cell because there are no additional pores required to fill the void volume in the structure. The HCP unit cell with a pore running between the upper and lower basal plane, in contrast, requires branch channels to fill the void volume in the cell.

The length of these pores is 2R, where R is the agglomerate radius. The effective radii of these channels is then assigned so that they contain the same surface area as the primitive cell.

$$2\pi R_{eff}(2R) = 2\pi R^2$$

$$R_{eff} = R/2$$

This compares with the minimum channel radius of

$$R_{min} = R((1/\cos 30)-1)$$

Since the pressure at which penetration occurs depends on R_{min}, mercury porosimetry underestimates the pore channel radius. The pressure should be multiplied by the scale factor, F

$$F = R_{min}/R_{eff} \sim 0.31$$

With this scale factor the surface area becomes $4.3 m^2/g$.

Appendix II. Growth of Monosized Powders by Controlled Agglomeration

In a dispersion, particle encounters occur due to Brownian motion, gravity, and convection. In dispersions of ultrafine particles, Brownian motion is the only significant cause of particle encounters. The nature of the forces between particles (attractive or repulsive) determine whether encounters results in permanent coagulation. Particle attraction is due to the van der Waals force, while electrostatic interactions of the diffuse ionic double-layers that surround particles in solution and short range interactions of adsorbed species generate repulsive forces.

The basic theory of these interactions in liquid dispersions containing electrolytes is developed in the DLVO (Derjaguin - Landau - Verwey - Overbeek)[76] treatment. The general form of the two-particle interaction energy curve is shown in Figure 27. Factors such as particle material, suspending liquid, pH, and electrolyte concentration affect features such as the height of the primary maximum and depth of the primary minimum.

The height of the primary maximum establishes the stability of a colloidal suspension; generally, particles will not coalesce at repulsive energies above 10 kT. The primary maximum height between particles (or agglomerates) of the same size scales roughly as the size of these interacting units. Thus, colloidal suspensions of large particles are more stable than those of small particles. Hogg et al.[77] and Israelechiavelli[78] analyzed repulsive and attractive interactions, respectively, between particles of different size; the primary maximum height obtained from these treatments can be approximated with

$$(1/W)_{mixed} = 1/2\{(1/W)_1 + (1/W)_2\}$$

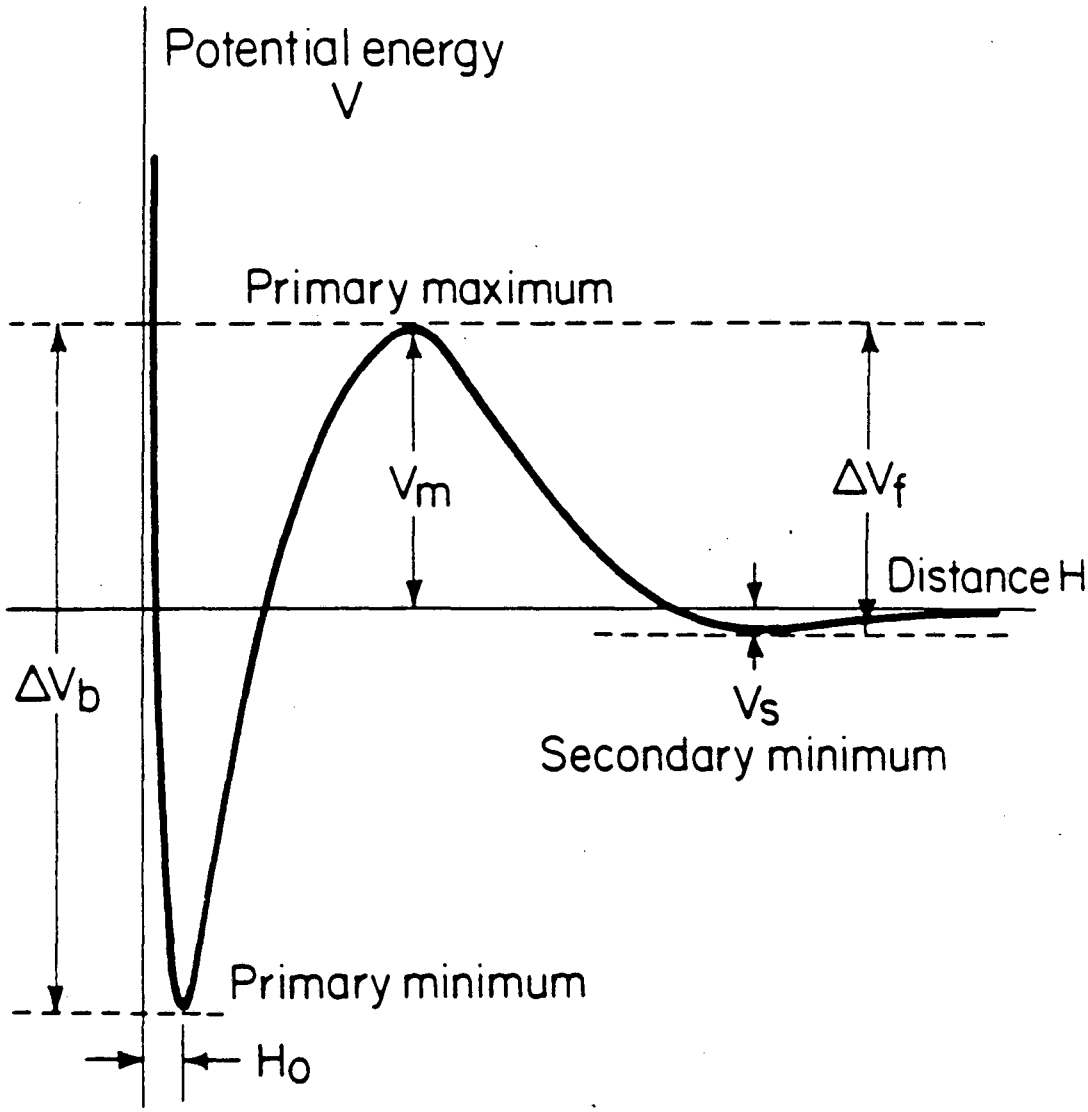

Figure 27. General form of the two-particle interaction energy versus surface separation distance (after ref. 23).

-- XBL 871-184 --

or

$$W_{mixed} = 2(W_1)(W_2)/(W_1 + W_2)$$

where W_{mixed} is the primary maximum of the mixed interaction of particle size (1) and (2) and W_1 and W_2 are the primary maximum heights corresponding to interactions between particles of size (1) and (2), respectively. One result is that the primary maximum in an encounter between a small particle and a much larger particle is essentially double the maximum for interactions between small particles. Thus, the growth rate of large agglomerates is always inhibited and there is a natural limit in the agglomerate size. This is a rather heuristic argument for the possibility of a stochastic monosized agglomerate growth process. A more rigorous approach to heterocoagulation requires modification of Fuchs[79] treatment of repulsive interactions in Smoluchowski's[80] model for the diffusional coalescence of particles to include corrections for agglomerate size. This is beyond the scope of this thesis.

Stabilization of large agglomerates appears to result in narrow size distribution of m-ZrO_2 prepared by thermal hydrolysis of zirconium salts.[34] Since agglomerates are actually composites of smaller agglomerates, their density is expected to be low. Agglomerate densities in Bleier's work are around 50%; particle alignment along preferred facets during agglomerate apparently raises agglomerate density. The agglomerate size distribution is relatively narrow. TiO_2 agglomerates do not appear to form by this mechanism because their densities are high (>65%) and the size distributions are exceedingly narrow.

An alternate possibility arises in the case of a shallow primary minimum and low primary maximum. This situation is somewhat analogous to the problem of nucleation and growth of precipitates. Agglomerates of

only a few particles have very low total binding energy and break apart under thermal action; consequently, stable agglomerates require the formation of nuclei of several particles. Subsequent growth of these nuclei is rapid because the primary maximum barrier is low. This rapid growth depletes the concentration of primary particles so that additional nucleation does not occur. The result is a very narrow size distribution of agglomerates. This appears to be the mechanism of monosized agglomerate formation in TiO_2. Onoda[81] has observed this process in the spontaneous two-dimensional ordering of suspensions of latex microspheres at a critical volume fraction.

Steric interactions of polymers adsorbed on particle surfaces can cause large repulsive forces as particles approach each other. This may aid in the formation of monosized secondary particles conditions where particle agglomeration would be a problem (low primary maximum and deep primary minimum). Surfactants can raise the primary minimum depth so that an agglomerate requires a large number of primary particles for stability. In this case, nucleation can only occur at primary particle concentrations. This confines nucleation to short times, and subsequent growth produces monosized agglomerates. At the neutral reaction conditions, monosized TiO_2 particles will have low stability against agglomeration. HPC may raise the primary minimum depth so that nucleation and growth of monosized agglomerates can occur.

REFERENCES:

1. L. H. Edelson and A. M. Glaeser, unpublished research.

2. H. Kent Bowen et al., "Basic Research Needs on High Temperature Ceramics for Energy Applications," Mat. Sci. and Eng. **44**, 1-56, (1980).

3. (a) H. Kent Bowen, "Advanced Ceramics," Scientific American. **255**, 168, (1986);
   (b) Joel P. Clark and Merton C. Flemings, "Advanced Materials and the Economy," ibid, 50;
   (c) Morris A. Steinberg, "Materials for Aerospace," ibid, 58;
   (d) W. Dale Compton and Norman A. Gjostein, "Materials for Ground Transportation," ibid, 92;
   (e)Richard S. Claassen and Louis A. Girifalco, "Materials for Energy Utilization" ibid, 102;
   (f) Robert A. Fuller and Jonathan J. Rosen, "Materials for Medicine," ibid, 118;
   (g) Tsu-Wei Chou, Roy L. McCullough and R. Byron Pipes, "Composites," ibid, 192.

4. C. Greskovich and J.H. Roslowski, "Sintering of Covalent Solids," J. Am. Ceram. Soc., **59** 336-343 (1976).

5. G. Onoda and L. L. Hench, Eds., Ceramics Processing Before Firing, John Wiley and Sons, NY, 1978.

6. M. F. Yan, R. M. Cannon, and H. K. Bowen; in Ceramic Microstructures '76, Ed. R. M. Fulrath and J. A. Pask eds., Westview Press, Boulder, CO, 1977, pp. 276-307.

7. C. Herring, "Effect of Change of Scale on Sintering Phenomena," J. Appl. Phys., **21**, 301-303 (1950).

8. W. D. Kingery and B. Francois, "Grain Growth in Porous Crystals", J. Am. Ceram. Soc., **48** [10] p. 546-47 (1965).

9. W. D. Kingery, H. K. Bowen, and D. Uhlmann, Introduction to Ceramics 2nd ed., J. Wiley and Sons, New York, 1978.

10. R. J. Brook, "Pore Grain Boundary Interactions and Grain Growth," J. Am. Ceram. Soc., **52** [1] 56-57 (1969).

11. F. M. A. Carpay, "Discontinuous Grain Growth and Pore Drag," J. Am Cer Soc, **60** [1-2] 82 (1977).

12. R. J. Speight and G. W. Greenwood, "Grain Boundary Mobility and Its Effect in Materials Containing Inert Gases," Phil Mag. **9** [100] 683 (1964).

13. M. Hillert, "On Theory of Normal and Abnormal Grain Growth," Acta Met., **13**, 227-238 (1965).

14. P. W. Voorhees and M. E. Glicksman, "Solution to the Multi-Particle Diffusion Problem with Applications to Ostwald Ripening -- II. Computer Simulations," Acta metall. **32** [11] 2013-2030 (1984).

15. W. H. Rhodes, "Agglomerate and Particle Size Effects on Sintering of Yttria-Stabilized Zirconia," J. Am. Ceram. Soc., **64**, (1), 19 (1981).

16. T. Vasilos and W. Rhodes, in Ultrafine-Grain Ceramics, J.J. Burke, N.L. Reed, and V. Weiss, Syracuse University, Syracuse, New York, 1970, 137-172.

17. P. H. Rieth, J. S. Reed, and A. W. Naumann, "Fabrication and Flexural Strength of Ultrafine-Grained Yttria-Stabilized Zirconia, Am. Ceram. Soc. Bull., **55** [8] 717-21, 727 (1963).

18. D. W. Johnson, D. J. Nitti, and L. Derrin, "High Purity Reactive Alumina Powders: II," ibid., **51** [12] 896-900 (1972).

19. D. E. Niesz and R. B. Bennett, "Structure and Properties of Agglomerates," pp. 61-73 in Ref 4.

20. R. T. Tremper and R. S. Gordon, "Agglomeration Effects on the Sintering of Alumina Powders Prepared by Auto-claving Metal," pp. 153-75 in Ref 4.

21. J. D. F. Ramsey and R. G. Avery, "Ultrafine Oxide Powders Prepared by Electron Beam Evaporation," J. Mat. Sci., **9** [10] 1681-88 (1974).

22. E. A. Barringer and H. K. Bowen, "Formation, Packing and Sintering of Monodisperse TiO_2 Powders," J. Am. Cer. Soc., **65**, C-199 - C-201 (1982).

23. E. A. Barringer, "The Synthesis, Interfacial Electrochemistry, Ordering and Sintering of Monodisperse TiO_2 Powders," Ph.D. Thesis, M.I.T., 1983.

24. M. F. Yan, W. W. Rhodes and L. Springer, "Low Temperature Sintering of TiO_2," Bull. Am. Ceram. Soc., **61** [3] 911 (1982). As Cited in Ref. 23.

25. (a) I. A. Aksay and C. H. Schilling, "Colloidal Filtration Route to Uniform Microstructures," in Proceedings of the International Conference and Utrastructure Processing Ceramic Glass Composites, 1983, pp. 43-47;
(b) Unpublished research on bimodal powders.

26. Blendell, "High-purity Alumina by Controlled Precipitation from Aluminum Sulfate Solutions," J. Am Cer Soc, **63** [6] 797-801 (1984).

27. J. Williams, "Characteristics of Fine Oxide Powders," in Science of Ceramics, Vol 2, Ed. G. H. Stewart, Academic Press, New York, 1965, pp. 3-18.

28. W. F. Sullivan and S. S. Cole, "Thermal Chemistry of Colloidial Titanium Dioxide," J. Am. Cer. Soc. 42 [3] (1959).

29. S. R. Yoganarasimhan, "Anatase-Rutile Transformation: Effect of Chloride Ion on the Transformation of Anatase Prepared by Hydrolysis of Titanium Tetrachloride," Ind. J. Chem., 1 358-360 (1963).

30. C. N. R. Rao, A. Turner and J. M. Honig, "Some Observations Concerning the Effect of Impurities on the Anatase-Rutile Transition," Can. J. Chem. 39, 498 (1961).

31. K. Masato, G. L. Messing, "Controlled Transformation and Sintering of a Boehmite Sol-Gel by alpha-Alumina Seeding," 68 [9] 500-505 (1985).

32. D. G. Pickles and E. Lilley, "Ultramicrotoming of Ceramic Powders for Electron Microscopy," J. Am. Ceram. Soc., 68 [9], C-222 - C-223 (1985).

33. D. G. Pickles and E. Lilley, in Extended Abstracts: American Ceramic Society, 88th Annual Meeting, Am. Cer. Soc, Columbus, OH, 1986, p 60; Am. Cer. Soc., 65, 502 (1986).

34. A. Bleier and R. M. Cannon, "Nucleation and Growth of Uniform m-ZrO_2," Mat. Res. Soc. Symp. Proc., 73, 71-78 (1986).

35. (a)J. H. A. van der Woude, P. L. de Bruyn and J. Pieters, "Formation of Colloidal Dispersions from Supersaturated Iron III nitrate solutions. III Development of Goethite at Room Temperature," Colloids and Surfaces, 9, 173 (1984);
(b) J. H. A. van der Woude and P. L. de Bruyn, "...V. Synthesis of Monodisperse Goethite Sols.," Colloids and Surfaces 12, 179 (1984).

36. E. Matijevic, "Monodispersed Colloids: Art and Science," Langmuir 2, 12 (1986).

37. D. H. Whitmore, T. Kawai, "Kinetics of Initial Sintering of Vacuum-Reduced Titanium Dioxide," J. Am. Cer. Soc. 45 [8] 375-379 (1962).

38. H. Anderson, "Initial Sintering of Rutile," ibid., 50 [5] 235-238 (1967).

39. A. G. Grotyohann and K. Herrington, "Sintering of Titanium Dioxide," ibid., 47 [1] 53-54 (1964).

40. K. V. K. Rao, S. V. Naidu and L. Iyengar, "Thermal Expansion of Rutile and Anatase," ibid., 53 [3] 124-126 (1970).

41. K. J. D. MacKenzie, "The Calcination of Titania. VII. Sintering of Rutile," Trans. J. Brit Cer Soc 74, 127-134 (1975).

42. K. J. D. MacKenzie, "The Calcination of Titania. VI. The Effect of Reaction Atmosphere and Electric Fields on the Anatase-Rutile Transformation," ibid., 74, 121-125 (1975).

43. K. J. D. MacKenzie, "The Calcination of Titania. V. Kinetics and Mechanism of the Anatase-Rutile Transformation in the Presence of Additives," ibid., **74**, 77-84 (1975).

44. K. J. D. MacKenzie, "The Calcination of Titania. IV: The Effect of Additives on the Anatase-Rutile Transformation," ibid., **74**, 29-34 (1975).

45. G. R. Miller and O. W. Johnson, "The Sintering of Conductive Rutile: A Model System for Sintering Electronic Ceramics," Mat. Sci, Res., V13, Ed. G. C. Kuczynski, Plenum Press, NY (1980) pp. 181-191.

46. H. M. O'Bryan, Jr. and G. Parravano, "On the Sintering of Single Crystal Rutile," Mat. Sci. Eng., **1**, 177-182 (1966).

47. P.G. Vergnon, F.E. Juillet, M.P. Astier and S.J. Teichner, "Sintering of Ultrafine Particles of Anatase and Delta Alumina," in Science of Ceramics, Eds., C. Brosset and E. Knopp, the Swedish Inst. for Silicate Research, 1970, pp. 47-62.

48. M. Astier, G. Brula, F. LeComte, J. P. Reymond and P. Vergnon, "Influence of the Structure, Pressing, Atmosphere and Doping on the Sintering of Spherical Particles of Titanium Dioxide," Mat. Sci. Monographs, 4: Sintering - New Developments, M. M. Ristic ed., Elsevier, New York, 150 (1979).

49. R. Demchak and E. Matijevic, "Preparation and Particle Size Analysis of Chromium Hydroxide Hydrosols of Narrow Size Distribution," J. Colloid Interface Sci., **31**, 257-262 (1969).

50. R. Brace and E. Matijevic, "Aluminum Hydrous Oxide Sols-I. Spherical Particles of Narrow Size Distribution," J. Inorg. Nucl. Chem., **35**, 3691-3705 (1973).

51. E. Matijevic, M. Budnick, and L. Meites, "Preparation and Mechanism of Formation of Titanium Dioxide Hydrosols of Narrow Size Distribution," J. Colloid Interface Sci., **61**, 302-311 (1977).

52. W. Stober, A. Fink, and E. Bohn, "Controlled Growth of Monodisperse Silica Spheres in the Micron Size Range," J. Colloid Interface Sci., **26**, 62-69 (1968).

53. D. W. Fuerstenau, D. Manmohan and S. Raghavan, "The Adsorption of Alkaline-Earth Metal Ions at the Rutile/Aqueous Solution Interface," in Adsorption from Aqueous Solutions, Ed., P. H. Tewari, Plenum Press, NY, 1981, pp. 93-117.

54. M. F. Yan, "Theoretical Studies and Device Application of Solute Segregation at Ceramic Grain Boundaries," J. Phys. Colloq, pp. C1269-C1283 (1986).

55. J.W. Cahn, "Impurity Drag Effect in Grain Boundary Motion," Acta Metall., **10** [9] 789-98 (1962).

56. (a) R. L. Coble, "Sintering Crystalline Solids. I. Intermediate and Final Stat Diffusion Models," J. App. Phys., **32** [5] 787-792 (1961); (b) R. L. Coble, "Sintering Crystalline Solids. II. Experimental Test of Diffusion Models in Powder Compacts," J. App. Phys., **32** [5] 793-799 (1961).

57. A. M. Glaeser, H. K. Bowen and R. M. Cannon, "Grain-Boundary Migration in LiF: I, Mobility Measurements", J. Am. Ceram., **69** [2] 119-125 (1986).

58. M. F. Yan, "Microstructural Control in the Processing of Electronic Ceramics," Mat. Sci. Eng., **48**, 53-72 (1981).

59. R. L. Coble and R. M. Cannon, "Current Paradigms in Powder Processing," in Processing of Crystalline Ceramics, Mat. Sci. Res., Vol. 11, Eds. H. Palmour, R. F. Davis, and T. M. Hare, Plenum Press, NY, 1978, pp. 151-170.

60. K. D.Reeve, "Non-Uniform Shrinkage in Sintering," Am. Ceram. Soc. Bull. **42** [8] 452 (1963).

61. R. Raj and M. F. Ashby, "Grain Boundary Sliding and Diffusional Creep, "Met. Trans. **2** [4] 1113-1127 (1971).

62. J. H. Jean and T. A. Ring, "Nucleation and Growth of Monosized TiO_2 Powders from Alcohol Solution," Langmuir **2**, 251-255 (1986).

63. M. M. Denn, Process Fluid Mechanics, Prentice-Hall, Englewood Cliffs, New Jersey, 1980, p. 55.

64. Autoscan 60, Scanning Mercury Porosimeter Operations Manual, Quantachrome corp, 1982.

65. E. W. Washburn, Proc. Nat. Acad. Sci., **7**, 115-116 (1921).

66. E. E. Underwood, "Quantitative Metallography," in Metals Handbook, Vol. 9, Amer. Soc. Met., Ohio, 1985, pp. 123-134.

67. S. Brunner, P. Emmett, E. Teller, "Adsorption of Gasses in Multimollecular Layers," J. Am. Ceram. Soc., **60**, 309-319 (1938).

68. Quantasorb Jr. Operation Manual, Quantachrome Corp., 1985.

69. D. E. Yates, "The Structure of the Oxide/Aqueous Electrolyte Interface," Ph.D. Thesis, University of Melbourne, Australia, 1975. As reported in ref 23.

70. B. D. Cullity, Elements of X-ray Diffraction, Addison Wesley, Reading, MA, 1978, p. 102.

71. J. Th. G. Overbeek, "Colloids, A Fascinating Subject: Introductory Lecture", in Colloidal Dispersions, Ed., J. W. Goodwin, The Royal Society of Chemistry, 1982, pp. 1-21. As reported in ref 23.

72. W. D. Harkins and G. Jura, J. Am. Chem. Soc., "Surfaces of Solids. X. Extension of the Attractive Energy of a Solid into an Adjacent Liquid of Film, The Decrease of Energy With Distance, and the Thickness of Films," J. Am. Chem. Soc., **66**, 919 (1944).

73. K. S. W. Sing, "Assessment of Microporosity," Chem. and Ind., 829-830 (1967). As reported in ref 23.

74. D. W. Readey, J. Lee, and T. Quadir, "Vapor Transport and Sintering of Ceramics," Proceedings of the 6th International Conference on Sintering and Related Phenomena, Notre Dame, Indiana, (1983).

75. W. D. Kingery and B. Francois, in Sintering and Related Phenomena, Ed. G. C. Kuczynski, N. A. Hooten, and C. F. Gibbon, Gordon and Breach, N.Y., 1967, p. 471. As reported in ref 74.

76. E. J. W. Verwey and J. Th. G. Overbeek, Theory of the Stability of Lyophobic Colloids, Elsevier, Amsterdam (1948).

77. R. Hogg, T. W. Healy, D. W. Fuerstenau, "Mutual Coagulation of Colloidial Dispersions," Trans. Faraday Soc., **62**, 1638-1651 (1966).

78. J. Israelechiavelli, Intermolecular and Surface Forces: with Applications to Colloidal and Biological Systems, Academic Press, London, 1985, pp 296.

79. N. Fuchs, "Uber die Stabilitat und Aufladung der Aerosole", Z. Phys., **89** 736-743 (1934).

80. M. Von Smoluchowski, "Versuch einer msthematischen Theorie der Koagulationskinetik kolloider Losungen," Z. Phys. Chem **92**, 129-168 (1917).

81. G. Onoda, personal communication.

LAWRENCE BERKELEY LABORATORY
TECHNICAL INFORMATION DEPARTMENT
UNIVERSITY OF CALIFORNIA
BERKELEY, CALIFORNIA 94720